Characterization of Glycan Features in Whole Biospecimens Using Glycan Node

Analysis and the Role of Low-density Lipoprotein Sialylation in Cancer Immunity

by

Jesús Aguilar Díaz de león

A Dissertation Presented in Partial Fulfillment
of the Requirements for the Degree
Doctor of Philosophy

Approved January 2021 by the
Graduate Supervisory Committee:

Chad Borges, Chair
Xu Wang
Peter Williams

ARIZONA STATE UNIVERSITY

May 2021

ABSTRACT

Glycans are complex biological sugar polymers that are commonly found covalently attached to proteins, lipids, and lipoproteins. About 50% of all mammalian proteins are glycosylated. Aberrant glycosylation is a hallmark of most types of cancer, and glycosylation changes that occur in this disease are known to facilitate tumor development. In this dissertation, a bottom-up approach to glycomics, "glycan node analysis", which is a method based on glycan linkage analysis that quantifies unique glycan features, such as "core fucosylation", "α2-6 sialylation", "β1-6 branching", and "bisecting GlcNAc", as single analytical signals by gas chromatography-mass spectrometry (GC-MS), was applied to cancer cell lines, antibodies, extracellular vesicles, and low density lipoproteins to understand the mechanisms leading to aberrant glycosylation in cancer, and to understand the role of blood plasma glycan sialylation in cancer immunity.

Specific tumor antigens such as β1-6-branching, β1-4-branching, bisecting GlcNAc, antennary fucosylation, and Tn antigen (GalNAc-Ser/Thr), were found to be regulated by IL-6 in HepG2 cells; fewer glycan features were regulated by IL-1β. Additionally, neuraminidase enzyme treatment of alpha-1 antitrypsin IgG demonstrates how glycan node analysis can be used to detect relative changes in "α2-6-sialylation" along with corresponding increases in terminal galactose.

Extracellular vesicles (EVs) derived from metastatic and non-metastatic cancer cell lines displayed upregulated or downregulated expression of several specific glycan nodes, particularly 3-GlcNAc, which represents hyaluronic acid. EVs displayed several glycan features that distinguished them from the whole blood plasma glycome. These results were promising for developing new diagnostic strategies in cancer.

A "liquid phase permethylation" procedure for glycan node analysis that does not require spin columns was applied for the first time to whole biological specimens, and it demonstrated potential clinical utility in detecting specific tumor antigens. Significantly different glycan node profiles were found among three cancer cell lines and in peripheral blood mononuclear cells from healthy donors.

Changes in glycosylation and mechanisms regulating glycan changes were studied extensively in cancer cells. Subsequently, it is reported how glycosylation changes can have an impact in cancer immunity. A novel role for oxidized-desialylated low density lipoprotein in cancer immunity is reported, and its implications in cancer and atherosclerosis are discussed.

DEDICATION

To my mother, Maria Teresa Díaz de león

To my father, José Aguilar

To my brother, José Aguilar Díaz de león,

To my sister, Maria Teresa Aguilar Díaz de león

To my nieces, Jazmine Guadalupe, Wendy Ailyn, Keyla Michelle, and my nephew,

Jesús Uziel.

To my grandfather, Miguel Aguilar (rest in peace)

To all my family

To my mentors and role models

Dr. Chad Borges

Dr. Marcia Levitus

ACKNOWLEDGMENTS

TABLE OF CONTENTS

Page

CHAPTER

   1   INTRODUCTION

LIST OF TABLES

LIST OF FIGURES

LIST OF ABBREVIATIONS

Glc	Glucose
Gal	Galactose
Man	Mannose
Xyl	Xylose
Fuc	Fucose
GlcA	Glucoronic Acid
GlcNAc	N-Acetyl-D-Glucosamine
GalNAc	N-Acetyl-D-Galactosamine
NeuAc	N-Acetylneuraminic Acid
GalCer	Galactosylceramide
Asn	Asparagine
Ser	Serine
Thr	Threonine
ALG	Asparagine-Linked Glycosylation
OST	Oligosaccharyltransferase
GnT	Glycosyltransferase
LacNAc	N-Acetyllactosamine
ppGalNAcT	Polypeptide-N-Acetyl-Galactosaminyltransferase
VNTR	"Variable Number of Tandem Repeats"
DMSO	Dimethyl Sulfoxide
TFA	Trifluoroacetic Acid
NaOH	Sodium Hydroxide
GC-MS	Gas Chromatography-Mass Spectrometry
PMAAs	Partially Methylated Alditol Acetates

XICs	Extracted Ion Chromatograms
GNA	Glycan Node Analysis
PTPRT	Receptor-Type Tyrosine-Protein Phosphatase T
ACP	Acute Phase Proteins
IL-6	Interleukin-6
IL-1β	Interleukin-1 Beta
IgG	Immunoglobulin G
Con A	Concavalin A
EVs	Extracellular Vesicles
SEC	Size-Exclusion Chromatography
PAR	Parental Cells
BR	Brain Tropic
LP	Liquid Phase
SP	Solid Phase
NK Cells	Natural Killer Cells
LAK Cells	Lymphokine Activated Killer Cells
PBMCs	Peripheral Blood Mononuclear Cells
HepG2	Hepatocellular Carcinoma Cell Line
K562	Leukemia Cell Line
Siglec	Sialic Acid Binding
LDL	Low-Density Lipoprotein
CD56 or NCAM	Neural Cell Adhesion Molecule
CD3	Cluster of Differentiation 3
NKG2D	Natural Killer Receptor
IFNγ	Interferon Gamma

ELISA	Enzyme Linked Immunosorbent Assay
TBARS	Thiobarbituric Acid Reactive Substances
MDA	Malondialdehyde
TBA	Thiobarbituric Acid
$CuCl_2$	Coper(II) Chloride

CHAPTER 1

INTRODUCTION

1.1 Glycan Structure and Composition, Types of Glycans, and Glycosyltransferase Specificity

Glycans are complex biological structures of multiple monosaccharides linked through glycosidic bonds. There are 8 frequently observed monosaccharides that constitute glycans in vertebrates. While there are over 10 major classes of biological monosaccharides [1], these 8 common monosaccharides can be divided into hexoses, deoxyhexoses, N-acetylhexosamines (HexNAcs), and sialic acids. The hexoses include; D-Glucose (Glc), D-Galactose (Gal), and D-Mannose (Man). The only common deoxyhexose is L-Fucose (Fuc). The HexNAcs include; N-acetyl-D-glucosamine (GlcNAc), N-Acetyl-D-galactosamine (GalNAc). The sialic acids include N-Acetylneuraminic acid (Neu5Ac or NeuAc) and, in non-human vertebrates, N-glycolylneuraminic acid (Neu5Gc). These monosaccharides can link to each other by glycosidic bonds and they can often form branches [2]. Glycotransferases are the enzymes that catalyze the glycosidic bonds that form glycan structures and/or branches by attaching sugars one by one with the help of sugar nucleotide donors in the endoplasmic reticulum [2]. Glycans are formed by the formation of glycosidic linkages between two or more monosaccharides. A glycosidic linkage is the bond formed between the anomeric carbon of one monosaccharide and any hydroxyl group of another monosaccharide. A glycosidic linkage can be formed in two possible stereoisomers (α or β) at the anomeric carbon (carbon 1) of a monosaccharide. A single monosaccharide can be involved in more than two glycosidic linkages, each serving as a branch point. For instance, a monosaccharide can have up to 5 positions for linkages with other monosaccharides (**Figure 1.1**). Once a glycosidic bond is formed, its configuration is kept

1

indefinitely, and therefore it can exist as α or β linkage. Glycosidic bonds can be hydrolyzed to generate its constituent monosaccharide structures [3].

1.1.1 Types of Glycans

A glycoconjugate is a molecule (e.g., a glycoprotein or a glycolipid) with one or more glycan units. About 50% of all secreted and membrane associated proteins of eukaryotic cells are glycosylated [4]. The attachment of many glycans to a polypeptide scaffold creates high diversity among glycoproteins. Some glycoproteins can contain from about 1% to more than 80% glycans by mass [5]. There are three common types of glycoconjugates; O-linked glycoproteins, N-linked glycoproteins, and lipid-linked glycoconjugates. In O-linked glycoproteins, an N-acetylgalactosamine (GalNAc) is attached to the hydroxyl (OH) of serine or threonine by the enzyme polypeptide-N-acetyl-galactosaminyltransferase (ppGalNAcT) forming an O-glycosidic bond. N-linked glycoproteins are initiated by the action of oligosaccharyltransferase, which transfers the pre-assembled glycan $Man_9Glc_3GlcNAc_2$ to the side chain of asparagine residues in the sequence Asn-X-Ser/Thr, where X can be any amino acid but proline [6]. Glucose is then cleaved away and additional sugar residues are attached to the GalNAc or Man residues by other glycotransferases, leading to the formation of complex glycan structures. Also, there are other types of glycans, such as proteoglycans, cytoplasmic glycoproteins, and GPI-anchored glycoproteins (**Figure 1.2**) [7]. Proteoglycans are formed with glycosaminoglycan groups that are covalently attached to proteins. An example of a glycosaminoglycan (GAG) is heparan sulfate. Hyaluronic acid GAGs can be attached to proteoglycans in the extracellular matrix, but hyaluronic acid is unique in that it does not contain sulfate, and it is not covalently attached to proteins [8]. Cytosolic glycoproteins constitute the O-GlcNAc glycoproteins, which have been found to regulate a plethora of

cellular processes such as transcription, cell signaling, and epigenetic modifications. O-GlcNAc modifications occur in cytosolic proteins, and it consists in the attachment of a single GlcNAc residue to a serine or threonine residue by an enzyme called O-GlcNAc transferase [9].

Another type of glycoconjugate are glycolipids. Glycolipids constitute a major portion of glycans in the blood, and in cell membranes [10]. The simplest glycolipid is galactosylceramide (GalCer), which is a glycosphingolipid. GalCer consists of a galactose residue attached to the C-1 hydroxyl group of a lipid moiety called ceramide, which is composed of a sphingosine and a fatty acid. An example of a complex glycosphingolipid is ganglioside, which is sialylated and branched (**Figure 1.3**). Most animals' glycolipids are glycosphingolipids. Additionally, the common glycan sequence found in several glycolipids is glucose attached to a lipid moiety, followed by the sequential addition of galactose and GlcNAc residues forming linear structures, such as N-acetyllactosamines [11].

Glycoproteins and glycolipids can be found in cell membranes and in circulation in blood plasma. Glycoproteins can carry N- and O-linked glycans at the same time. For instance, glycophorin A, which is abundant in human red blood cells, contains 1 N-linked and 15 O-linked glycans [12].

1.1.2 Glycosyltransferase Specificity

Glycotransferases assemble monosaccharides into linear and branched glycan chains. There are over 200 genes that encode for glycotransferases in eukaryotes. Most glycotransferases catalyze a group transfer reaction in which a monosaccharide from a

sugar nucleotide donor is transferred to a protein or acceptor substrate. Examples of sugar nucleotide donors include UDP-Gal, GDP-Fuc, or CMP-Sia. The acceptor substrates can be polypeptides, lipids, monosaccharides, oligosaccharides, and small organic molecules, and even DNA. Glycotransferases act sequentially, such that the product of one enzyme yields a preferred acceptor substrate for the subsequent action of another. The result is a linear or branched glycan composed of monosaccharides linked to one another. Glycotransferases display high specificity for their nucleotide sugars, their acceptor substrates, and the linkages they direct (α or β). An example of glycotransferase specificity is the human B blood group α1-3 galactosyltransferase. This enzyme adds a galactose residue in an α1-3 linkage only to the galactose containing fucose in α1-2 linkage. If prior modifications are made, such as adding a sialic acid instead of a fucose, no reaction occurs. Similarly, if the galactose residue acceptor does not contain fucose, no reaction occurs by the enzyme [13].

In addition to glycotransferases that elongate glycan chains, there are glycotransferases that are involved in the initiation of the synthesis of glycoproteins and glycolipids. Such glycotransferases attach pre-formed glycans to either a polypeptide or a sphingolipid base, and these glycotransferases also display strict donor and acceptor specificity (As discussed below).

1.2 Glycan Biosynthesis

1.2.1 N-Glycan Biosynthesis

The glycosylation machinery is not template driven as with the synthesis of DNA and proteins. Glycan biosynthesis is the result of a complex network of factors such as; sugar nucleotide donors, glycosyltransferases, glycosidases, extracellular factors (such as

growth factors and cytokines), pH of the ER and Golgi, competition reaction between glycotransferases, and localization of glycotransferases in Golgi and ER [6]. N-glycosylation starts in the ER membrane with the synthesis of the oligosaccharide. N-glycosylation occurs co-translationally, which means that it occurs while the protein is being synthesized. Building of the N-glycan is initiated by the transfer of GlcNAc-P from the sugar nucleotide donor UDP-GlcNAc to dolichol pyrophosphate (Dol-P), a lipid like molecule. The transfer is catalyzed by the enzyme DPAGT1, yielding Dol-PP-GlcNAc [14]. The action of glycosyltransferases ALG13, ALG14, ALG1, ALG2, and ALG11 elongate the glycan by adding one more GlcNAc and five mannose residues generating Dol-PP-$GlcNAc_2Man_5$. ALG glycotransferases were discovered using Yeast as a genetic model, in which Asparagine-Linked Glycosylation (ALG) mutants in yeast helped to identify the glycotransferase genes responsible for N-glycan elongation in the ER. Hence, for this reason, such glycotransferases are abbreviated ALG. The RFT1 protein translocates the Dol-PP-$GlcNAc_2Man_5$ to the ER lumen. Then in the ER lumen, the subsequent action of other ALG glycotransferases make the lipid linked oligosaccharide Dol-PP-$GlcNAc_2Man_9Glc_3$ [6, 15].

The entire glycan structure of 14 sugars containing 9 mannose residues, 3 glucose residues, and 2 GlcNAc residues ($Man_9Glc_3GlcNAc_2$) is transferred from the Dol-P lipid molecule to the Asn residue of a protein by the oligosaccharyltransferase (OST) complex on the luminal side of the ER membrane. OST complex recognizes an asparagine (Asn) residue in the context of the sequence Asn-X-Ser/Thr, where X can be any amino acid but proline. Even though Asn is similar in structure to glutamine, the extra carbon on the glutamine chain is not tolerated by the OST complex, and hence it is not recognized by the OST complex (glycosyltransferase specificity). Also, although OST transfers the

5

oligosaccharide to the Asn-X-Ser/Thr sequon, transfer to this sequence does not always occur due to conformational or other constrains during glycoprotein folding. Additionally, because the OST complex is specific to the Asn-X-Ser/Thr sequence, proteins with such amino acid sequence are said to have *potential* N-glycosylation sites [16]. After the oligosaccharide is transferred to Asn residues on glycoproteins, ER membrane anchored glucosidase I (MOGS) cleaves the terminal α1-2Glc residue. During glycoprotein folding, soluble glucosidase II (PRKCSH) enzyme sequentially removes the second and third α1-3Glc residues from the oligosaccharide, yielding $Man_9GlcNAc_2$. Before exiting the ER, α-mannosidase I (MAN1B1) removes the terminal α1-2Man from the central arm of $Man_9GlcNAc_2$ to yield $Man_8GlcNAc_2$. After the glycoprotein has been trimmed in the ER, it will redirect to the Golgi for further modifications. Depending on the availability of α-mannosidase I, most glycoproteins exiting the ER will carry N-glycans with either 8 or 9 mannose residues [17].

The glycoprotein with the high mannose oligosaccharide ($Man_8GlcNAc_2$) exits the ER and enters the Golgi where it is further modified by glycotransferases and glycosidases. In the *cis*-Golgi, α1-2 mannosidases IA, IB, and IC remove the α1-2Man residues from the $Man_8GlcNAc_2$ oligosaccharide to give $Man_5GlcNAc_2$. This modification enables GnT-I or MGAT1 in the *medial* Golgi to add a β1-2 linked GlcNAc residue to α1-3 mannose branch in the core structure of $Man_5GlcNAc_2$, yielding $GlcNAcMan_5GlcNAc_2$. After this step, most of the N-glycans are trimmed by mannosidase IIA and IIX, which remove α1-3 and α1-6-linked Man residues from $GlcNAcMan_5GlcNAc_2$, yielding $GlcNAcMan_3GlcNAc_2$. The N-glycans that are not trimmed by mannosidase IIA and IIX form hybrid N-glycan structures by the action of other glycotransferases. After the two mannose residues are removed, a second β1-2 GlcNAc linked residue is added to the α1-

6

6 linked man of the core structure by MGAT2 or GnT-II. This gives rise to the precursor of complex N-glycans, which are then formed by the action of other glycotransferases [17].

The common core structure that is common to all N-glycans is Manα1–6(Manα1–3) Manβ1–4GlcNAcβ1–4GlcNAcβ1-Asn-X-Ser/Thr. There are three different types of N-glycans; complex, high mannose, and hybrid. High mannose chains result from the initial stage in the biosynthesis of N-linked glycans, after they exit the ER. Complex chains result from the removal of mannose residues from high mannose chains by glycosidases and the addition of other sugar residues such as fucose, sialic acid, GlcNAc, and galactose in the Golgi. A hybrid oligosaccharide chain contains a branched of the high mannose type and a branched of the complex type that also occurs in the Golgi [6, 17].

1.2.2 N-Glycan Branching

There are three types of sugar modifications and/or branching that can further add to the heterogeneity of N-glycan structures, which occur at the Golgi. There can be 1) sugar additions to the core structure, 2) additional branching by the addition of GlcNAc residues, and 3) decoration or "capping" of additional branch structures by other sugars [6] N- glycan core modifications result by the addition of fucose α1-6 linked to the GlcNAc attached to the asparagine residue in the core structure, which is catalyzed by the fucosyltransferase 8 (Fut 8). Additional branching to the N-glycans can be made by the action of other glycotransferases [6, 17]. Regulation of additional branching is largely a function of the level of expression of the relevant glycotransferases, such as GnT-V or GnT-IV, level of sugar nucleotide donors, and glycotransferase competition of substrate. An example of additional branching is β1-6 branching, which results in the addition of GlcNAc β1-6 linked to the α1-6 linked mannose of the core structure by the action of GnT-V or MGAT5. β1-4

branching results by the addition of GlcNAc β1-4 linked to the α1-3 mannose of the core structure by the enzyme GnT-IV or MGAT4. Such branching can be further elongated by the addition of β-linked galactose residue to the GlcNAc, which by the sequential addition of GlcNAc and galactose residues form N-acetyllactosamines or LacNAc sequences. N-acetyllactosamines can be initiated in two different ways. Galactose can be added in a β1-4 linkage to the GlcNAc residue of the additional branch, generating what is called a type 2 glycan unit. Galactose residues can also be added in a β1-3 linkage to obtain a type 1 unit. These LacNAc sequences can be further decorated or "capped" at the end by the addition of sialic acid, fucose, galactose, N-acetylgalactosamine, and sulfate. Capping sugars are most commonly α-linked. Therefore, core structure modifications, additional branching, and "capping" or decoration with additional monosaccharides can give rise to highly heterogeneous mixtures of complex N-glycan structures, which are commonly found on mature N-linked glycoproteins. (**Figure 1.4)** [6] [18].

1.2.3 O-Glycan Biosynthesis

As opposed to N-glycan synthesis, there are no lipid linked intermediates and glycosidases involved in O-glycan synthesis. O-linked glycosylation starts in the Golgi by the addition of monosaccharide units to a completed polypeptide chain. Building of the O-glycan is initiated by the transfer of N-acetylgalactosamine (GalNAc) to a serine or threonine residue of a polypeptide, which is catalyzed by the enzyme polypeptide-N-acetyl-galactosaminyltransferase (ppGalNAcT). Although there is not an identified amino acid sequence that accepts GalNAc residues, proline residues near the GalNAc addition site are usually favorable for O-glycosylation, whereas charged amino acids seem to interfere with O-glycosylation. The locations of O-glycans are specified by the secondary or tertiary structure of the protein, and there is not a common sequence as with N-glycans

[19].O-linked glycosylation is an essential process since all mammalian cell types express ppGalNAcTs. There are 21 ppGalNAcTs, with high sequence identity, and other 9 glycotransferases involved in O-glycosylation. The subcellular localization in the Golgi of these enzymes determines the degree of O-glycans synthetized by a cell. For example, if a ppGalNAcT is localized to a late compartment of the Golgi, incomplete or shorter O-glycans will be produced. In addition, as observed in N-glycosylation, glycotransferase specificity is a key feature for O-glycosylation as well. For instance, one ppGalNAcT cannot attach a GalNAc residue until an adjacent serine or threonine residue is glycosylated by a different ppGalNAcT. An example of heavily O-glycosylated proteins are mucins, which contain as much as 80% glycan by mass. Mucins are found in mucous secretions, and in cell membranes with the glycan exposed to the external microenvironment. Mucins have repeated peptide stretches called "variable number of tandem repeats" (VNTR), which are rich in serine and threonine residues, which serve as O-GalNAc acceptor sites. VNTR are also rich in proline residues, which facilitate O-GalNAc glycosylation [20].

There are four common O-glycan core structures, which can be further substituted by other sugars. The most common core structure of O-glycans found in many glycoproteins and mucins is the core 1 structure Galβ1-3GalNAc-, which forms the core of longer and complex structures. Core 2 O-glycans contain a β1,6-linked GlcNAc attached to the GalNAc of core 1. This type of structure is also commonly found in mucins and glycoproteins. Core 3 structures have an α1,6-linked sialic acid and a β1,3-linked GlcNAc attached to the GalNAc. Core 4 structures have a β1,6-linked GlcNAc and a β1,3-GlcNAc attached to the GalNAc (**Figure 1.5**). All of the core structures can be sialylated. Elongation of core 1 and core 2 structures is catalyzed by β1,3-N-

acetylglucosaminyltransferase. Terminal structures of O-glycans may contain fucose, sialic acid, and N-acetylglucosamine in both α and β linkages. Core 2 structures are regulated during activation of lymphocytes, cytokine stimulation, and embryonic development. In cancer, there is altered expression of the enzymes responsible for core 2 O-glycosylation. Some of the 5 hydroxylysine (Hyl) residues of collagen are joined to D-galactose via an O-glycosidic bond. Some proteoglycans are joined to their glycosaminoglycans via a Gal-Gal-Xyl-Ser structure. Cytosolic and nuclear glycoproteins contain GlcNAc-Ser/Thr moieties in which GlcNAc is the only sugar attached to the protein (**Figure 1.5)** [19].

1.2.4 Glycan Structure Common to all Glycans

Common to N- and O- linked glycans as well as glycolipids are terminal N-acetylglucosamine (GlcNAc) residues which, with the subsequent addition of galactose residues and GlcNAc residues, can form poly-N-acetyllactosamines (**see Figure 1.4)**. Hence, some glycoproteins and glycolipids are modified with poly N-acetyllactosamines. These type of glycan modifications are common among glycolipids and glycoproteins. The A, B, and H blood group antigens are glycans presented on the type 1, type 2 N-acetyllactosamines [21]. N-acetyllactosamines are synthesized by the alternating actions of β1,4-galactosyltransferases and β1,3 N-acetylglucosaminyltransferases. On N-glycans, poly N-acetyllactosamines occur mainly on the β1,6-branch, which is catalyzed by GnT-V. In O-glycans, poly N-acetyllactosamines occur on the β1,6 GlcNAc transferred by a core 2 β1,6GlcNAcT. In glycolipids, poly N-acetyllactosamines occur on the glucose β-linked to the ceramide. In addition, such N-acetyllactosamines can be further decorated with the attachment of additional sugars such as fucose, galactose, N-acetylglucosamine, and sialic acids, all of which can be α or β linked. N-acetyllactosamines can carry

additional branched, elongated structures. GlcNAc residues can be added to the galactose residues in a β1,6 linkage, which is catalyzed by β1,6 N-acetylglucosaminyltransferases. These GlcNAc residues can be extended by the addition of galactose and GlcNAc residues, forming additional N-acetyllactosamines [21].

1.3 Glycans and Cancer

1.3.1 Cell Surface Glycosylation

Cancer metastasis is still the major cause of cancer deaths worldwide [22]. Evidence from tissue specific glycosylation studies have revealed that abnormal glycosylation on cancer cell surfaces is one of the mechanisms by which cancer cells evade an immune response to survive longer in the host and facilitate metastasis [23]. Examples of abnormal glycosylation in cancer include incomplete or truncated glycan structures [24], increased branching [25], increased sialylation [26], and sometimes decreased core fucosylation in some cancers [27]. An example of increased branching includes β-1,6-GlcNAc branching, which results due to upregulation of MGAT5 or GnT-V enzyme [25]. An example of decreased or truncated glycosylation includes the Tn antigen (GalNAc-Ser/Thr), which is often found in mucins derived from tumors and not found in normal mucins [28]. These glycan modifications facilitate cancer proliferation and metastasis [29]. For example, increased β-1,6-GlcNAc branching can result in the formation of poly N-acetyllactosamines, which are elongated glycan structures. N-acetyllactosamines are usually recognized by glycan binding proteins such as Galectin-3, and binding of Galectin-3 to glycoproteins with increased poly-N-acetyllactosamines impedes natural killer cell recognition and activation, which subsequently results in immune evasion by cancer cells [30]. Also, the catalytic activity of tumor suppressor proteins can be suppressed by increased expression of poly-N-acetyllactosamines. For example, PTPRT acts as a

phosphatase protein to regulate phosphorylation of tumorigenic proteins such as STAT3, and when PTPRT is modified with poly-N-acetyllactosamines, Galectin-3 binding masks its catalytic activity, preventing STAT3 dephosphorylation, and inducing STAT3 translocation to the nucleus where it induces the transcription of tumorigenic proteins that drive cell proliferation [31].

1.3.2 Blood Plasma Protein Glycosylation

In addition to abnormal cell surface glycosylation, abnormal glycosylation of circulating glycoproteins in the blood is commonly observed [32]. Abnormal glycosylation of highly abundant blood plasma glycoproteins is a feature that is known to be a hallmark of nearly every type of cancer [33]. In lung cancer patients, five major glycan features that are elevated relative to healthy individuals are terminal fucosylation, α2-6-sialylation, β1-6-branching, β1-4-branching, and outer arm fucosylation [34]. These changes are stage dependent as these levels increase dramatically from stage I to stage IV in lung cancer. Other types of cancer, such as ovarian cancer and bladder cancer, also display similar characteristics, with α2-6-sialylation being elevated in both [35]. The role that these abnormal glycan features within highly abundant blood plasma proteins play in cancer development is not well understood, and what is most striking is that such changes are not derived directly from the tumor. Such glycan changes come from healthy hepatocytes and B cells/plasma cells since the vast majority of plasma glycoproteins are produced by the liver and by the immune system (as antibodies) [36]. Therefore, cancer induced changes to the immune system and hepatocytes are more likely responsible for the glycan structural changes observed in the blood.

1.4 Effect of Inflammatory Cytokines on Regulating Glycosylation in Mammalian Cells

1.4.1 Inflammatory Cytokines Regulate N-Glycan Branching on Blood Plasma Glycoproteins

It has been discussed that malignant transformation is accompanied by abnormal glycosylation [33]. An understanding of the biochemical mechanisms regulating abnormal glycosylation in cancer can provide new targets for therapy efficacy and diagnosis [37]. However, little is known about the factors that drive abnormal glycosylation in cancer. The level of glycosylation depends on several factors, such as the level of glycosyltransferase expression, nucleotide sugar donor availability, and cytokine expression. For instance, constant GnT-V over expression has been reported in several tumors, and its overexpression is associated with tumor development. However, few documented mutations in glycosyltransferase genes have been reported [38], which means that upstream factors or pathways are responsible for the altered expression of glycosyltransferase activity in cancer cells. These upstream factors are most likely cytokines since there are studies demonstrating how certain cytokines alter glycosyltransferase activity [39–45], although the exact molecular pathway is not always well defined. Cytokines are important players in mediating innate and adaptive immunity, and they are important in activating T-cells and other immune cells. In response to infection, tissue injury, or cancer, several inflammatory processes cause the activation of immune cells, such as macrophages and monocytes, that are responsible for host protection. These immune cells secrete cytokines which in turn have the ability to activate other immune cells [39]. The cytokines involved in stimulation of pro- and anti-inflammatory processes are referred to as inflammatory cytokines. One of the many targets of inflammatory cytokines are hepatocytes. Hepatocytes secrete acute phase

13

proteins or plasma proteins that constitute about 50% of all blood plasma glycoproteins [40]. It has been shown that inflammatory cytokines, such as IL-6, IL-1β, and TNF-α, can not only alter genes encoding acute phase proteins, but they can also alter glycosylation of acute phase proteins [41, 42, 44, 45]. A technique called "crossed affinity immunoelectrophoresis" with a lectin Concanavalin A (Con A) as a ligand was first used to discover glycosylation changes of acute phase proteins upon cytokine stimulation [43]. Con A binds only with bi-antennary glycans, but it does not bind to tri- or tetraantennary glycans. This led to the finding that inflammatory cytokines increased branching of N-glycans in acute phase proteins [45]. These studies, however, were limited since a complete glycan profile was not provided, and other glycosylation changes, besides increased branching, might not have been observed.

1.4.2 Inflammatory Cytokines Regulate Abnormal Cell Surface Glycosylation

Cytokines, such as IL-6, IL-1β, IL-5, and IL-10, are commonly found elevated in many types of cancers, including pancreatic cancer and lung cancer, and they are known to increase the expression of several oncogenic proteins that facilitate tumor development [46–52]. These cytokines are also known to regulate cell surface glycosylation in different cell lines. For instance, IL-6 and IL-1β are known to regulate the expression of specific glycosyltransferases involved in the synthesis of tumor specific antigens in several cancer cells: In gastric cancer cells, IL-6 and IL-1β are known to regulate the expression of several fucosyltransferase and sialyltransferase genes that are involved in the synthesis of sialylated Lewis antigens [53]. In hepatocellular carcinoma cells, IL-6 induces the production of fucosylated haptoglobin [54]. In pancreatic cancer cells, IL-6 and IL-1β were found to regulate the expression of tumor associated sialylated antigens such as SLe^x [55]. Additionally, IL-10 is known to regulate fucosylation in epithelial cells [56], and IL-5

14

is known to increase sialylation of secreted IgA in B-lymphoma cells [57]. The common belief is that abnormal glycosylation is the result of the inflammatory aspect of cancer. However, the Borges lab has provided evidence that, at least in blood plasma/serum, cancer causes changes in glycosylation above and beyond inflammation alone from some of the cancers that have been studied in which the control samples were from inflammation-positive patients, but glycan changes occurred beyond what was observed in the controls [34]. Overall, the immune network, the inflammatory aspect of cancer, and inflammatory cytokines indicate that multiple pathways could be involved in regulating the complex machinery of plasma protein glycosylation in cancer patients.

1.5 Sialylation in Cancer Immunology

1.5.1 Natural Killer Cells and Lymphokine Activated Killer Cells

The immune system is capable of recognizing and destroying cancer cells [58]. Natural killer (NK) cells are part of the innate immune system, and they comprise about 5-15 % of all lymphocytes. NK cells express CD16 and CD56 receptor, but they do not have the component of the T cell receptor CD3 [59]. In NK cell immunotherapy for cancer, NK cells are used to kill cancer cells that lack MHC-1. Therefore, those cells that lack MHC-1, and cannot be targeted by T-cells, are the ideal target cells for NK cells [60]. NK cells are commonly used in patients for leukemia treatment [61]. However, NK cells show limited clinical efficacy in clinical trials. The limited efficacies have to do with the inhibitory signals found in the tumor microenvironment, such as sialic acids, MHC expressing cells, and expansion of regulatory T cells [62].

The central goal of anti-cancer immunotherapy is to activate cytotoxic lymphocytes and enhance their cytotoxic activity against cancer cells [63]. Among the many

immunotherapy methods being considered for anti-cancer therapy, the use of lymphokine activated killer cells has been translated into clinical studies [64]. When peripheral blood mononuclear cells (PBMCs) are stimulated with interleukin-2 (IL-2) cytokine, they are transformed into lymphokine activated killer (LAK) cells. LAK cells are composed of NK cells and NKT cells. NKT cells express CD16 and CD56 receptors, but they also express the T-cell receptor CD3 [65]. Therefore, these cells can target both, MHC-1 expressing cells and cells that lack MHC-1. LAK cells were first introduced by Rosenberg et al in 1985 for the treatment of metastatic melanoma, and 11 of 25 patients showed significant tumor regression, with one patient exhibiting complete tumor regression [66]. However, a low clinical response rate was reported in phase II and phase III trials using LAK cells in combination with IL-2. The low response in later trials was explained by the expansion of regulatory T-cells induced by IL-2 and by prevention of NK cell attack from the inhibitory receptor killer cell immunoglobulin-like receptor (KIRs) [67]. Today, even though LAK cells are not widely used, LAK cell immunotherapy is still being used in some clinical trials in combination with other forms of therapy. For instance, it has been shown that LAK cell immunotherapy in combination rituximab in patients with follicular lymphoma is safe and may delay disease progression [64].

Immune cell mediated cancer therapy is commonly attempted to eradicate tumors in clinical research [60]. Another commonly used method is adoptive T-cell therapy, in which tumor infiltrating T-cells (TILs) are isolated from the primary tumor, activated with IL-2 cytokines, expanded, and transplanted back into the patient. The process of cell isolation and activation is similar as in T-cells and NK cells [68]. Therefore, an understanding of the mechanisms that lead to NK cell or LAK cell impairment could be of great importance for improving NK/LAK cell and T cell immunotherapy.

1.5.2 Role of Sialylation in Regulating Lymphocyte Cytotoxicity

The most critical step in cancer metastasis is when cancer cells disseminate into blood circulation [69]. In circulation, cancer cells are exposed to immune cells, such as natural killer (NK) cells and T-cells, that patrol and kill cancer cells to avoid their dissemination. However, cancer cells have evolved different mechanisms to evade an immune response. Recent studies have shown that increased expression of sialic acids on the surface of cancer cells is one of the mechanisms by which cancer cells evade the cytotoxicity activity of NK cells and T-cells [70]. NK cells are part of the innate immune response, and they express both inhibitory and activating receptors on their surface. Sialic acid binding immunoglobulin-type lectin 7 (Siglec-7) is an inhibitory receptor expressed on NK cells, and cancer cells evade NK-cell dependent killing by enhancing Siglec-7 receptor-mediating signaling using sialic acids on the cell surface [71]. Another study found that tumor infiltrating lymphocytes show enhanced expression of Siglec-9 receptor (an inhibitory receptor on T cells), and cancer cells evade T-cell cytotoxicity by engaging Siglec-9 signaling using sialic acid overexpression on their surface [72]. *These studies suggest that increased expression of sialic acids in blood plasma glycoproteins will also engage Siglec receptors on NK cells and T-cells to block their killing activity against cancer cells, facilitating dissemination and metastasis of cancer. However, to date there are not any studies that show how abnormal sialic acid bearing blood plasma glycoproteins protect cancer cells from an immune response.*

Additionally, it has been extensively studied how cancer cells use cell surface glycans to evade the cytotoxicity activity of immune cells in circulation [73], yet it is not well understood how blood plasma glycans facilitate evasion of the immune response. Some studies suggest that glycosylation changes in blood plasma glycoproteins facilitate

tumor development and metastasis by facilitating evasion of the natural immune response to cancer [74]. Other studies suggest that abnormal glycosylation in the blood "coats" tumor cells, protecting them from the killing activity of immune cells such as natural killer cells (NK cells) [75]. Blood plasma glycoproteins display increased N-glycan branching and subsequently increased expression of sialic acids on the terminal glycan [76]. Such sialic acids likely engage NK cells or CD8-T cells through binding of their inhibitory sialic acid binding immunoglobulin-type lectin (siglec) receptors, resulting in immune evasion. This suggested mechanism is supported by the fact that tumor secreted glycoproteins with increased sialic acids, such as osteopontin, engage the siglec-9 receptor on T cells and inhibits their cytotoxicity activity [77]. Specific glycan features, such as increased sialylation in circulation, could engage inhibitory siglec receptors on natural killer (NK) cells and T-cells and inhibit their cytotoxic activity against cancer cells.

As explained above, elevated sialylation is one of the many glycan features that are elevated in blood plasma glycoproteins in cancer, and research studies on how this is beneficial to cancer are scarce. Additionally, while increased levels of sialic acid content on glycoproteins appears to be a driver for tumor development, in other cases low levels of sialic acids can promote the development of other diseases, such as atherosclerosis [78], as described below.

1.6 Desialylated Blood Plasma Low-Density Lipoprotein in Atherosclerosis

1.6.1 Carbohydrate and Chemical Composition of Low-Density Lipoprotein

Blood plasma low-density lipoprotein (LDL), also known as the "bad" cholesterol, plays an important role in the development of atherosclerosis because of its capability to deliver cholesterol from the liver to other cells in circulation and the arterial wall [79]. LDL particles

are about 3 million Daltons in total molecular weight and are composed of apolipoprotein B-100 (apoB-100), a phospholipid monolayer, and a hydrophobic core which makes up about 75% of LDL particle weight. ApoB-100 has 16 asparagine residues that are glycosylated and up to 24 potential N-glycosylation sites. Glycans constitute about 5-9 % of ApoB-100 molecular weight. There are two types of glycan chains on ApoB-100; one type of chain contains N-acetylglucosamine (GlcNAc) and mannose (Man) residues, and the other type of chain contains GlcNAc, Man, and Galactose (Gal) residues connected to sialic acids. The phospholipid part of LDL contains diacylglycerol, ceramide, phosphatidylcholine, sphingomyelin, and phosphatidylethanolamine. The hydrophobic core contains cholesterol esters, non-esterified cholesterol, and triglycerides. In addition to transporting cholesterol, LDL also transports gangliosides, which are sialic acid rich. Gangliosides are believed to contain most of the sialic acids present in LDL particles. The glycolipid part of LDL contains galactosamine and glucose monosaccharides [78].

1.6.2 Atherogenic Role of Desialylated Low-Density Lipoprotein

The search for atherogenic LDL in the blood stream of patients with coronary atherosclerosis led to the discovery of LDL particles with low levels of sialic acids, referred to as desialylated LDL [80]. Compared to healthy controls, patients with coronary atherosclerosis showed significantly lower levels of sialic acids on LDL particles, but no significance difference was found in the levels of GlcNAc, Gal, and Man residues [81]. Desialylation of LDL appears to be a hallmark of atherosclerosis since this grants the ability of LDL to induce atherogenic changes in cells. *In vitro* desialylated LDL and isolated LDL from patients with atherosclerosis induce intracellular lipid accumulation in smooth muscle cells. LDL isolated from healthy controls shows no significant induction of intracellular lipid accumulation, whereas LDL isolated from patients with coronary

atherosclerosis induces increased intracellular content of triglycerides and cholesterol esters [81]. Desialylation of LDL plays a key role in enhancing the uptake of LDL by cells, leading to increased intracellular accumulation of cholesterol esters. The enhanced uptake of desialylated LDL and low degradation of ApoB-100 causes the intracellular accumulation of cholesterol esters. The uptake of native LDL is controlled by LDL receptors, but desialylation of LDL allows LDL particles to enter arterial walls via other pathways [82].

Desialylation likely occurs in the blood stream, however, the exact mechanisms on how this posttranslational modification occurs is not well understood. Evidence suggests that desialylation might be an early event that leads to smaller, denser, more electronegative, and oxidized LDL particles, all of which are referred to as multiple modified LDL that cause atherogenic changes in cells [83]. Therefore, elucidation of the molecular mechanism by which LDL is desialylated is important. One hypothesis is that LDL undergoes desialylation in the blood. For instance, one study showed that when native LDL was treated with trans-sialidase that was isolated from lipoprotein deficient serum, desialylation of LDL occurred [84]. This desialylated LDL then induced accumulation of cholesterol esters in human aortic intimal cells [84]. While this may be a possible mechanism, other factors might be involved, such as cytokines, which are known to regulate glycosylation of glycoproteins.

1.6.3 LDL Oxidation and a Method for its Quantification

In addition to desialylation of LDL, oxidation of LDL is an also an important mediator in the development of atherosclerosis. Studies have shown that when LDL is both desialylated and oxidized, its atherogenic capability is much higher [85]. In fact, studies have shown

that desialylated LDL is more easily oxidized than native LDL [86], leading to the hypothesis that desialylation is an early even that leads to LDL oxidation. Therefore, a rapid, reliable, cheap, and general method to determine oxidative modification of LDL is needed for studies of LDL in atherosclerosis and other diseases. The most commonly used and preferred assay for LDL oxidation studies is the thiobarbituric acid reactive substances (TBARS) assay [87]. Malondialdehyde (MDA) has been widely used as a marker of lipid peroxidation due to its facile reaction with thiobarbituric acid (TBA) that leads to the formation of MDA-TBA$_2$ conjugates. These conjugates absorb in the visible spectrum at 532 nm and produces a pink color. The major source of TBARS in LDL are the unsaturated fatty acids arachidonic acid and docosahexaenoic acid [87]. Because other molecules derived from lipid peroxidation can also react with TBA, this assay is considered to measure thiobarbituric acid reactive substances (TBARS) [88] and is readily applicable to LDL.

1.6.4 Low-Density Lipoprotein in Cancer

Little is known about the role of LDL in tumor development, and little research has been done on the role of oxidized-desialylated LDL in cancer. However, some studies suggest that LDL, free cholesterols, and lipids can inhibit NK cell cytotoxicity against cancer cells [89]. One study showed that LDL uptake inhibits the antitumor functions of γδT-cells [90], which express NK receptors that determine their antitumor cytotoxicity. A different study found that NK cells with increased intracellular lipid accumulation display decreased cytotoxicity effects [89]. These studies suggest that enhanced uptake of LDL by NK cells inhibits their antitumor functions. However, little is known about how oxidation and desialylation of LDL affects uptake and cytotoxicity of NK cells. There is one study that shows how oxidation of LDL by polymorphonuclear leukocytes inhibits NK activity in a

dose response manner [91], yet the exact mechanism on how this occurs is not well defined. In this dissertation, a new role for oxidized and desialylated LDL in modifying LAK cell activity is discussed in chapter 5.

As discussed above in sections 1.3-1.6, glycosylation changes, such as sialylation, in cancer and in atherosclerosis are extremely important since they can have an impact on disease progression and development. The first step towards understanding glycan function in disease is to understand glycan structural changes. Therefore, there is a need for new glycomics methods that can quantify specific changes in glycosylation and that are able to provide reliable and reproducible results. In the next section, it will be discussed the commonly used methods for glycan analysis (top down glycomics), and a bottom up glycomics approach (glycan node analysis), which was used to conduct this research.

1.7 Glycan Analysis Methods

1.7.1 Intact Glycan Analysis; Top Down Glycomics

Glycosylation changes in cancer are well recognized in medicine, and their potential clinical utility has been suggested [92]. There are several glycomics methods that are commonly used to profile glycosylation in cells and in blood plasma. For example, Lectin microarrays are a technology that was recently developed in 2005 for the analysis of glycan epitopes [93]. Microarrays consist of glycan binding proteins or lectins immobilized to a glass support that bind to certain glycan epitopes. These immobilized lectins are incubated with a fluorescently labeled sample that reveals which epitopes bind to the lectins. One of the disadvantages of lectin microarrays are structural limitations since the exact glycan structures are not revealed. Mass spectrometry (MS) techniques overcome

such structural limitations since MS instruments are often coupled to chromatographic techniques that allow separations of glycans facilitating structural analysis [94]. Additionally, controlled fragmentation of ions by tandem mass spectrometry (MS/MS), a feature commonly used in intact glycan analysis, allows the analysis of glycan sequences and it gives an additional insight into glycan structure [94]. For intact glycan analysis, MS methods often employ high-performance liquid chromatography (HPLC) to achieve sample separation. However, the MS method that does not use a sample separation technique is the Matrix-Assisted Laser Ionization Time-of-Flight Mass-Spectrometry (MALDI-TOF MS), which is a method with high-throughput and automation potential. HPLC-MS and MALDI-TOF MS methodologies often use the PNGase F enzyme to release N-glycans from pre-isolated glycoproteins and biological samples [95]. These studies, however, are often limited to N-glycan analysis since there is not an enzyme that efficiently releases O-linked glycans.

1.7.2 Bottom Up Glycomics; "Glycan Node Analysis"

In addition to the top down glycomics techniques, a bottom up glycomics technique, referred to as "glycan node analysis", has proven effective at detecting multiple classes of glycans in whole biological specimens. Glycan node analysis allows a broad analysis of multiple types of glycans, such as N-linked, O-linked, and lipid linked glycans, as compared to top down glycomics methods that are often limited to N-glycoproteins. The glycan node analysis involves the chemical deconstruction of glycans from whole biospecimens into its monosaccharide constituents in such a way that monosaccharide identity, branching, and glycan linkages are captured as single analytical signals by GC-MS (**Figure 1.6**) [96]. This technique has been applied to whole blood plasma or serum from hundreds of patients with cancer, and it has been shown effective at generating

23

specific glycan nodes that distinguish cancer patient plasma from that of healthy matched controls [34, 35, 97]. Another advantage of using glycan node analysis over intact glycan analysis methods is that several glycan nodes can be used as molecular surrogates of glycosyltransferase activity [96]. One of the limitations of glycan node analysis, however, is that at least 100 µg of glycoprotein sample are needed for analysis. The first step in glycan node analysis is the permethylation procedure. Permethylation allows the release O-linked glycans, and it provides stability to glycans, as discussed below.

1.7.2.1 Solid Phase Permethylation

Permethylation is a technique commonly used for glycan sample preparation prior to MS analysis. Permethylation improves sensitivity in mass spectrometry, it facilitates determination of glycan composition, such as linkages, branching points, and monosaccharide identity. Permethylation provides stability to isolated glycan structures and increases volatility of glycans. Glycan node analysis uses the spin column permethylation procedure developed by Kang et al [98] and Goetz et al [99], and further adapted and modified by Borges et al [96, 100]. The use of a strong base, such as sodium hydroxide, and a polar aprotic organic solvent, such as dimethyl sulfoxide (DMSO), are employed in the permethylation reaction with iodomethane as the permethylating reagent. A direct reaction between iodomethane and glycans does not seem possible because no permethylated product is obtained after mixing these reagents [101]. The presence of a strong base, such as sodium hydroxide, is needed to deprotonate the hydroxyl groups on carbohydrates and generate alkoxyl groups because alkoxide is a more powerful nucleophilic agent than carbohydrate hydroxyl. A methylating reagent (iodomethane) in the presence of alkoxyl groups generates methyl esters by the nucleophilic attack of the hydroxyl ion (alkoxyl group) on the methylating reagent (**Figure 1.7**) [99]. Permethylation

is carried out in polar aprotic solvent, such as DMSO, to give more efficient permethylation. It has been shown that the permethylation reaction is faster in a polar solvent [102]. Additionally, DMSO dissolves carbohydrates, but it does not dissolve sodium hydroxide. Hence, solid sodium hydroxide beads are commonly used since these will collect the water produced during permethylation reaction. The process of using of solid sodium hydroxide beads for permethylation of glycans is commonly known as solid phase permethylation, and it commonly involves the use of spin columns packed with sodium hydroxide beads [103]. However, solid phase permethylation can be cumbersome and somewhat expensive because of its requirement for spin columns.

One of the functions of permethylation is to release O-glycans from proteins. The hydroxyl ions or permethylation base abstract a hydrogen from the α-carbon of either serine or threonine. This results in a double bond between the α-carbon and the β-carbon of serine or threonine. Formation of such doble bond results in cleavage of β-carbon of serine or threonine from the oxygen on the reducing end of the O-linked glycan. The cleavage generates an alkoxide that then reacts with iodomethane that ultimately results in permethylation of the free reducing end of the O-glycan (**Figure 1.7**) [99]. Although this study suggests that O-glycan release occurs more efficiently when proteins are denatured, the exact release efficiency of O-glycans by permethylation is not exactly known. However, when O-glycans (3-GalNAc, 3,6-GalNAc) are quantified by glycan node analysis, results are consistent enough to give acceptable % CV, as shown by Borges et,al [96, 100].

1.7.2.2 Hydrolysis, Reduction, and Acetylation

After permethylation, the next steps in glycan node analysis are hydrolysis, reduction, and acetylation, which were adapted from Heiss et al [104]. Hydrolysis is carried out with 2 M trifluoroacetic acid at 120 °C for two hours. During hydrolysis, partially methylated monosaccharides are generated, and all the N-linked and lipid-linked glycans are released (**Figure 1.7**). Evidence is provided in Borges et al [96] that the monosaccharides from N-glycans and lipid link glycans are released during hydrolysis. After hydrolysis, partially methylated monosaccharides are reduced to alditols with sodium borohydride. Reduction allows the capture of linear structures in order to avoid formation of isomers during GC-MS analysis. The last step in glycan node analysis is acetylation which forms a partially methylated alditol acetate (PMAA). In acetylation, all the hydroxyl groups that were formed during hydrolysis are acetylated, forming a unique pattern of methyl and acetyl groups that corresponds to the linkage pattern of a monosaccharide as it existed in the original glycan polymer (**Figure 1.7**) and providing the molecular basis for separation and quantification by GC-MS (**Figure 1.7).** Monosaccharides with charged groups like carboxyls, sulfates and even amines are not detected by this approach [96].

A)

B) Manα(1-6)-Man-Manα(1-3)
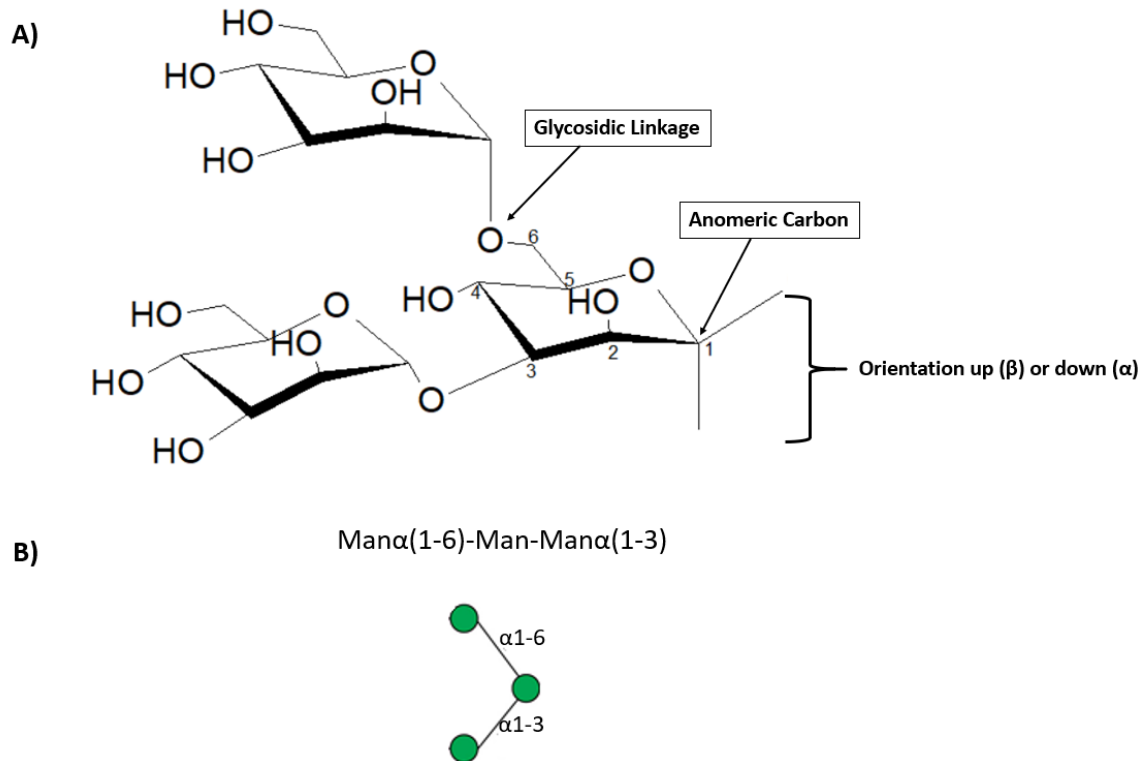
Figure 1.1. Representative structure of a 3-6-linked branched α-D-mannose trisaccharide. A) Chair monosaccharide mannose (Man) structures linked by glycosidic bonds forming a common core structure of N-linked glycans. B) Cartoon representation of glycan structure shown in A.
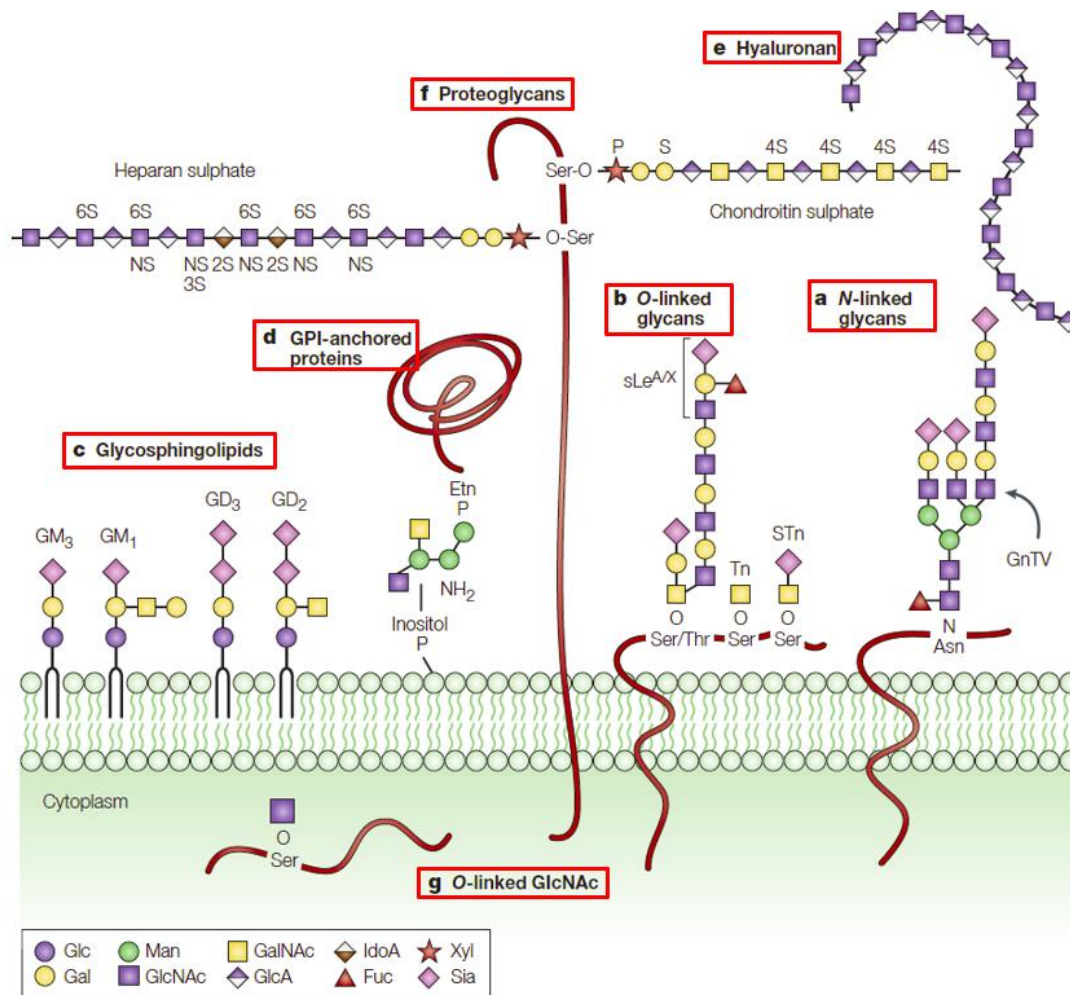
Figure 1.2 Common classes of glycans in mammalian cells. a) N-linked glycans on glycoproteins are covalently bound to Asn residues. **b)** O-linked glycans are found covalently linked to Ser or Thr residues on glycoproteins and mucins. **c)** Glycosphingolipids consist of the lipid ceramide linked to one or more sugars. **d)** Glycosylphosphatidylinositol (GPI)-linked proteins are anchored in the outer leaflet of the plasma membrane by a glycan covalently linked to phosphatidylinositol. Glycosaminoglycans can occur as free chains (hyaluronan; **e)** or as covalent complexes with proteoglycan core proteins (heparan sulphate, chondroitin sulphate and dermatan sulphate, a type of chondroitin-sulphate-containing iduronic acid (IdoA)). **f)** Proteoglycans participate in growthfactor activation and cell adhesion. **g)** Various cytoplasmic and nuclear proteins contain O-linked N-acetylglucosamine (O-GlcNAc). Some glycoconjugates can be tethered to the plasma membrane as depicted or secreted into the extracellular matrix. In some cases, hybrid molecules exist, containing more than one type of glycan. Sugars are represented by coloured geometric symbols. Glc, glucose; Gal, galactose; Man, mannose; GlcNAc, N-acetylglucosamine; GalNAc, N-acetylgalactosamine; GlcA, glucuronic acid; Fuc, fucose; Xyl, xylose; Sia, sialic acid. (This figure was adapted with permission from ref.[7]. Copyright 2005, Nature Publishing Group).
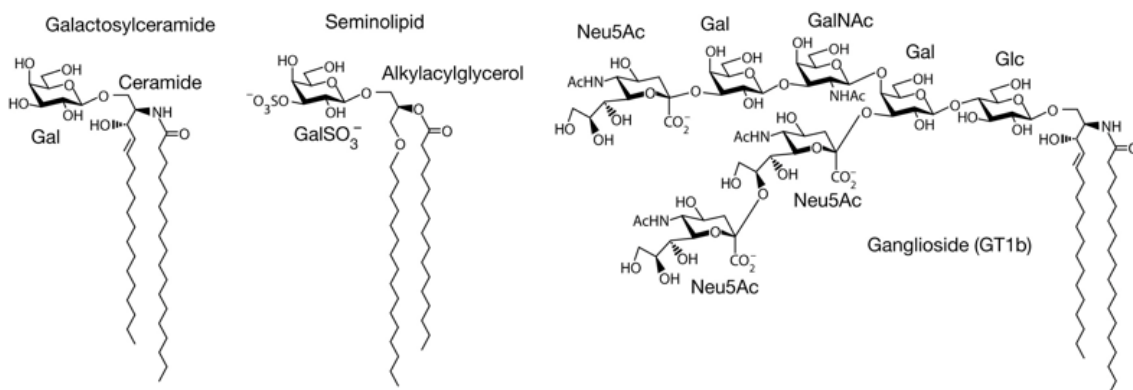
Figure 1.3. Structures of representative glycosphingolipids (GSLs) and glycoglycerolipids. GSLs, such as GalCer, are built on a ceramide lipid moiety that consists of a long-chain amino alcohol (sphingosine) in amide linkage to a fatty acid. In comparison, glycoglycerolipids, such as seminolipid, are built on a diacyl or acylalkylglycerol lipid moiety. Most animal glycolipids are GSLs, which have a large and diverse family of glycans attached to ceramide. Shown is one example of a complex sialylated GSL, GT1b (IV^{3}Neu5AcII^3[Neu5Ac]$_2$Gg$_4$Cer). (This figure was adapted with permission from ref.[11]. Copyright 2015-2017 by The Consortium of Glycobiology Editors, La Jolla, California).
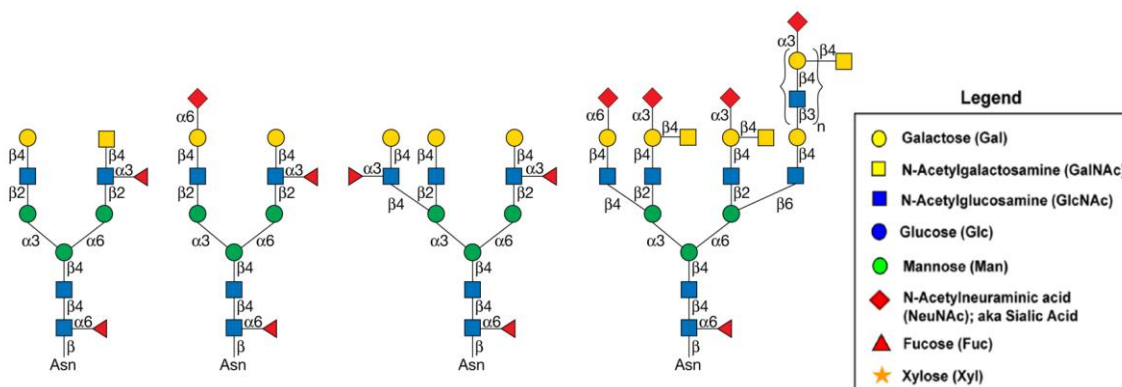
Figure 1.4. Typical complex N-glycans found on mature glycoproteins. A LacNAc unit (bracketed) on any branch may be repeated many times. (This figure was adapted with permission from ref.[6]. Copyright 2015-2017 by The Consortium of Glycobiology Editors, La Jolla, California).
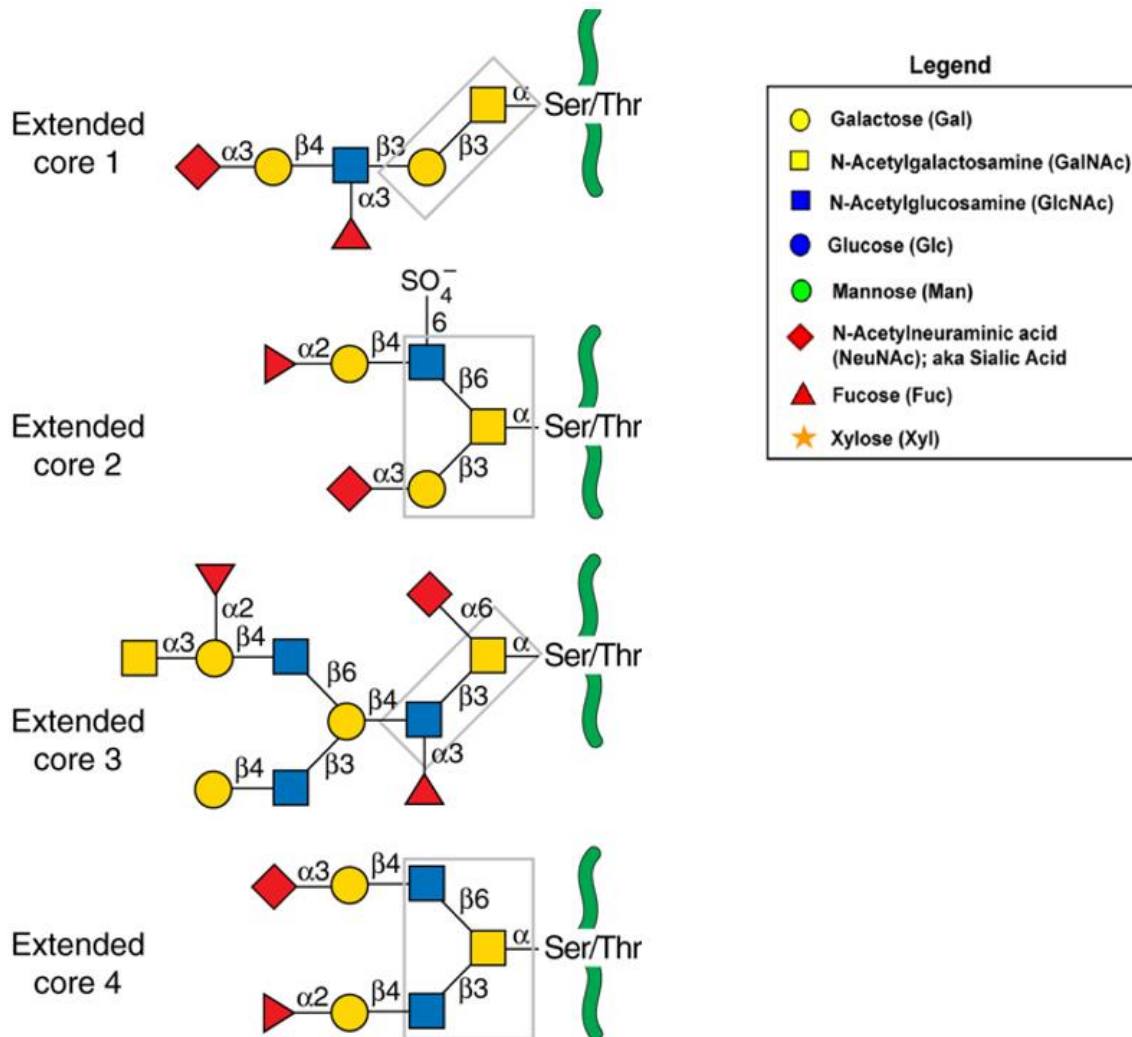
Figure 1.5. Common core O-linked glycans. Attached to the mucin are complex O-GalNAc glycans with different cores identified by gray boxes. Extended core 1, 2, 3, or 4 O-GalNAc glycans are from human respiratory mucins and the extended core 3 O-GalNAc glycan is from human colonic mucins. All four core structures (in boxes) may be extended, branched, and terminated with Fuc, Sia, or blood group antigenic determinants. Core 1 and 3 O-GalNAc glycans may also carry α2-6 Sia linked to the core GalNAc. Green lines are protein. (This figure was adapted with permission from ref.[19]. Copyright 2015-2017 by The Consortium of Glycobiology Editors, La Jolla, California).
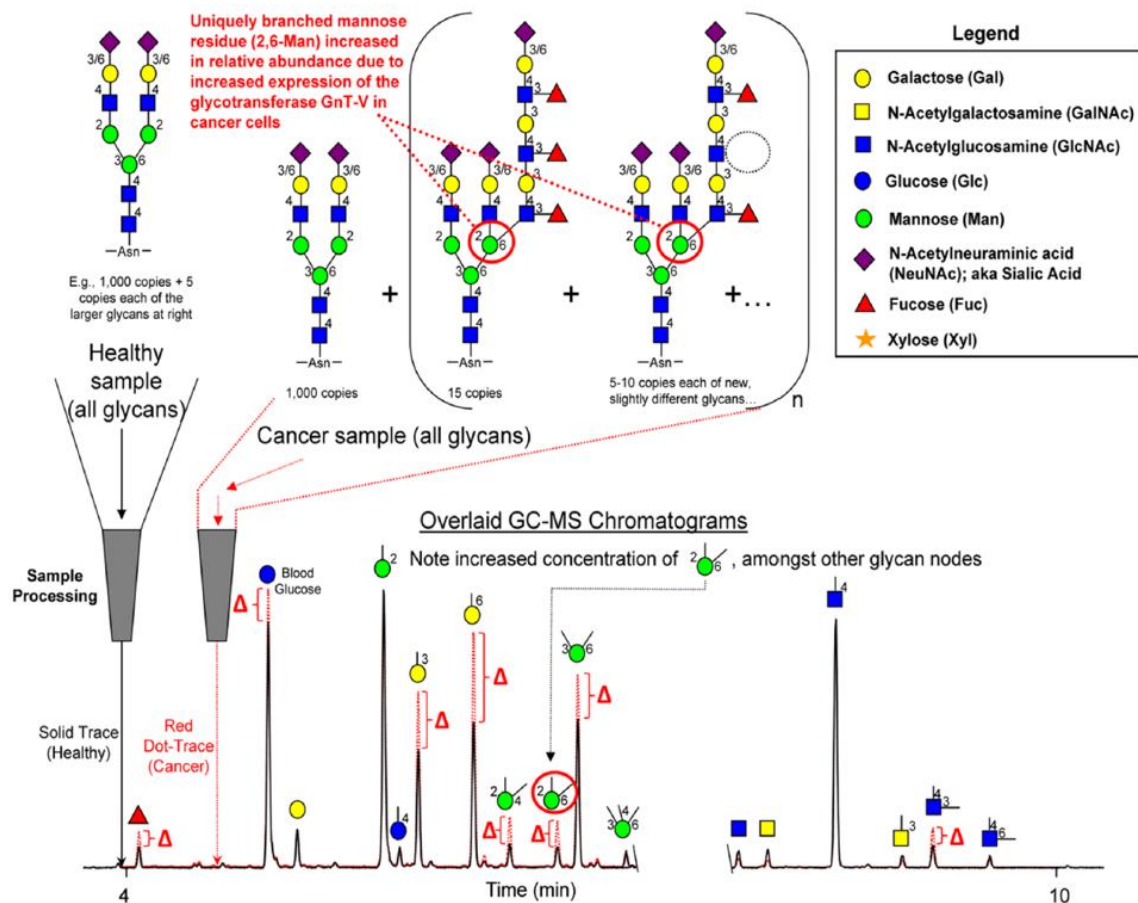
Figure 1.6. Conceptual overview of the glycan "node" analysis concept. The procedure consists of applying glycan linkage (methylation) analysis to intact glycoproteins, whole biofluids or, in this case, unpurified cell culture supernatant. Intact normal and abnormal glycans including O-glycans, N-glycans, and glycolipids are processed and transformed into partially methylated alditol acetates (PMAAs), each of which corresponds to a particular monosaccharide-and-linkage-specific glycan "node" in the original polymer. As illustrated, analytically pooling together the glycan nodes from among all the aberrant intact glycan structures provides a more direct surrogate measurement of abnormal glycosyltransferase activity than any individual intact glycan while simultaneously converting unique glycan features such as "core fucosylation," "α2-6 sialylation," "bisecting GlcNAc," and "β-1-6 branching" into single analytical signals. Actual extracted ion chromatograms from 9 µl blood plasma samples are shown. Numbers adjacent to monosaccharide residues in glycan structures indicate the position at which the higher residue is linked to the lower residue. (This figure was adapted with permission from ref.[96]. Copyright 2013 American Chemical Society).

31
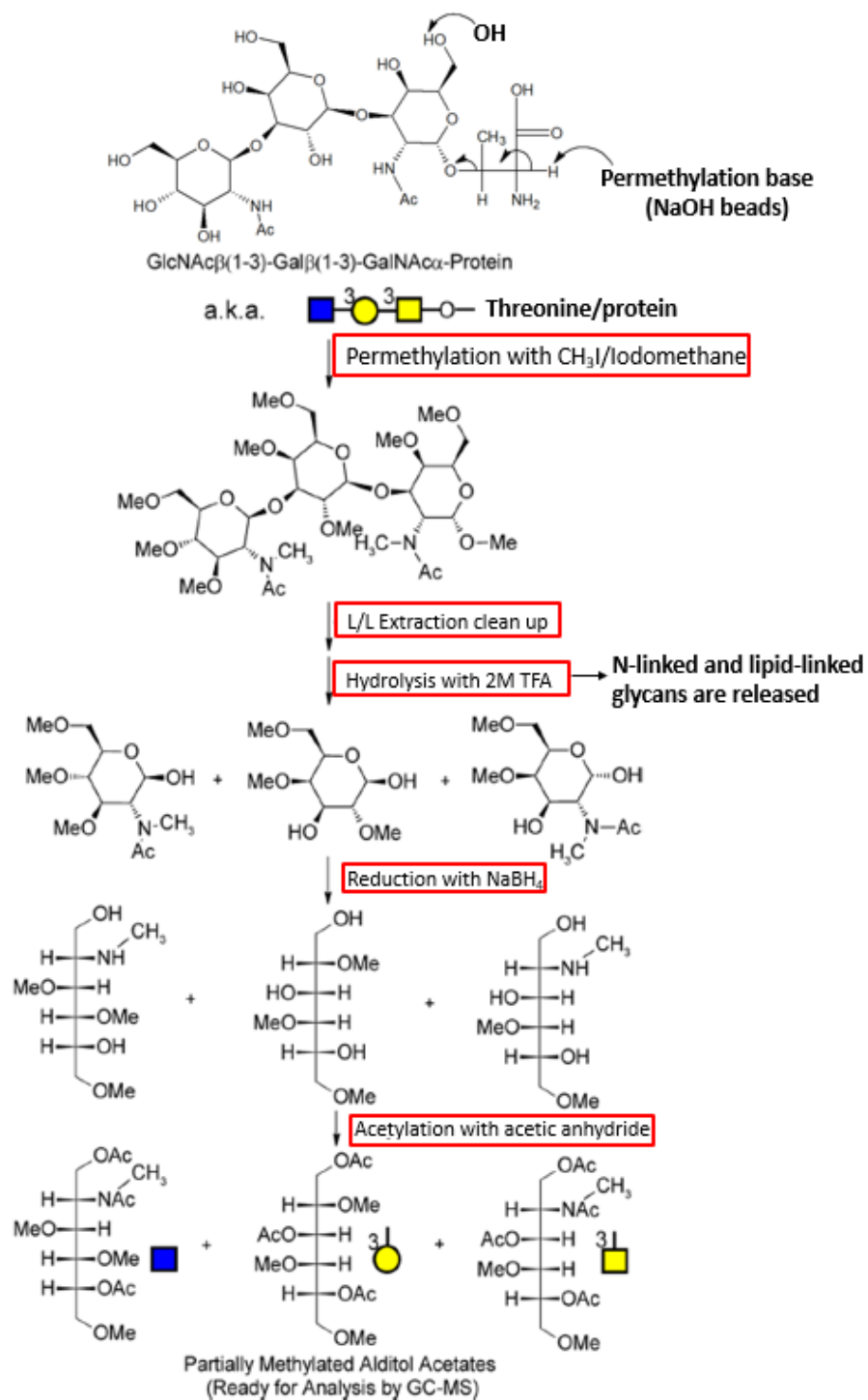
Figure 1.7. Molecular overview of the glycan "node" analysis procedure. O-linked glycans are released during permethylation, while N-linked glycans and glycolipids are released during acid hydrolysis. The unique pattern of stereochemistry, methylation and acetylation in the final partially methylated alditol acetates (PMAAs) corresponds to the unique glycan "node" in the original glycan polymer and provides the molecular basis for separation and quantification by GC-MS. (Figure adapted with permission from ref.[96]. Copyright 2013 American Chemical Society).

CHAPTER 2

GLYCOSYLATION CONSISTENCY PROFILING IN CELL CULTURE SUPERNATANT

AND ANTIBODIES USING GLYCAN NODE ANALYSIS AND GC-MS

2.1 Introduction

Glycosylation is a common posttranslational modification of mammalian proteins. About 50% of all mammalian proteins are glycosylated [4]. Glycoproteins can be secreted by cells or found in cell membranes, and their glycans play pivotal roles in cell recognition [4], immune evasion [71], and cell signaling [31]. There are over 200 known human glycosyltransferase genes that encode for glycosyltransferase enzymes, each of which assembles glycans in a strict donor, acceptor, and linkage-specific manner [13].

Aberrant glycosylation is common in cancer. Glycosylation changes that occur in this disease are known to help facilitate tumor metastasis [92]. In the antibody therapeutic industry, changes in glycosylation can severely impact antibody stability and biological function [105]. In both cases, cell culture systems are employed to either study glycosylation in cancer cell lines or to produce antibodies with consistent glycosylation so that their pharmacodynamics and pharmacokinetics will remain constant. In most cases, altered expression of glycosyltransferases serves as the immediate upstream cause of structural changes in glycosylation [105].

While abnormal glycosylation within cancer cells has been extensively studied [40, 54, 106], relatively little is known about the mechanisms leading to aberrant glycosylation of the numerous highly abundant blood plasma proteins in cancer, the vast majority of

which are secreted by either the liver or B-cells/plasma cells (i.e., IgG) and are the major analytical target of serum glycomics studies [107].

Additionally, structural characterization of therapeutic antibody glycans is required under regulatory guidelines because changes in antibody glycosylation tend to be the major source of batch to batch variability during their production [108]. It is thus important to track therapeutic antibody glycosylation changes to ensure batch to batch consistency and the proper function of the antibody.

Glycans are complex sugar polymers containing a variety of different monosaccharides, α-linkages or β-linkages, linear and branched forms, and sometimes repeating units, all of which add high heterogeneity to the glycan structure and makes the analysis of glycans a difficult task [5]. New methods that expedite the quantification of unique glycan features and that can point directly to dysregulated glycosyltransferases in cell culture supernatant would help facilitate a better understanding of the mechanisms regulating the glycan structures of secreted glycoproteins. Additionally, new methods for the direct quantification of specific glycan features in antibodies could help facilitate improved batch to batch glycosylation consistency profiling.

Glycan methylation analysis (a.k.a., glycan linkage analysis) that takes place via generation of partially methylated alditol acetates (PMAAs) and subsequent analysis by GC-MS has been widely used in the past to systematically deconstruct pre-isolated glycans in order to obtain linkage and branching information [98, 109–111]. Over the past few years this approach has been adapted to the analysis of whole biofluids and employed it as a biomarker development tool in blood plasma/serum [34, 35, 96, 97, 100, 112]. In

34

short, the technique involves the simultaneous chemical deconstruction of N-, O-, and lipid linked glycans in a manner that both conserves and facilitates relative quantification of uniquely linked monosaccharides (glycan nodes). In doing so, the approach captures unique glycan features, such as "core fucosylation", "α2-6-sialylation", "β1-6-branching", "β1-4-branching", and "bisecting GlcNAc", as single analytical signals, some of which serve as 1:1 molecular surrogates of glycosyltransferase activity [96] (**Figures 1.6 & 1.7**). As such, application of this approach to profiling the glycosylation of proteins produced by cultured cells should provide a direct means of tracking specific glycan features that reflect important changes in cellular biology and impact the function of secreted glycoproteins and antibodies.

A detailed methodology for the adaptation of this approach to the analysis of glycoproteins in cell culture supernatants and to antibody glycosylation profiling is reported. Analysis of glycan nodes in cell culture supernatant is reproducible and consistent on a day-to-day basis. As an example for the application of the assay, the effect of IL-6 and IL-1β cytokines on secreted hepatocyte glycoprotein glycan node profiles is demonstrated using HepG2 cells as target cells. Specific tumor antigens such as β1-6-branching,β1-4-branching, antennary fucosylation, bisecting GlcNAc, and the Tn antigen (GalNAc-Ser/Thr) were found to be regulated by IL-6.Terminal galactosylation was found to be regulated specifically IL-1β. Additionally, neuraminidase enzyme treatment of alpha-1 antitrypsin IgG demonstrates how the method can be used to detect relative changes in "α2-6-sialylation" along with corresponding increases in terminal galactose.

2.2 Experimental Procedures

2.2.1 Materials

HepG2 cells (Cat. No. HB-8065) and Eagle's Minimum Essential Medium (EMEM) (Cat. No. 30-2003) were purchased from ATCC. Fetal bovine serum (FBS) (Cat. No. FB-11) was purchased from Omega Scientific. Sterile 1X PBS pH 7.4 1L (Cat. No. 101642-262) and trypsin 0.25 % 1X (Cat. No. 16777-166) were purchased from VWR. Alpha-1-antitrypsin antibody (Cat. No. A0012) was purchased from Dako. Neuraminidase (Sialidase) from Clostridium perfringens (Cat. No. 11585886001, pkg of 5 U), which cleaves terminal sialic acids that are α2,3-, α2,6-, or α2,8-linked to Gal, GlcNAc, GalNAc, AcNeu, GlcNeu, in oligosaccharides, glycolipids, N- or O-linked glycoproteins, was purchased from SIGMA. Amicon Ultra - 4 3K MWCO centrifugal spin filters (Cat. No. UFC800324) were purchased from Fisher Scientific. Spin columns (0.9 ml) with plugs and polyethylene frits (Cat. No. 69705) was purchased from Thermo Fisher Scientific. HEPES (Cat. No. H3375-250G), DMSO (Cat. No. D8418-1L), sodium hydroxide beads (Cat. No. 367176-2.5KG), acetonitrile (Cat. No. 539996-1KG), iodomethane (Cat. No. I8507-500G), chloroform (Cat. No. 650498-4L), sodium chloride (Cat. No. S7653-1KG), sodium phosphate dibasic (Cat. No. S7907-500G), sodium phosphate monobasic (Cat. No. S8282-500G), trifluoroacetic acid (TFA) (Cat. No. 299537-500G), ammonium hydroxide (Cat. No. 320145-50ML), glacial acetic acid (Cat. No. 27225-1L-R), and acetic anhydride (Cat. No. 539996-1KG), were purchased from SIGMA. Sodium borohydride (Cat. No. 71321-100G) was purchased from Fluka). Methanol (Cat. No. A452SK-4) and dichloromethane (Cat. No. D143SK-4) were purchased from Fisher Chemical. GC-MS autosampler vials (Cat. No. 03-377K) were purchased from VWR. Teflon-lined pierceable caps, 9mm (Cat. No. C500-51G) were purchased from Thermo Fisher Scientific. GC consumables were purchased from Agilent (Santa Clara, Ca), and MS consumables were acquired from Waters (Milford, MA).

2.2.2 Cell Culture and Cell Supernatant Processing

HepG2 cells were grown in T75 flasks at 37^0C in 5% CO_2 under semi-confluent conditions for 3 days in 10% FBS-supplemented EMEM media. FBS-containing media was removed, and cells were washed 3 times with sterile 1X PBS, and once with serum-free EMEM media. Cells were incubated with 3 ml of serum free EMEM medium for 48 hours. Media was collected and changed every 24 hours. Media was collected over the last 24 hours, and it was centrifuged at 1000 g for 5 min to pellet any cell debris, and supernatant was concentrated by spin filtration. Three ml of cell culture media were placed into a 4-ml Amicon 3K centrifugal spin filter and centrifuged in a swing bucket rotor at 2950 x g for 30 minutes at room temperature. Final volume was about 500 µl. Media was resuspended in 3 ml of 10X HBS buffer and centrifuged again at 2950 x g for 30 minutes. Two more washes were performed with 10X HBS buffer, with the third wash centrifuged for 50 minutes, yielding a final volume of approximately 100 µl.

2.2.3 Induction Experiments with Cytokines IL-6 and IL-1β

For induction experiments with cytokines, the Mackievicz protocol was adapted [40]. Briefly, HepG2 cells were grown for 3 days in FBS medium. After 3 days, FBS medium was removed, and cells were washed 3X with sterile 1X PBS and once with serum free medium to remove any FBS related proteins. Then cells were incubated with 3 ml of serum free medium and 50 ng/ml of cytokine (IL-6 or IL-1β) with replacement of medium and cytokine every 24 hours for a maximum period of 48 hours. Serum free medium was collected over the last 24 hours, centrifuged at 1000 g for 5 min, and supernatant was concentrated 30-fold using a 4-ml Amicon 3K centrifugal spin filter (MW Cutoff 3 kD), as described above. Three technical replicates per biological replicate (12 µl each) were made for glycan node analysis.

2.2.4 Antibody Preparation

Pre-purified alpha-1 antitrypsin antibody (IgG) was concentrated to 10 mg/ml, and 10 µl (100 µg) were aliquoted for glycan node analysis. For the desialylation of alpha-1 antitrypsin antibody, intentionally low amounts of neuraminidase enzyme were used to induce only partial desialylation of IgG; To 1.7 µl of antibody (100 µg), 2 µl of a 0.1 M sodium acetate buffer pH 5 and 1 µl of neuraminidase enzyme (0.1 milliunits) were added. The final pH of the sample was checked to be around 5 using Hydrion pH papers. Samples were incubated for 4 hours at 37 °C. After incubation, final pH was brought back to 7 with 1 µl of a 0.5 M sodium bicarbonate solution. Then, final volume was brought to 10 µl with water and glycan node analysis was performed.

2.2.5 Glycan Node Analysis

Permethylation of concentrated cell culture medium and IgG: Twelve µl of whole concentrated cell medium or 10 µl of antibody were added to a 1.5 ml polypropylene test tube. To this, 270 µl of dimethylsulfoxide (DMSO) and 105 µl of iodomethane were added. This solution was mixed and added it to a plugged 1 ml spin column containing sodium hydroxide beads, previously preconditioned with 400 µl of acetonitrile and two rinses with 400 µl of DMSO. Samples were mixed gently with the sodium hydroxide beads 3 to 4 times for 10 minutes using the tip of a 200 µl pipette tip. Then, columns were unplugged and centrifuged them at 10,000 g for 15 sec to collect sample, leaving any NaOH residues behind. Immediately after, 300 µl of acetonitrile were added to the columns to wash off any sample left on the column. Samples and acetonitrile wash were transferred to a silanized glass tube containing 3.5 ml of 0.2 M sodium phosphate buffer, pH7 containing 0.5 M NaCl. To this, 1.2 ml of chloroform were added. L/L extractions were performed 3

times with the sodium phosphate buffer, saving the chloroform layer every time. Then, the chloroform was dried under a nitrogen stream in a heating block set at 74 ^{0}C.

Hydrolysis and reduction of permethylated glycans: A 2 M TFA solution was prepared. Then, 325 µl of the 2 M TFA solution were added to each sample, and tightly capped them to prevent evaporation. Then samples were heated at 120 ^{0}C for 2 hours. TFA was removed by drying sample under nitrogen stream in a heating block set at 74 ^{0}C. For the reduction of monosaccharides, 475 µl of 10 mg/ml sodium borohydride in 1 M ammonium hydroxide were added to each tube and allowed it to react for 1 hour. Then, 63 µl of methanol were added to each sample to remove any residual borate, followed by 125 µl of 9:1 methanol: acetic acid. Each time, samples were dried under nitrogen in a heating block set at 74 ^{0}C. To complete the drying process, the samples were placed in a vacuum chamber (e.g., vacuum desiccator) at room temperature for at least 20 minutes.

Acetylation: After drying, 18 µl of DI water were added to each sample, and mixed residues until they were completely dissolved. Then, 250 µl of acetic anhydride were added to each tube, mixed thoroughly, and sonicated in a water batch for 2 minutes. Samples were incubated at 60° C for 10 minutes, followed by addition of 230 µl of TFA, and incubating again at 60°C for 10 minutes. Then, 1.8 ml of dichloromethane and 2 ml of DI water were added to each sample. L/L extraction was performed twice with water, removing the top layer (containing water) and saving the dichloromethane layer (bottom layer) every time. The dichloromethane layer was placed into silanized autosampler vials and dried samples under nitrogen in a heating block at 60 ^{0}C. Samples were reconstituted with 50 µl of acetone, and placed onto the GC-MS autosampler rack.

Gas Chromatography-Mass Spectrometry (GC-MS): A gas chromatograph coupled to a time-of-flight (TOF) mass spectrometer was used here. One microliter of each sample was injected in split mode (1:10) onto a silanized glass liner containing a small plug of silanized glass wool held at a temperature of 280 ^{0}C. Using helium as the carrier gas, samples were transferred onto the GC column, which is maintained at an initial temperature of 165°C for 0.5 min, followed by ramping the temperature at 10 ^{o}C per minute to 265°C then immediately ramping at 30°C per minute to 325°C and holding for 3 min. Samples eluting from the column were transferred to the mass spectrometer at a transfer line temperature of 250 ^{o}C. They were then subjected to electron ionization at 70 eV and 250 ^{o}C, and analyzed from *m/z* 40-800 by TOF-MS in which transients were summed and recorded every 0.2 s.

Data Analysis: Identification of each glycan node was made by comparing retention times with those from known partially methylated alditol acetates (PMAAs)-e.g., such as those obtained by Borges et al [96]., and mass spectra were verified through comparison with the mass spectral library of PMAAs at the University of Georgia's Complex Carbohydrate Research Center website (https://www.ccrc.uga.edu/databases/index.php#). Each glycan node was quantified by the sum of the integrals of a specific set of extracted ion chromatogram peaks using QuanLynx software. Integrated peaks were exported to an Excel spreadsheet to normalize the area of each glycan node by dividing each individual hexose glycan node by the sum of all hexoses, and each individual HexNAc glycan node by the sum of all HexNAcs.

2.2.6 Western Blotting

Cells were washed twice with cold sterile 1X PBS and incubated with lysis buffer (500 mM TRIS-HCl, 150 mM NaCl, 1% NP-40, 0.1% sodium azide, 2 mM Na_3VO_4, 1 mM NaF, and a 1X protease inhibitor mixture) for 10 minutes. Protein concentrations were determined using bicinchonic acid (BCA) assay with BSA as a standard. To 15 µg of protein were added 2 µl 4X gel loading buffer (1M Tris-HCl, 10% SDS, glycerol) and 2 µl of 2% 2-mercaptoethanol. Protein samples were boiled at 95 °C for 10 minutes, loaded into a 4-20% denaturing gel, and run at 180 V for 45 minutes. Proteins were transferred to a nitrocellulose membrane for 1 hour and 15 minutes at 20 V. The blotted membrane was blocked with 5% milk in 1X PBST for one hour, followed by overnight incubation with 1 µg/ml GnT-V antibody. The next day, blotted membrane was washed 3 times with 1X PBST and incubated with secondary antibody for one hour. The membrane was washed 4 times, and bands were detected by chemiluminescence.

2.3 Results

2.3.1 Optimization of Concentration Factor and Chromatographic Background in Cell Media

Secreted glycoproteins tend to be too diluted in cell culture media (at least from HepG2 cells) to provide adequately strong GC-MS based extracted ion chromatogram (XIC) peak intensities. Thus, semi-confluent HepG2 cells were incubated with only 3 ml of serum free media for 48 hours, which is enough to cover the cells in T75 flasks. Reducing the amount of media does not affect cell viability, and the cells sustain well for up to 72 hours. However, even at a protein concentration of about 200 µg/ml glycan nodes could still not be detected upon analysis by GC-MS (data not shown). Thus, whole culture media needed to be concentrated about 30-fold to reach good signal to noise ratios for each of the glycan nodes. To reach this high concentration factor, evaporative concentration and spin

filtration methods were used. These two methods are well-accepted and commonly used for concentrating protein solutions [113].

For evaporative concentration, HepG2 cell culture media was concentrated 30-fold using a SpeedVac Concentrator at 50 °C, pressure 3 mbar. However, the major disadvantage of using evaporative concentration was the formation of a precipitate during the process and high chromatographic background in blank media for three of the glycan nodes of interest, such as 2-Man, 2,6-Man, and 3,4-Gal nodes (data not shown). The signals in the blank media that interfere with the signal of interest appear to have the same ionization spectra and retention times as the glycan nodes of interest, and they appear to be much higher in blank media likely because components in the media are being consumed by the cells. Selecting for ions specific for the glycan nodes of interest did not solve this problem since those same ions are found in blank media as well. Even though the media supposedly does not contain any glycans, some its components appear to have the exact same electron ionization patterns and retention times as these three glycan nodes. Additionally, aiming for a high concentration factor leads to the formation of a precipitate, and this is less than ideal for the analysis of glycans. Because this method concentrates entire protein samples, precipitate likely occurs due to the presence of salts and other components in the media that decrease protein solubility and lead to the formation of protein aggregates [114]. Such protein aggregates can be broken down and resuspended thoroughly and used for glycan node analysis by GC-MS. However, resuspending a precipitate is time consuming. Therefore, due to these challenges, concentrating whole culture media by evaporative concentration methods was deemed unsuitable for the analysis of glycan nodes.

On the other hand, concentrating culture media by spin filtration helps solve the problems associated with evaporative concentration. Three milliliters of culture media and blank media were concentrated 30-fold using Amicon spin filter devices with a molecular weight cutoff of 3 kDa. About 10 mg of albumin (a non-glycosylated protein) were added to the blank media to provide a retentate since about three washes with HEPES buffer were performed to help remove low molecular weight components in the media. A cleaner chromatographic background was obtained, and no precipitate was formed using this approach (**Figure 2.1**). Because during spin filtration protein samples are concentrated by separating small molecules from large molecules, low molecular weight components in the media that were forming the precipitate and interfering with the signal of interest were removed. The disadvantage of using spin filtration for glycan node analysis is that some glycolipids maybe lost during the process. Nevertheless, this approach seemed to work better at removing high chromatographic background in blank media (**Figure 2.1**) and at preventing the formation of a precipitate.

2.3.2 Validation of Analytical Precision for Glycan Nodes observed in Cell Culture Supernatant using Spin Filtration

Concentrating the cell culture media by spin filtration gave XIC peaks with the highest signal-to-noise ratio and low overall chromatographic background. Intraday and interday precision of glycan node analysis was validated using this approach. HepG2 cells were seeded in 20 T75 flasks, and they were grown for 3 days in FBS medium and with serum free medium for 48 hours. Serum free medium was collected from across all flasks, centrifuged at 1000 g for 5 minutes, and supernatant was stored in a single container (bulk sample) at -80 °C. Serum free medium was concentrated 30-fold by spin filtration and analyzed by glycan methylation analysis on three different days (6 technical replicates per

day from the same bulk sample). The area of each chromatographic peak was integrated using MassLynx software, each glycan node was normalized, and the percent coefficient of variation (% CV) was calculated per day for each set of samples and on all three days. Variation per day and on all three days was low (**see Table 2.1**). Results show the assay is consistent and reproducible on three different days.

2.3.3 Changes in Glycan Nodes upon Cytokine Induction

Inflammatory cytokines, such as IL-6 and IL-1 beta, are known to regulate the expression of specific glycotransferases involved in the synthesis of tumor specific antigens in gastric cancer cells [53], hepatocellular carcinoma cells [54], and pancreatic cancer cells [55]. With this background in mind, we sook to understand how inflammatory cytokines, such as IL-6 and IL-1beta, regulate the way HepG2 cells glycosylate their secreted glycoproteins. HepG2 cells were induced with 50 ng/ml of cytokine (IL-6 or IL-1 beta) for 72 hours with replacement of media every 24 hours. Induction experiments were conducted with each cytokine individually. After IL-6 treatment, the relative abundance of 2,4-Man and 2,6-Man glycan nodes increased significantly, while the relative abundance of 2-Man decreased significantly (**Figure 2.2A & B)**. 2,4-Man and 2,6-Man represent β1,4- and β1,6-branching, respectively. Increased β1,6-branching and β1,4-branching correspond to upregulation of GnT-V and GnT-IV glycotransferases, respectively [13]. Therefore, increased abundance of 2,4-Man and 2,6-Man nodes are indicative of increased branching on N-glycans, and this explains the reduction in 2-Man node (**Figure 2.2A & B**). 2,6-Man is a molecular surrogate of GnT-V activity, hence, increased abundance of 2,6-Man node was likely due to the upregulation of GnT-V by IL-6. To confirm this, a Western blot was performed to check for the expression levels of GnT-V enzyme in HepG2 cells stimulated with IL-6. As expected, IL-6 upregulates the expression

levels of GnT-V in HepG2 cells, which causes increased β1,6-branching in glycoproteins secreted by HepG2 cells (**Figure 2.2C & D**). Additionally, the relative abundance of t-Gal and 3,4-GlcNAc nodes increased significantly, while the relative abundance of 3-Gal, 3,4,6-Man, 4-GlcNAc, 3-GalNAc, and 3,6-GalNAc nodes decreased significantly upon IL-6 treatment (discoveries were made using multiple t-tests with the Holm–Sidak method for multiple comparisons correction, and a two tailed t-test for Western blot data), see **Figure 2.2**.

It was observed that the 3,4-GlcNAc node increased significantly in IL-6 treated cells (**Figure 2.3B**). The 3,4-GlcNAc node represents antennary fucosylation. This glycan node forms when fucose gets attached to an N-glycan arm/antenna at GlcNAc that would have only been 4-linked. The increase expression of glycosyltransferases GnT-V and GnT-IV create a greater opportunity for antennary fucosylation to occur because GnT-V and GnT-IV enzymes add a GlcNAc residue in a β1,6-linkage or β1,4-linkage to a mannose of an N-glycan. This then creates a greater opportunity for the action of other glycosyltransferases, such as fucosyltransferases, to attach a fucose to the new GlcNAc on the N-glycan antenna (**See Figures 1.6, 2.2 & 2.3B**). Additionally, a concomitant significant decrease in 4-GlcNAc confirms increased antennary fucosylation (See **Figure 2.3B**).

When HepG2 cells were stimulated with IL-1beta, the relative abundance of t-Gal increased significantly, while the relative abundance of 2-Man decreased (discoveries were made using the Two-stage linear set up procedure of Benjamini, Krieger and Yekutieli, with Q = 1 %) (**Figure 2.3C & D**). Changes in 2,4-Man and 2,6-Man were observed, and although such changes were not significant, together may explain the

reduction in 2-Man node that causes it to be significant (**Figure 2.3C & D**). We performed a Western blot to verify expression of GnT-V enzyme upon cytokine treatment, and although the expression levels of GnT-V appear to go up, such changes were not significant (data not shown).

2.3.4 Application of Glycan Node Analysis to study Antibody Glycosylation

Changes in glycosylation in therapeutic antibodies can severely impact their pharmacokinetics and pharmacodynamics [105]. Hence, it is extremely important to quantify antibody glycosylation and ensure batch-to-batch reproducibility. Here we show the applicability of the glycan node analysis procedure in quantifying specific IgG antibody glycan features, such as sialylation, and how these can be impacted by low amounts of neuraminidase activity. The pre-isolated rabbit alpha-1 antitrypsin antibody (IgG) was treated with 0.1 milliunits of neuraminidase enzyme, and glycan node analysis was performed on the desialylated samples. Results revealed a statistically significant increase in terminal galactose, and a significant decrease in 3-linked galactose and 6-linked galactose, indicating an overall decrease in terminal neuraminic acid. There were no significant changes for the other glycan nodes (**Figure 2.4A & B**). These results showed how such subtle changes in neuraminidase activity can be captured using glycan node analysis.

2.4 Discussion

Abnormal glycosylation in cancer appears to be under the influence of cytokines [115]. Inflammatory cytokines such IL-6 and IL-1β have been known to regulate specific glycan features of acute phase proteins [45]. However, detail structural changes in glycan structures on glycoproteins induced by cytokines have not been provided. Here we described a bottom-up glycomics approach (glycan node analysis) to quantify specific

glycan features in cell HepG2 cell culture supernatant. Increased production of N-glycan branching (2,6-Man and 2,4-Man nodes) was found to be regulated by IL-6 using glycan node analysis. Previous reports have suggested that bisecting GlcNAc and branching are two N-glycan modifications that are inversely correlated [106]. For example, increased branching on N-glycans results in decreased modifications with bisecting GlcNAc, or increased expression of GnT-V or GnT-IV enzymes result in suppression of GnT-III enzyme [106]. Our glycan node analysis results confirmed these observations since the relative abundance of 3,4,6-Man or bisecting GlcNAc decreased significantly as increased branching (β1,6- branching and β1,4- branching) occurred simultaneously upon IL-6 treatment (**Figure 2.3A**).

3-GalNAc and 3,6-GalNAc nodes are the common core structure in O-glycans, and these two glycan nodes were downregulated by IL-6 and IL-1β, as suggested by our glycan node analysis (**Figure 2.3B**). In cancer cells, O-glycosylation appears to be truncated, and this results in the Tn antigen (GalNAc-Ser/Thr), which is a common tumor antigen [28]. The enzymes responsible for O-glycosylation are varied, and hence it is difficult to track the enzyme that is being upregulated or downregulated. The mechanisms that lead to truncation in O-glycosylation are not well understood. With our glycan node analysis, we were able to unravel a novel role of IL-6 and IL-1β in regulating truncation in O-glycosylation, a process commonly seen in cancer [33].

Additionally, a common glycan alteration of hepatocellular carcinoma tissues is antennary fucosylation [116]. Here we found that IL-6 regulates antennary fucosylation in the secreted glycome of hepatocellular carcinoma cells (HepG2 cells). Increased antennary fucosylation is also present in blood plasma glycoproteins of hepatocellular

carcinoma patients [117]. Our glycan node analysis approach allowed us to show how inflammatory cytokines, such IL-6, can cause alterations in antennary fucosylation of glycoproteins secreted by hepatocellular carcinoma cells.

Aberrant glycosylation in cancer seems to be under the influence of internal and external environmental factors [115]. New methods that allow the quantification of glycan structure in cell culture supernatant are required to understand the mechanisms regulating the glycan structures of secreted glycoproteins. Numerous studies have focused on understanding the mechanisms regulating abnormal glycosylation in cancer cells using intact glycan analysis and genetic analysis [29]. For example, using intact glycan analysis, Klasic et al. identified DNA hypomethylation as a possible mechanism for regulating abnormal glycosylation of blood plasma glycoproteins in HepG2 cells [106], in which the MGAT3 gene was suggested to be responsible for glycan changes. MGAT3 or GnT-III regulates bisecting GlcNAc in N-glycans [118]. Our glycan node analysis method allowed us to identify detail structural changes upon cytokine stimulation and specific tumor antigens such as increased N-glycan branching, bisecting GlcNAc, and truncation in O-glycosylation were identified as single analytical signals.

Additionally, the glycan node analysis procedure allowed us to quantify subtle changes in IgG sialylation upon neuraminidase treatment. Therefore, the glycan node analysis procedure has the potential to be used in the therapeutic industry as a tool to quantify glycosylation changes in antibodies. The advantage of this method over others is that specific antibody glycan features, such as mannosylation, terminal galactosylation, terminal GlcNAc, α2,3-sialylation, and α2,6-sialylation, can be quantified as single analytical signals.

2.5 Conclusion

A glycan linkage analysis procedure that uses GC-MS (glycan "node" analysis) was applied for the first time to cell culture supernatant and IgG antibodies to quantify linkage-related glycan features. Glycan "node" analysis is the process by which pooled glycans within complex biological samples are chemically deconstructed in way that facilitates the analytical quantification of uniquely linked monosaccharide units (glycan "nodes"). It is based on glycan methylation analysis (a.k.a. linkage analysis) that has historically been applied to pre-isolated glycans. Thus, when using glycan node analysis, unique glycan features within whole biospecimens such as "core fucosylation", "α2-6-sialylation", "β1-6-branching", "β1-4-branching", and "bisecting GlcNAc", are captured as single analytical signals by GC-MS. Here we have described the use of this methodology in cell culture supernatant for studies of the mechanisms regulating glycan structure of blood plasma proteins, and in the analysis of IgG glycans. The effect of IL-6 and IL-1β cytokines on secreted hepatocyte protein glycan features was demonstrated; likewise, the impact of neuraminidase treatment of IgG was illustrated. For the majority of glycan nodes, the assay is consistent and reproducible on a day-to-day basis; because of this, relatively subtle shifts in the relative abundance of glycan features could be captured using this approach.
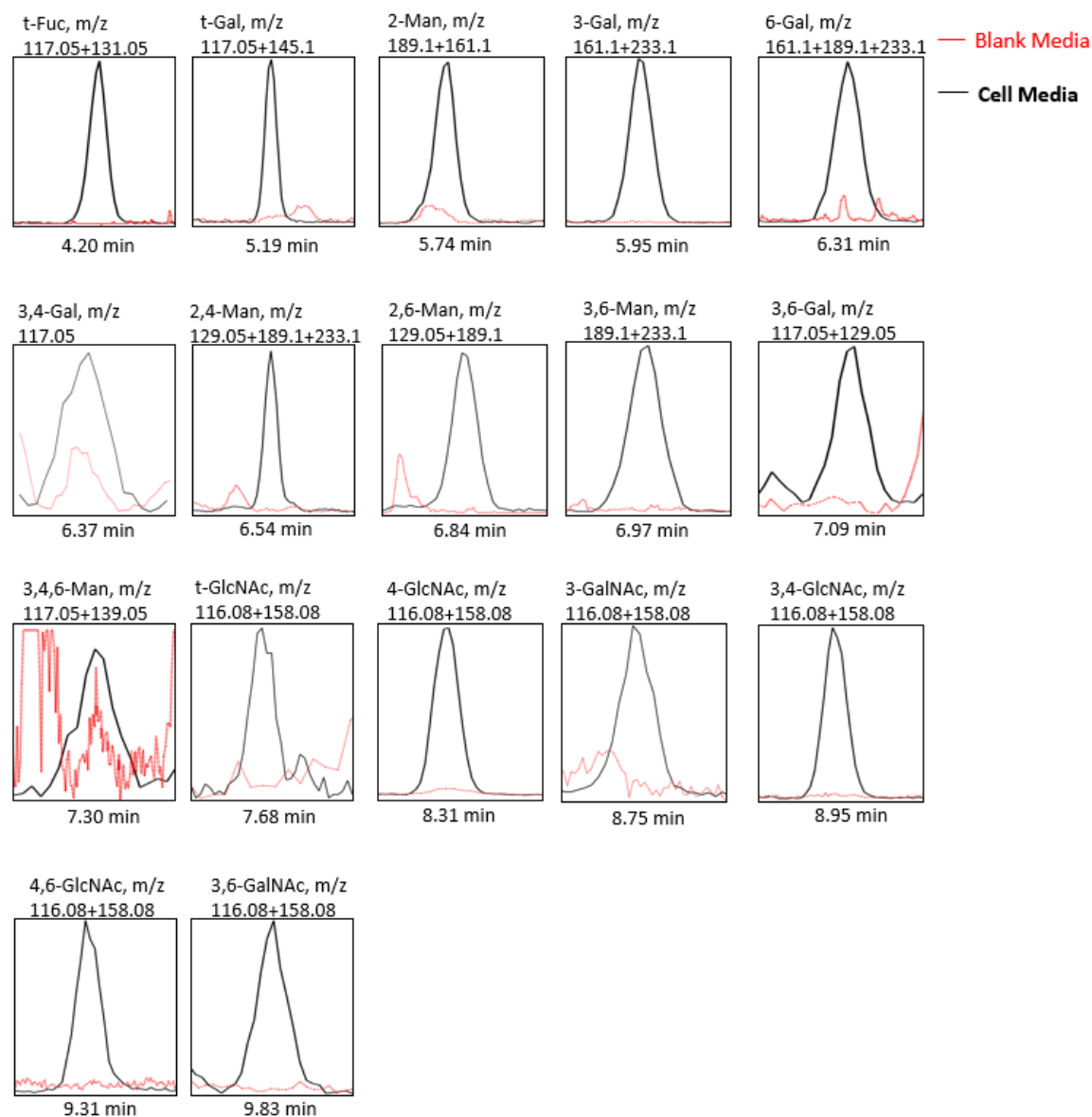
Figure 2.1. Summed extracted ion chromatograms (XICs) for the 17 glycan nodes found in HepG2 cell culture media. Raw XIC traces for EMEM media that was never exposed to cells are shown in red (i.e., "Blank Media"); raw XIC traces for EMEM media exposed to cells then processed by spin filtration (see experimental procedure section) are shown in black (i.e., "Cell-Exposed Media"). Retention times listed correspond to the XIC peak apex.
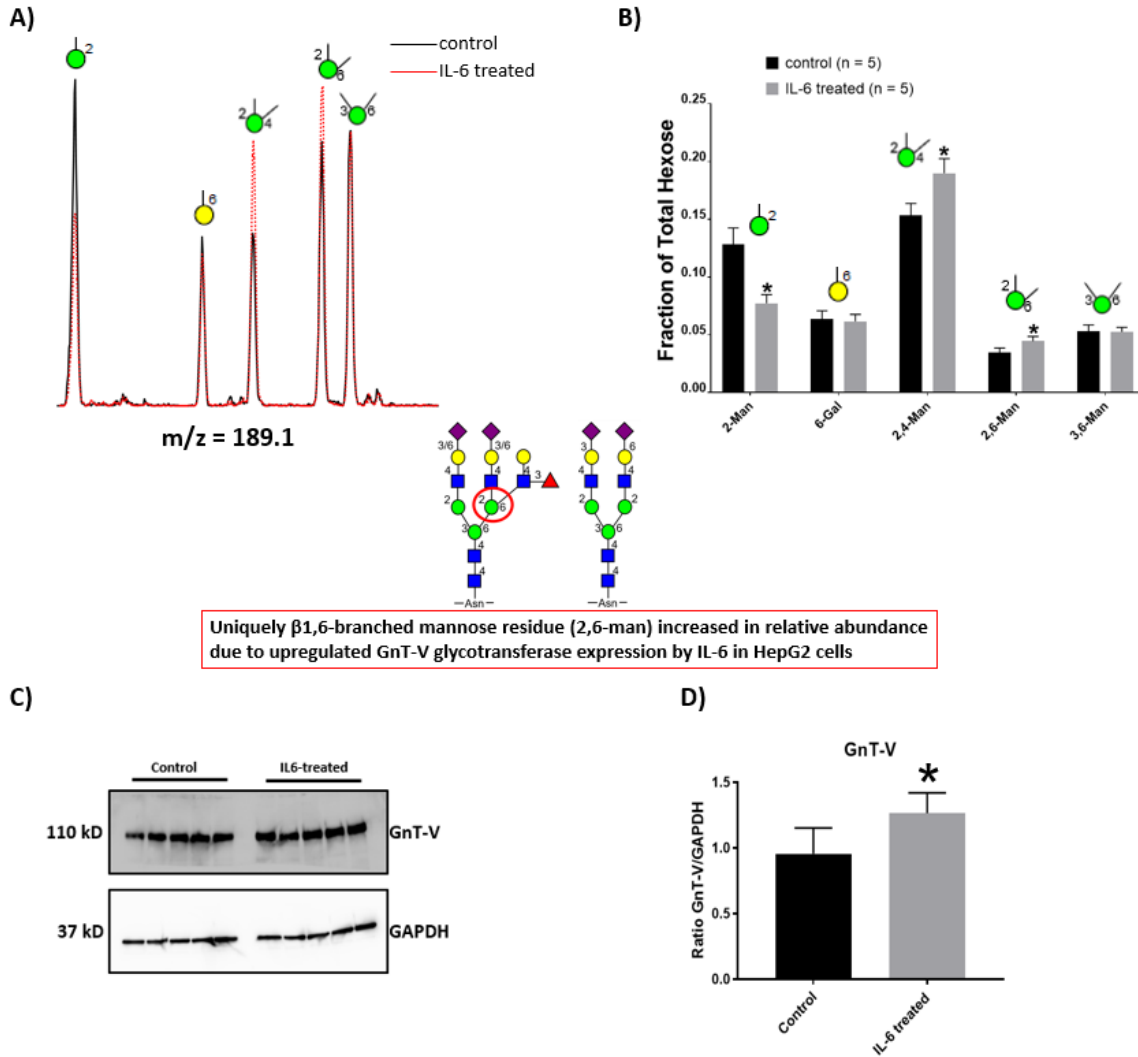
Figure 2.2. IL-6 regulates glycosyltransferase GnT-V expression in HepG2 cells. Cells were grown in media containing 10% FBS for 3 days until 70% confluence then washed to remove FBS (See experimental section) and incubated with 3 ml of FBS-free media containing 50 ng/ml IL-6. Media was collected and replaced with fresh IL-6-containing media every 24 h for a total cytokine exposure period of 48 h, as previously done by Mackievicz et al. [43]. Control cells were cultured in the same way but in the absence of added cytokine. A). Extracted ion chromatogram at m/z 189.1 show a significant decrease in 2-linked mannose (2-Man), and a significant increase in 2,4-linked mannose (2,4-Man) and 2,6-linked mannose (2,6-Man) as determined by glycan node analysis. B). Extracted ion chromatograms corresponding to each glycan node shown in A were normalized to the summed area of all hexoses. C). Qualitative Western blot data showing and increase in GnT-V enzyme in HepG2 cells upon IL-6 stimulation. D). Quantitative summary of illustrative data shown in C showing each band normalized to GAPDH protein control. Error bars represent standard deviation. * Indicates statistically significant differences between control and IL-6-treated cells (p < 0.001). Statistical

51

significance determined using multiple t-tests with the Holm–Sidak method for multiple comparisons correction for part B, and for part D a two-tailed t-test was performed using GraphPad v8.2.
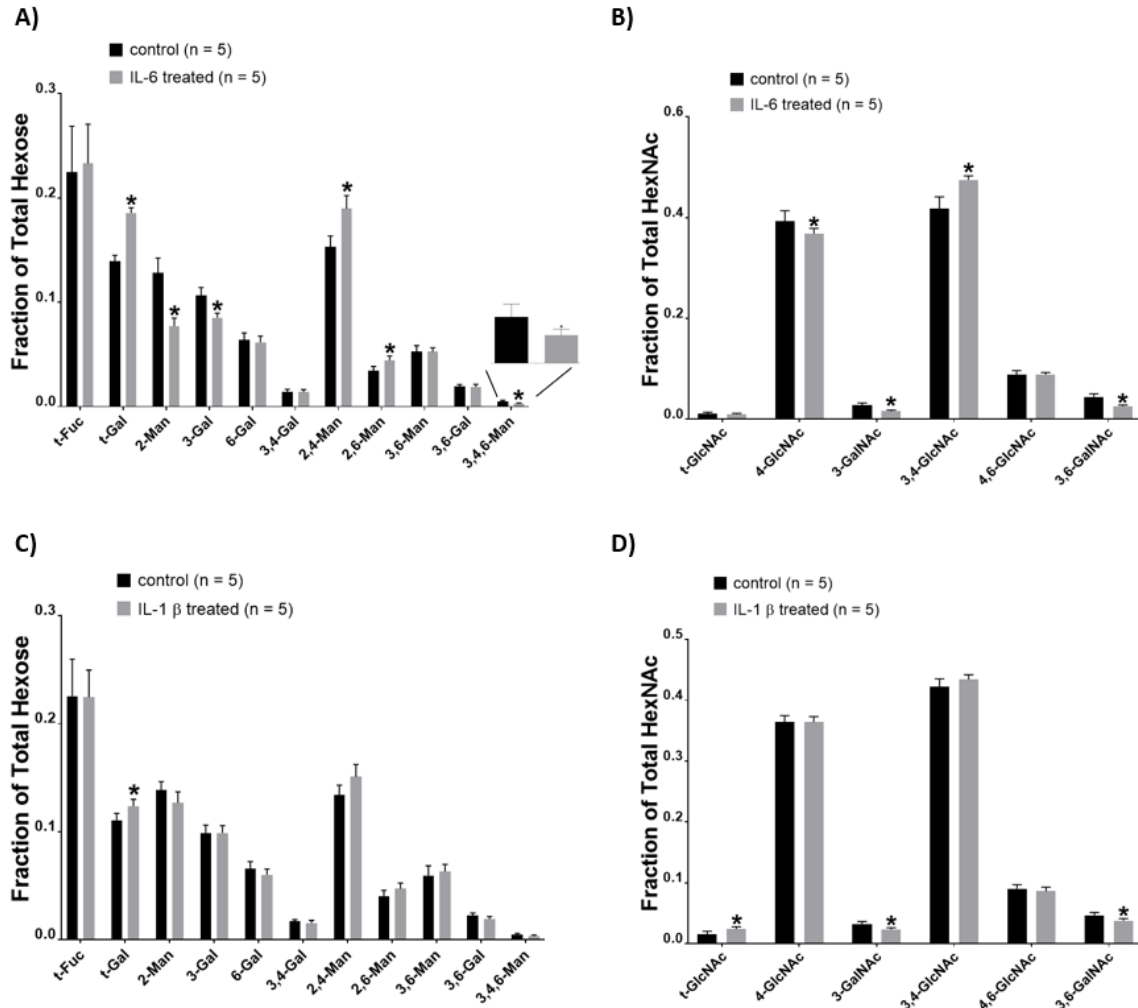
Figure 2.3. Complete glycan node profile in HepG2 cell culture supernatant with different cytokine stimulation. Cells were grown in media containing 10% FBS for 3 days until 70% confluence then washed to remove FBS and incubated with 3 ml of FBS-free media containing 50 ng/ml IL-6 (a and b) or IL-1β (d and c). Media was collected and replaced with fresh cytokine-containing media every 24 h for a total cytokine exposure period of 48 h, as previously done by Mackievicz et al. [43]. Control cells were cultured in the same way but in the absence of added cytokine. Extracted ion chromatograms corresponding to each glycan node were normalized to the summed area of all hexoses (a and c) or HexNAcs (b and d) (as appropriate per that particular glycan node). Error bars represent standard deviation. * Indicates statistically significant differences between control and cytokine-treated cells ($p < 0.001$). Statistical significance determined using multiple t-tests with the Holm–Sidak method for multiple comparisons correction (GraphPad v8.2).
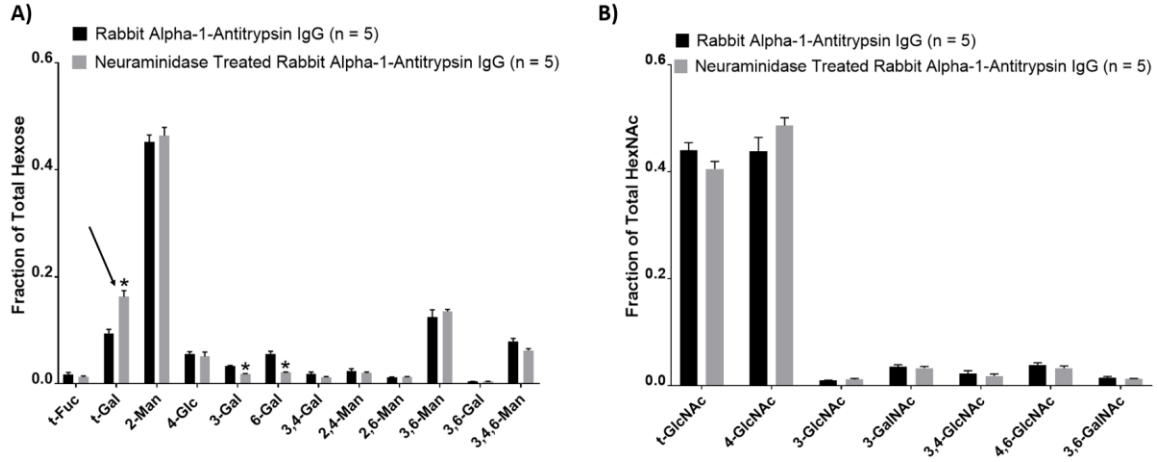
Figure 2.4. Glycan node analysis of IgG Antibodies. Glycan nodes from rabbit anti-alpha-1 antitrypsin IgG (A and B) before and after treatment of the antibody with neuraminidase enzyme. Rabbit anti-alpha-1 antitrypsin IgG (A and B) were treated with 0.1 milliunits/ml of neuraminidase enzyme. Significant decreases in 6-linked and 3-linked galactose were observed along with an increase in terminal galactose (t-Gal), indicating an overall decrease in terminal neuraminic acid residues. Error bars represent standard deviation. * Indicates statistically significant differences between untreated and neuraminidase-treated antibody ($p < 0.001$). Statistical significance determined using multiple t-tests with the Holm–Sidak method for multiple comparisons correction (GraphPad v8.2).

Table 1. Analytical Reproducibility of Glycan Nodes in HepG2 Cell Culture Supernatant [a]

Specific Glycan Feature	Glycan "node"	Intra-Assay CV[b,c]						Inter-Assay CV[b,c]	
		Day 1 (n = 6)		Day 2 (n = 6)		Day 3 (n = 6)		All 3 days (n = 18)	
		% of all Hexoses or HexNAcs	CV	% of all Hexoses or HexNAcs	CV	% of all Hexoses or HexNAcs	CV	% of all Hexoses or HexNAcs	CV
	Hexoses								
Terminal Fucose	t-Fuc	19.5	15	17.5	19	19.2	10	18.9	14
Terminal Galactose	t-Gal	10.6	8	10.4	4	10.5	6	10.5	6
	2-Man	11.4	3	11.8	4	11.5	9	11.5	6
	4-Glc	ND[d]	ND	ND	ND	ND	ND	ND	ND
	3-Man	ND	ND	ND	ND	ND	ND	ND	ND
	2-Gal	ND	ND	ND	ND	ND	ND	ND	ND
	3-Gal	11.7	3	12.2	5	11.8	7	11.7	5
α2-6-sialylation	6-Gal	6.3	4	6.7	6	6.4	10	6.5	7
	3,4-Gal	1.6	11	1.4	8	1.5	11	1.5	11
	2,3-Gal	ND	ND	ND	ND	ND	ND	ND	ND
β1-4-branching	2,4-Man	15.3	4	16.2	7	14.9	5	15.5	6
	4,6-Glc	ND	ND	ND	ND	ND	ND	ND	ND
β1-6-branching	2,6-Man	3.8	7	4.4	4	4.2	7	4.2	8
	3,6-Man	5.8	6	6.6	6	6.0	11	6.1	9
	3,6-Gal	3.1	5	3.3	4	3.2	5	3.3	5
Bisecting GlcNAc	3,4,6-Man	0.89	18	0.94	12	0.88	16	0.94	15
	HexNAcs								
	t-GlcNAc	1.9	4	1.9	5	1.9	13	1.9	7
	t-GalNAc	ND	ND	ND	ND	ND	ND	ND	ND
	4-GlcNAc	32.0	4	32.4	2	31.0	7	31.8	5
	3-GlcNAc	ND	ND	ND	ND	ND	ND	ND	ND
	3-GalNAc	5.4	3	5.4	5	5.3	7	5.3	5
	6-GlcNAc	ND	ND	ND	ND	ND	ND	ND	ND
Antennary Fucosylation	3,4-GlcNAc	40.7	3	40.1	1	41.1	3	40.8	3
	4-GalNAc	ND	ND	ND	ND	ND	ND	ND	ND
	6-GalNAc	ND	ND	ND	ND	ND	ND	ND	ND
	4,6-GlcNAc	10.7	5	10.5	2	10.1	4	10.5	5
	3,6-GalNAc	8.4	6	8.6	3	7.9	9	8.1	7

[a]HepG2 cells were seeded in T75 flasks, and they were grown for 3 days in FBS medium until 70 % confluency and then with serum free medium for 48 hours. Serum free medium was collected from across all flasks, centrifuged at 1000 g for 5 minutes, and supernatant was stored in a single container (bulk sample) at -80 °C. Serum free medium was concentrated 30-fold by spin filtration and analyzed by glycan methylation analysis on three different days (6 replicates per day from the same bulk sample).

[b]In general, glycan nodes with the lowest precision (highest % CV values) are those with the lowest relative abundance.

[c]These results are consistent with those observed in whole blood plasma/serum [96, 100].

[d]ND indicates not detected, but it has been previously detected in other biomatrices [96].

CHAPTER 3

GLYCAN NODES OF PLASMA AND CELL DERIVED EXTRACELLULAR VESICLES

3.1 Introduction

Extracellular vesicles (EVs) are nano-sized particles generated by all cells. EVs mediate near and long-distance intercellular communication through transfer of bioactive molecules, such as nucleic acids, proteins, lipids, and metabolites, in normal physiological processes, and in pathological processes [119]. EVs are divided into two categories; ectosomes and exosomes. Ectosomes are vesicles that are released from plasma membranes and have a size range of about 50 nm to 1 μm in diameter. Exosomes have an endosomal origin since they are released from the exocytosis of multivesicular bodies, and they have a size range of about 40 to 160 nm in diameter [119]. EVs carry several functions in cell biology, such as cell signaling, immune response balance, cell proliferation, angiogenesis, gene transcription and translation regulation, cell migration and metastasis [120].

Recent reports have shown that changes in glycan structures can have an impact on EV function in cancer cells, affecting cell communication and the uptake of EVs by recipient cells [121]. Therefore, studies involving EVs in biology will also have to focus on EV glycosylation through glycomics approaches to better understand the function of glycans in EV biology and their potential for diagnosis and prognosis in cancer. However, even though glycomics methods have been widely applied to understand protein glycosylation [95], their application to EVs is still limited, and studies on EV glycomics are scarce.

EVs are present in almost all body fluids, including blood plasma, and they show high stability at 4 $^{\circ}$C for 24 hours [122]. The clinical utility of EVs in the diagnosis and therapy of cancer has been shown [123]. For instance, EVs represent a promising cancer serum-based biomarker since they show higher diagnostic accuracy than carcinoembryonic antigen (CEA) [124]. Identification of changes in glycosylation on EVs can also provide a target for potential diagnosis and therapy for cancer. However, the plasma EV glycome has been mostly overlooked, primarily due to technical challenges in glycan analysis. Previous studies on the plasma glycome have focused on the N-glycome as a promising diagnostic modality for longitudinal monitoring [125, 126]. Additionally, some studies have found that certain plasma glycans (beyond N-linked glycans) are elevated in cancer patients when compared to healthy controls [34, 35, 97]. However, outside of a few studies targeting specific EV glycoproteins/proteoglycans or glycolipids [127–129], only a single study has assessed glycan expression levels in plasma based on association with EVs, and this analysis was limited to N-linked glycosylation [130].

In this study, we first applied the glycan node analysis (GNA) procedure, a medium-throughput method for analyzing carbohydrates [96], to quantify differences in glycan expression in metastatic and non-metastatic breast cancer cell line-derived EVs. We then evaluated the utility of the GNA in healthy donor-matched whole plasma and plasma-derived EVs to understand which glycans are expressed in EVs in order to improve diagnostic readouts and identification of novel therapeutic targets in plasma-derived EVs. GNA is a molecularly bottom-up gas chromatography-mass spectrometry (GC-MS)-based approach to glycan linkage analysis [96, 100]. This method can be applied directly to complex biological matrices, covers all major classes of glycans, and condenses and captures unique glycan features, such as core fucosylation, α2-6-

56

sialylation, bisecting N-acetylglucosamine (GlcNAc), and β1-6 branching, as single analytical signals, some of which serve as direct molecular surrogates for the activity of specific glycosyltransferases. Therefore, GNA is often capable of providing unique information that may remain undetected with conventional methods [96, 100].

To date, GNA of whole blood plasma or serum from hundreds of patients has proven effective at detecting and predicting progression, reoccurrence, and/or survival in lung cancer [34, 97] and bladder cancer [35]. The implementation of an additional EV isolation step prior to GNA has the potential to improve the clinical sensitivity and specificity of plasma glycan nodes as cancer biomarkers, as tumor-derived EVs play a critical role in cancer formation and progression and can be detected in circulation [124].

The present study shows differences in glycan expression in metastatic and non-metastatic cancer cell-derived EVs specific glycan features, such as hyaluronic acid. Also, this study represents the first broad analysis of glycan expression (multiple glycan classes) in healthy donor plasma-derived EVs, and it shows the potential to be used for detecting specific glycan changes in healthy vs cancer plasma-derived EVs.

3.2 Experimental Procedures

3.2.1 Materials

Materials were acquired from the following sources: acetone from Avantor Performance Materials (Center Valley, PA, USA); methanol from Honeywell Burdick & Jackson (Muskegon, MI, USA); acetonitrile, methylene chloride, pierce spin columns (900 µL volume, Cat. No. 69705), GC-MS autosampler vials, Pierce bicinchoninic acid assay (BCA) Protein Assay Kit, dimethylsulfoxide (DMSO), iodomethane (99%, Cat. No. I8507),

chloroform, trifluoroacetic acid (TFA), ammonium hydroxide, sodium borohydride, acetic anhydride, sodium acetate and sodium hydroxide beads (20-40 mesh, Cat. No. 367176) from Sigma-Aldrich (St. Louis, MO, USA); GC consumables from Agilent (Santa Clara, CA, USA); MS consumables from Waters (Milford, MA, USA).

3.2.2 Collection of Exosomes

Cell derived EVs and blood plasma derived EVs samples suspended in water were obtained from our collaborators at Mayo clinic. They isolated EVs using Izon qEV original 70 nm SeriesTM size-exclusion chromatography (SEC) columns and followed manufacturer instructions. For plasma derived EVs, elution fractions were counted in 0.5 mL intervals beginning after the void volume of 3 mL had passed through the column. Elution fractions seven through nine were pooled for analysis as 'fraction 1' (for a total of 1.5 mL) and elution fractions ten and eleven were pooled for analysis as 'fraction 2' (for a total of 1.0 mL). These two size exclusion fractions were isolated from each of three different blood plasma donors. For GNA this process was repeated for each donor plasma sample in quadruplicate (four technical replicates for each fraction).

3.2.3 Glycan Node Analysis of Exosomes

EV samples suspended in water were concentrated by speed-vac to obtain final protein concentrations of 10-25 mg/mL, as measured by a BCA. Whole plasma samples and concentrated EV samples were directly subjected to permethylation following addition of internal standard as described below:

Permethylation, nonreductive release, and purification of glycans: Blood plasma or concentrated EV samples (10 µL) were added to 1.5 mL snap-cap polypropylene tubes, followed by the addition of DMSO (270 µL). Sodium hydroxide beads (~ 0.7 g) were

collected in a ~ 1 mL Pierce spin column and washed with acetonitrile (ACN, 350 µL) followed by two rinses with DMSO (350 µL). The sample was combined with DMSO (270 µL) and iodomethane (105 µL) followed by immediate vortexing. The sample was then added to the pre-conditioned NaOH beads in the plugged microfuge spin column. The sample was allowed to sit in contact with the NaOH beads for 11 minutes with occasional gentle stirring. The microfuge spin column was then unplugged and spun into a 2 mL sample collection tube for 30 s at 5,000 rpm (1,000 g in a fixed-angle rotor). The collected sample solution was quickly transferred into a silanized 13 x 100 mm glass test tube containing 0.5 M NaCl in 0.2 M sodium phosphate buffer (pH 7) (3.5 mL). To maximize glycan recovery, the NaOH beads were washed twice with ACN (300 µL) with all spun-through liquid immediately transferred into the same silanized glass test tube. Liquid/liquid (L/L) extraction was then carried out by adding chloroform (1.2 mL) to each test tube, which was then capped and shaken well. After brief centrifugation to separate the layers, the upper aqueous layer was discarded and replaced with 0.5 M NaCl solution in 0.2 M sodium phosphate buffer (pH 7) (3.5 mL). After three L/L extraction rounds, the chloroform layer was recovered and dried under a gentle stream of nitrogen in a heater block set to 74 °C.

Hydrolysis, reduction, and acetylation: To perform acid hydrolysis, 2 M TFA (325 µL) was added to each sample followed by heating at 121 °C for two hours. Samples were then dried under a gentle stream of nitrogen in a heater block set to 74 °C. To reduce the sugar aldehydes, freshly made 10 mg/mL sodium borohydride in 1 M ammonium hydroxide (475 µL) was added to dissolve each sample, followed by incubation at room temperature for one hour. To remove excess borate, methanol (MeOH, 63 µL) was added, mixed well and dried under nitrogen, followed by adding 9:1 (v/v) MeOH:acetic acid (125

µL) which was dried in like fashion. Samples were then fully dried in a vacuum desiccator for 20 minutes. To acetylate hydroxyl groups introduced by the acid hydrolysis step, deionized water (18 µL) was added to each test tube to dissolve any precipitates. This was followed by addition of acetic anhydride (250 µL) and sonication in a water bath for two minutes. Each sample was then incubated for ten minutes at 60 °C, followed by mixing with concentrated TFA (230 µL) and incubation again at 60 °C for ten minutes. To clean up the sample mixture prior to GC-MS, L/L extraction was performed twice after adding dichloromethane (1.8 mL) and deionized water (2 mL) to each sample. The upper aqueous layer was discarded each round and the organic layer was then transferred to a silanized autosampler vial and dried under nitrogen. Each sample was reconstituted in acetone (90 µL) and then capped in preparation for injection onto the GC-MS.

GC-MS: Samples were analyzed on an Agilent A7890 gas chromatograph equipped with a CTC PAL autosampler (Agilent Technologies, Santa Clara, CA, USA) coupled to a Waters GCT (time-of-flight: TOF) mass spectrometer (Milford, MA, USA). For each sample, 1 µL of the 120 µL total volume was injected at a split ratio of 20:1 onto a hot (280 °C), silanized glass liner (Cat. No. 5183-4647, Agilent Technologies, Santa Clara, CA, USA) containing a small plug of silanized glass wool. Volatilized sample components were separated on a 30-m DB-5ms GC column using helium as the carrier gas at a constant flow rate of 0.8 mL/minute. The GC oven temperature was initially kept at 165 °C for 0.5 minutes, then increased to 265 °C at a rate of 10 °C/minute, followed by immediate ramping to 325 °C at a rate of 30 °C/minute and finally held at 325 °C for 3 minutes. As sample components entered the mass spectrometer, they were subjected to electron ionization (70 eV, 250 °C). Positive-ion mode mass spectra from individual TOF pulses over a m/z range of 40-800 were summed every 0.1 seconds. The mass spectrometer

was tuned and calibrated daily with perfluorotributylamine to ensure reproducible relative abundances of electron ionization (EI) ions and mass accuracy within 10 ppm.

Data processing: Summed extracted-ion chromatogram (XIC) peak areas for all glycan nodes were integrated with Quanlynx 4.1 software. A list of ions corresponding to each glycan node can be found elsewhere. Peak areas were automatically integrated and manually verified, then exported to a spreadsheet for further analysis. Individual hexoses were normalized to the sum of all endogenous hexoses, and individual N-acetylhexosamines (HexNAcs) were normalized to the sum of all endogenous HexNAcs. This approach provided relative glycan node profiling and therefore direct comparison of glycan node profiles between EV and plasma samples. It does not facilitate quantitative comparisons between different glycan nodes within the same sample. Notably, terminal mannose is not chromatographically or mass spectrally resolved from terminal glucose (which is mostly derived from free blood glucose). If specific hexoses or HexNAcs were not reported as present, it was because their summed extraction ion chromatogram signal-to-noise ratio was less than ten.

3.3 Results

3.3.1 Glycan Nodes of Cancer Cell Derived Exosomes

Numerous significant differences were observed between EV glycan nodes derived from a metastatic breast cancer cell line (brain tropic BR) and those from the parental breast cancer cell line (PAR). 3-linked N-acetylglucosamine (3-GlcNAc), 3-linked N-acetylgalactosamine (3-GalNAc), 3,4-linked galactose (3,4-Gal), 3,6-linked galactose (3,6-Gal), and 3-linked galactose (3-Gal) nodes were elevated in brain tropic BR derived EVs relative to PAR derived EVs. Out of these elevated glycan nodes, 3-GlcNAc was most

strikingly elevated in brain tropic derived EVs compared to PAR derived EVs (**Figure 3.1A**). We have observed that 3-GlcNAc node is barely detected by GC-MS in other biological samples such as blood plasma [100]. However, as shown here, in EVs, 3-GlcNAc is highly abundant. 3-GlcNAc is derived primarily from hyaluronic acid [96]. To confirm that hyaluronic acid produces 3-GlcNAc, a glycan node analysis procedure was performed on a hyaluronic acid standard. GC-MS data on the hyaluronic standard revealed the same chromatographic peak with the same underlying mass spectra and retention time as 3-GlcNAc observed in EVs (data not shown). Elevated hyaluronic acid in EVs derived from cancer cells was also confirmed in the Wolfram lab by ELISA (Data not shown). Additionally, the relative abundance of 4-GlcNAc, 4,6-GlcNAc, 2,4-Man, 2,6-Man, and 6-Gal glycan nodes were elevated in PAR derived EVs compared to brain tropic BR derived EVs (**Figure 3.1A**).

In contrast to breast cancer cell lines, for melanoma cells, 3-GlcNAc node was found to be elevated in the parental melanoma cell line (A75)-derived EVs as compared to the metastatic melanoma brain tropic (BR)-derived EVs (**Figure 3.1B**). Whereas, 4-linked N-acetylglucosamine (4-GlcNAc), 3-GalNAc, an unknown GlcNAc, 4,6-linked N-acetylglucosamine (4,6-GlcNAc), and 3,6-N-acetylgalactosamine (3,6-GalNAc) were significantly increased in the EVs from metastatic melanoma BR relative to parental melanoma cell derived EVs (**Figure 3.1B**).

3.3.2 Glycan Nodes of Plasma Derived Exosomes

In this study, healthy donor plasma was used as a source material for EVs, and it was collected in fractions by size exclusion chromatography (SEC) (**See Figure 3.2 and section 3.2.2**). We then applied the GNA procedure to EVs derived from normal donor

blood plasma samples to see if there was a significant difference between the blood plasma glycome and EV glycome. There was a lack of statistically significant differences in GNA data from four size-exclusion chromatography (SEC) technical replicates from each donor, and data were statistically pooled to facilitate comparisons. Numerous significant differences were observed between EV glycan node profiles (fraction 1 and fraction 2 combined) and those from plasma of the same donor (**Figure 3.3**). 3-Gal, 3-GalNAc, and 3,6-GalNAc residues were most strikingly and consistently elevated in EVs relative to whole plasma across all donors. The most likely explanation for this phenomenon is that there is an increased relative abundance of proteoglycans (i.e., glycosaminoglycans/GAGs) in EVs relative to whole plasma. In particular, these specific glycan nodes correspond to the unmodified hexoses and HexNAcs present in chondroitin sulfate and dermatan sulfate (3-GalNAc) as well as type II keratan sulfate (3-Gal and 3,6-GalNAc) [131]. Modified hexoses and HexNAc, such as those containing sulfate, phosphate or carboxyl groups, are not detected by the method [96]. Significantly elevated 4-linked xylose (4-Xyl) in EVs of two of the three donors accords well with this assignment, as this node serves as the reducing-end sugar attached directly to serine in chondroitin sulfate, dermatan sulfate and heparan sulfate GAGs, but is generally not observed in N-, O-, or lipid-linked glycans. Likewise, enrichment of branched mannose residues in EVs is consistent with increased type I keratan sulfate.

Compared to plasma EVs, whole plasma was relatively enriched in 4-linked glucose (4-Glc), 6-linked glucose or mannose (which were indistinguishable by GC-MS; 6-Glc/6-Man), 3,4-linked N-acetylglucosamine (3,4-GlcNAc), and 3,4-Gal (**Figure 3.3**). The most likely sources of 4-Glc and 6-Glc in plasma are lactose (4-Glc), glycogen fragments (4- and 6-Glc) glycosylphosphatidylinositol (GPI)-anchored proteins. 3,4-

63

GlcNAc represents antennary fucosylation and 3,4-Gal is most commonly found in glycolipids [96].

A lack of statistically significant differences was observed between healthy donor EV glycans (**Figure 3.4**), indicating that the EV glycome profile may be consistent across healthy donor plasma. Similarly, a lack of statistically significant differences was observed between EV fractions 1 and 2, which held true across all three healthy plasma donors (**Figure 3.5**), demonstrating that these SEC-EV fractions can be pooled for glycan expression analysis (which was done in figures 3.2 and 3.3).

3.4 Discussion

In this study we found that hyaluronic acid or hyaluronan was significantly elevated in metastatic breast cancer cell-derived EVs relative to non-metastatic parental breast cancer cell-derived EVs. These results suggest that hyaluronic acid could play an important role in breast cancer metastasis. Other studies have shown that hyaluronic acid is upregulated in cancer, and that its overexpression promotes tumor development [132, 133]. Additionally, increased expression of hyaluronic acid binding protein 1 has been correlated with poor prognosis in breast cancer [134]. Hence hyaluronic acid represents an important target for cancer treatment.

On the contrary, in this study we also found that the parental melanoma cancer cell-derived EVs had increased levels of hyaluronic acid relative to the metastatic melanoma cell-derived EVs. These results appeared to correlate well with what others have found. For example, it has been shown that highly aggressive melanoma cell lines shed significant amounts of CD44 from the cell surface and secrete its ligand hyaluronic

acid [135]. A different study found that reduced CD44 and hyaluronic acid levels on cell surfaces were associated with poor prognosis in clinical stage I cutaneous melanoma [136]. In both studies, it's shown how reduced levels of hyaluronic acid on cell surfaces enhances the metastatic capacity of melanoma cancer cells. Our glycan node analysis results revealed that metastatic melanoma cancer cells secrete EVs with lower amounts of hyaluronic acid, suggesting a different mechanism by which melanoma cells metastasize.

The additional findings from this study indicate that glycan profiles of plasma-derived EVs are distinct from donor-matched whole plasma (e.g. the former has higher relative proteoglycan content), and that EV glycans do not substantially differ among a small set of healthy donors. Moreover, this study demonstrates that plasma EV fractions from SEC can be pooled for analysis, as glycan expression does not significantly differ among fractions. The results also reveal that glycan nodes corresponding to those observed in the GAG residues of proteoglycans such as chondroitin sulfate, dermatan sulfate, type I keratan sulfate, or type II keratan sulfate are relatively enriched on healthy plasma EVs. Chondroitin sulfate-decorated serglycin has previously been observed in serum-derived EVs and found to play an important role in tumor-derived EV protein cargo loading [128]. Heparan sulfate and chondroitin sulfate-bearing syndecan-1 has been identified as a potential plasma EV-based marker of glioma [129]. Future studies, however, are necessary to fully elucidate the potential biological roles of the aforementioned biomolecules in this context.

The distinct glycan expression profile of EVs compared to whole plasma is promising for developing new diagnostic strategies. In particular, GNA of EVs is likely to

be an important, cost effective, and time-efficient future method to assess glycan-dependent health from a simple blood draw, as EVs have been associated with multiple disease conditions [137–140]. Additionally, GNA of plasma EVs coupled with follow-up targeted studies could provide further understanding of various disease conditions and identification of potential therapeutic targets. GNA of plasma EVs may also aid in understanding therapeutic mechanisms involved in plasma-based therapies. This study represents the first broad analysis of glycan expression in plasma-derived EVs (based on all major glycan classes, not just N-glycans), and future studies with more samples will be necessary to further assess potential scientific and medical applications.

3.5 Conclusion

Glycan node analysis (GNA) was applied for the first time to quantify specific glycan features in extracellular vesicles (EVs) derived from cancer cell lines and metastatic cells, as well as EVs derived from normal blood plasma. The glycan node 3-GlcNAc represented hyaluronic acid, and its expression was upregulated in metastatic breast cancer cell-derived EVs relative to parental breast cancer cell-derived EVs. However, 3-GlcNAc was significantly downregulated in the parental melanoma cell-derived EVs relative to the metastatic melanoma cells. The 3-GalNAc node was upregulated in both of the metastatic cancer cell-derived EVs relative to their parental cancer cell-derived EVs. The 3-GalNAc node could come from proteoglycans, but it could also come from O-linked glycans.

EV glycan vs plasma glycan profiles revealed significant differences among the glycan nodes. For instance, 3-Gal, 3-GalNAc and 3,6-GalNAc residues were most strikingly and consistently elevated in EVs relative to whole plasma across all donors. Also, 4-Xyl, an indicator of GAGs/proteoglycans, was significantly elevated in EVs relative

to whole plasma. In whole plasma, 4-Glc, 6-Glc/6-Man, which were indistinguishable by GC-MS,, 3,4-GlcNAc, and 3,4-Gal were elevated relative to EVs. These results suggest that GNA of EVs represents a promising tool for profiling glycans in cancer.
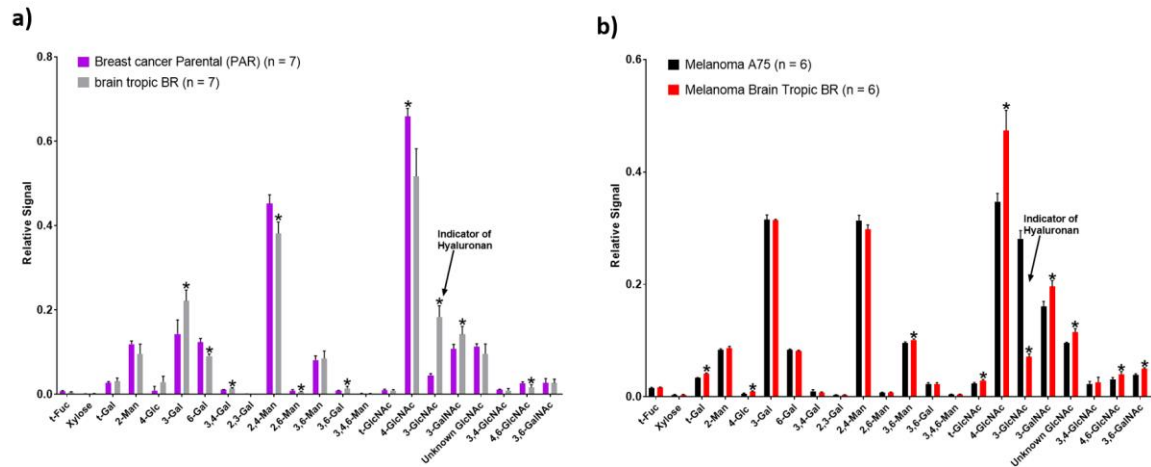
Figure 3.1. Comparison of EVs from four different cancer cells. Data represent extracted ion chromatogram (XIC) peak areas for each hexose or N-acetylhexosamine (HexNAc) within each sample that were normalized to the sum of all hexose or HexNAc XIC peak areas for that sample. * indicates statistical significance among glycan nodes derived from metastatic vs non metastatic cell-derived Evs (p<0.001). Error bars represent standard deviation. Statistical significance determined using multiple t-tests and the Holm-Sidak method for multiple comparison correction in Graphpad.
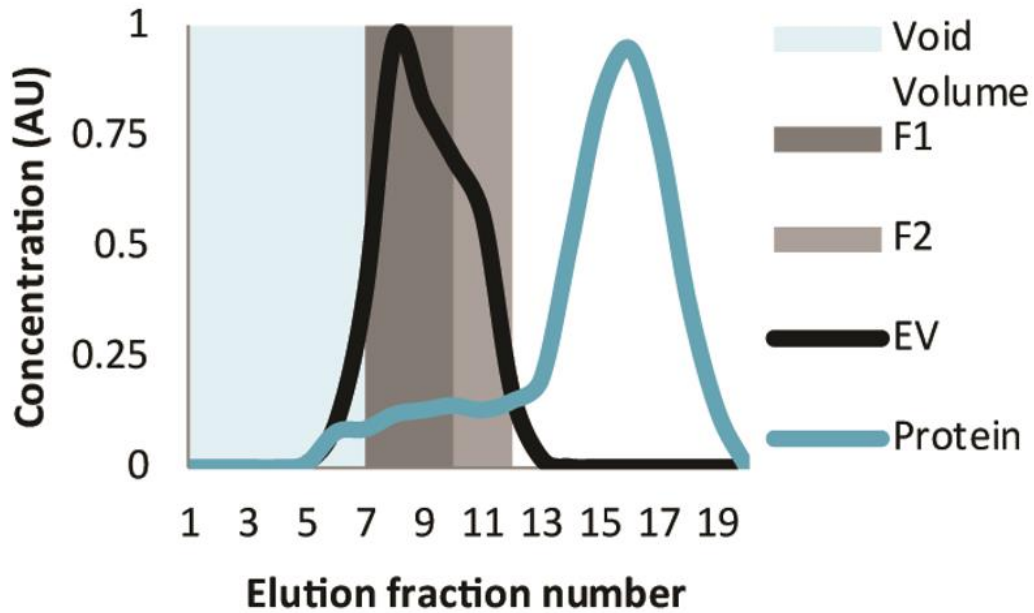
Figure 3.2. **Size-exclusion chromatography (SEC). Izon qEV original 70 nm SeriesTM size-exclusion chromatography (SEC) columns** were used to collect EV fractions from 500 µL of plasma according to the manufacturer's instructions. Elution fractions seven through nine were pooled for analysis as 'fraction 1' (for a total of 1.5 mL) and elution fractions ten and eleven were pooled for analysis as 'fraction 2' (for a total of 1.0 mL). These two size exclusion fractions were isolated from each of three different blood plasma donors. For GNA this process was repeated for each donor plasma sample in quadruplicate (four technical replicates for each fraction) These data were acquired by the Wolfram lab.
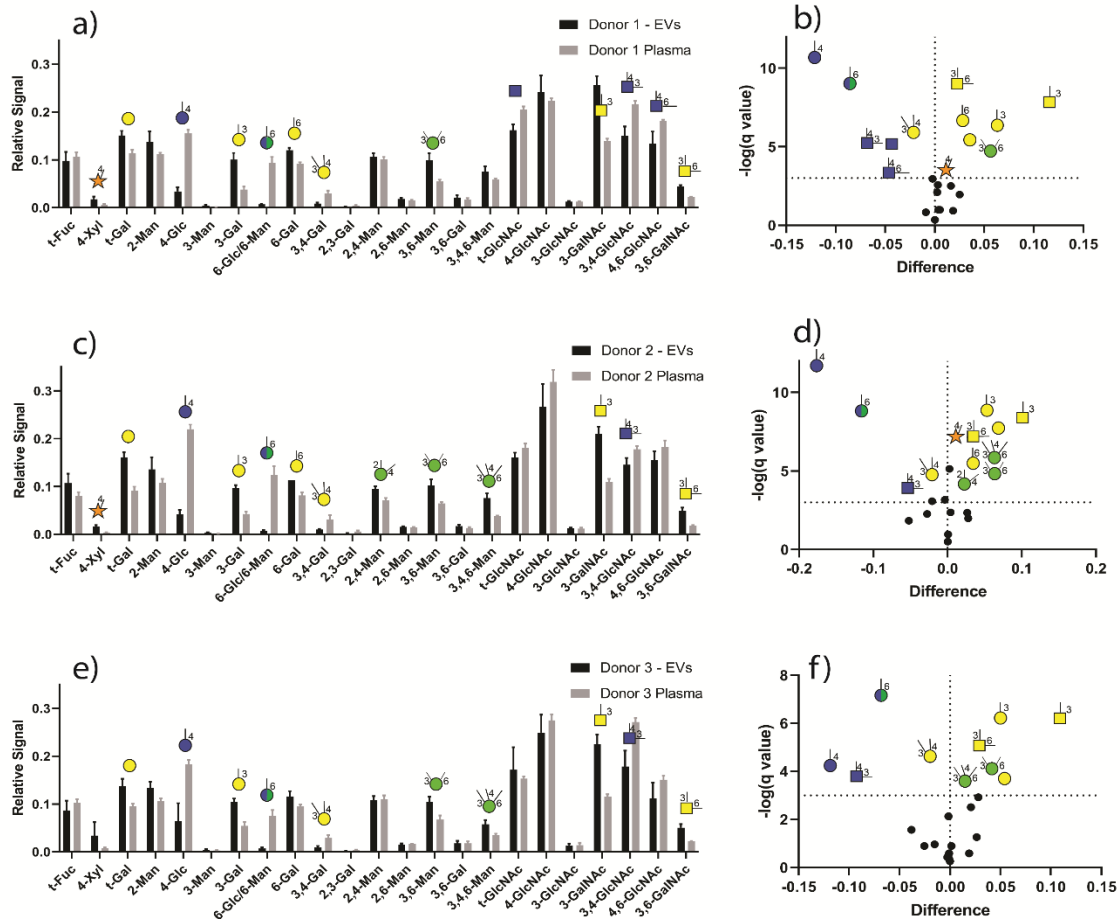
Figure 3.3. Comparison of EV vs. plasma glycan node profiles from three "normal" donors. Data represent extracted ion chromatogram (XIC) peak areas for each hexose or N-acetylhexosamine (HexNAc) within each sample that were normalized to the sum of all hexose or HexNAc XIC peak areas for that sample. Glycan nodes that were significantly different with regard to their relative abundance in EVs vs. plasma are summarized in the volcano plots (b,d,f) and depicted as their cartoon representations (defined by the x-axis in each bar graph (a,c,e)). For each glycan node, significant differences were determined by the Student's t-test without assuming equal variance between groups. To correct for multiple comparisons, the false discovery rate was set at 0.1% according to the two-stage step-up procedure of Benjamini, Krieger and Yekutieli. Data represent mean ± s.d. (n = 8 for EVs and n = 6 for plasma).
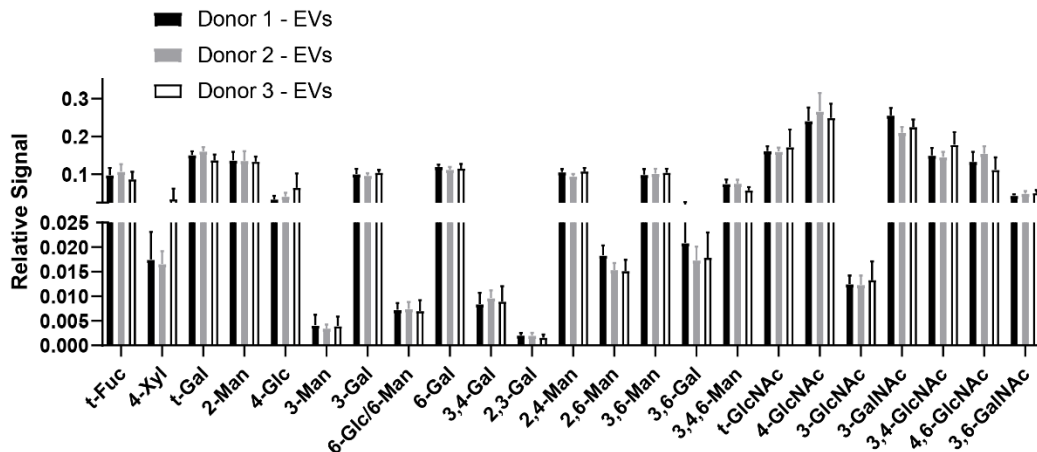
Figure 3.4. Comparison of EV glycan node expression across donors. Data represent XIC peak areas for each hexose or HexNAc within each sample that were normalized to the sum of all hexose or HexNAc XIC peak areas for that sample. For each glycan node, differences between all pairwise combinations of donors were searched for with t-tests, using the two-stage linear step-up procedure of Benjamini, Krieger, and Yekutieli, with Q = 0.1% to correct for false discoveries. No significant differences were observed. Data represent mean ± s.d. (n = 8).
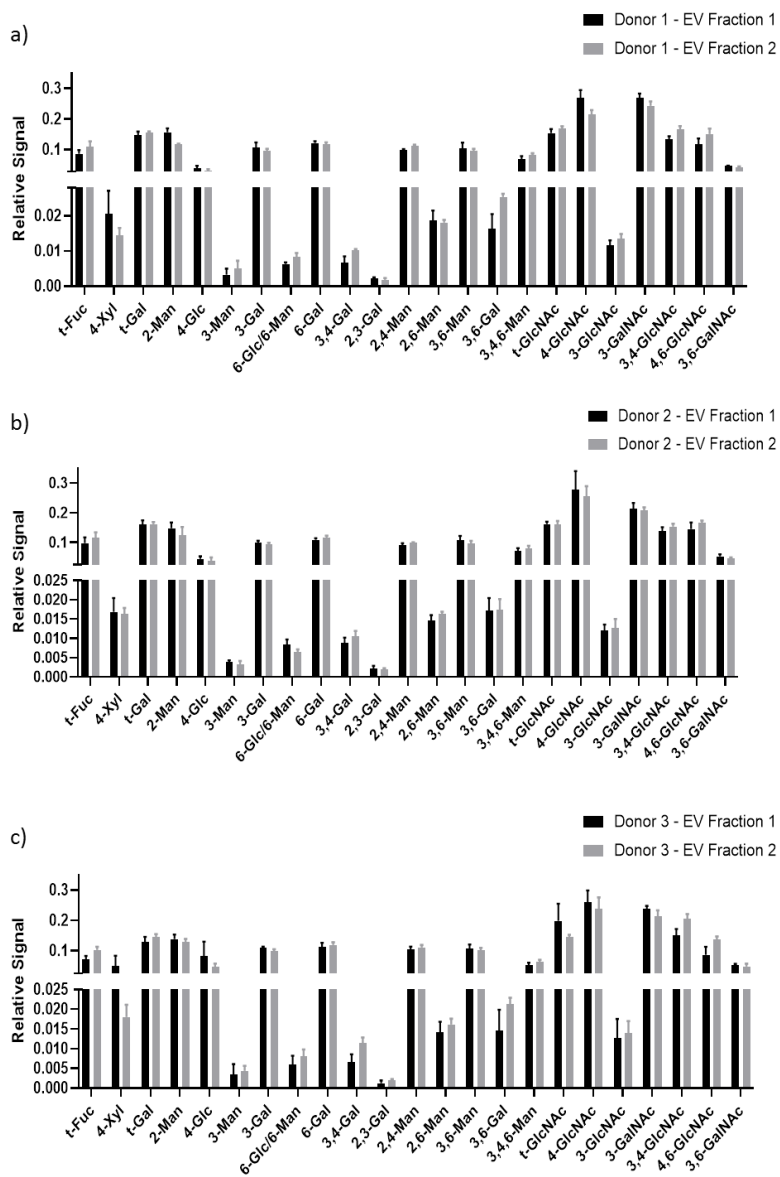
Figure 3.5. Comparison of EV fraction 1 (pooled elution fractions 7-9) and fraction 2 (pooled elution fractions 10-11) from each donor. Comparison of EV glycan nodes between SEC fractions 1 and 2 for each of three different donors (a-c). Data represent XIC peak areas for each hexose or HexNAc within each sample that were normalized to the sum of all hexose or HexNAc XIC peak areas for that sample. For each glycan node, differences between fractions were searched for with a t-test, using the two-stage linear step-up procedure of Benjamini, Krieger, and Yekutieli, with Q = 0.1% to correct for false discoveries. No significant differences were observed. Data represent mean ± s.d. (n = 4).

CHAPTER 4

COMPARISON OF PERMETHYLATION METHODS FOR PROFILING GLYCAN

NODES OF MEMBRANE GLYCOPROTEINS

4.1 Introduction

Mammalian cells express a dense and complex array of complex carbohydrate structures on their surface, which are usually attached to membrane glycoproteins, glycolipids, and proteoglycans. They are all, collectively, referred to as the glycocalyx [141]. Different cell types express different sets of glycans, and significant glycosylation changes occur during development and cell differentiation [142, 143]. Additionally, glycosylation changes are known to occur during malignant transformation [144]. Cancer cells often overexpress certain glycan features that allow them to inhibit an immune response or metastasize to other organs [144]. For instance, hepatocellular carcinoma cells are known to have increased expression of core-α1,6-fucosylated triantennary glycans [116]. Increased sialylation and increased N-glycan branching are among other glycan features that elevated in cancer cells [76]. The potential of changes in glycan features as clinical biomarkers of cancer are now well recognized in clinical medicine. However, translation into practice has not been well established because there is a need for new glycan analysis technologies that can give reliable and reproducible results [145].

Mass spectrometric methods have been largely used for glycan analysis because of their sensitivity and the enormous amount of data that are collected. Derivatization of glycans by permethylation is a useful method that is commonly used with mass spectrometry for the analysis of glycans [94]. Permethylation often improves sensitivity in mass spectrometry and it facilitates determination of glycan composition, including linkages, branching points, and monosaccharide identity. Permethylation provides stability

to isolated glycan structures and increases volatility of glycans [111]. Methods based on glycan permethylation analysis have historically been applied to pre-isolated glycans [146]. Over the years there has been a great amount of effort to simplifying permethylation procedures for efficient glycan analysis. In 1984, Ciucanu and Kerek introduced a permethylation procedure based on the use of powered sodium hydroxide as a base to deprotonate hydroxyl groups on carbohydrates, dimethyl sulfoxide (DMSO) as the solvent, and iodomethane as the permethylation reagent [147]. However, large quantities of sample were needed for this procedure, and it was found to be a hazardous task [148]. The Ciucanu procedure was later optimized by different groups that introduced a solid phase permethylation procedure based on packing of powered sodium hydroxide in spin columns [98, 99, 111], commonly known as solid phase permethylation [112]. This new spin column-based procedure helped minimize oxidative degradation and peeling reactions, and low quantities of glycans (picomole to femtomole) were needed for analysis, which was not previously achieved by the Ciucanu procedure.

In 1991, Anumula and Taylor developed a rather different permethylation procedure, which was found to be a rapid and simple method for permethylation at the time [148]. This new procedure consisted in the preparation of a gel-like NaOH-DMSO reagent for permethylation of carbohydrates. The NaOH-DMSO reagent acted as the base to deprotonate hydroxyl groups and generate the alkoxide groups that would react with iodomethane to generate the permethylated glycans. The NaOH-DMSO reagent preparation consisted in the suspension of methanol with 50% sodium hydroxide at a 2:1 ratio followed by dilution with DMSO. This mixture is washed several times with DMSO and centrifuged to generate a gelatinous precipitate (NaOH-DMSO) that is then reconstituted in DMSO and used as the permethylation base [148]. Other researchers

have implemented this procedure, and it is commonly used today for the permethylation of pre-isolated glycans or isolated glycoproteins in intact glycan analysis [149, 150]. However, the Anumula and Taylor procedure has never been applied to whole biological specimens.

In 2013, the optimized Ciucanu spin column-based procedure (or solid phase permethylation procedure) was adapted by Borges et al and incorporated trifluoroacetic acid (TFA) hydrolysis, reduction, and acetylation steps for linkage analysis of monosaccharide units ("glycan nodes") in whole biospecimens by GC-MS [96]. This methodology has been applied to blood plasma, and its clinical performance has been assessed with regard to its ability to generate glycan nodes that distinguish cancer patient plasma from that of healthy matched controls [34, 35, 97]. When using glycan node analysis, specific glycan features within whole biospecimens such as "core fucosylation", "α2-6-sialylation", "β1-6-branching", β1-4-branching", antennary fucosylation, and bisecting GlcNAc, are captured as single analytical signals by GC-MS [96, 100].

Here we have adapted the Anumula and Taylor procedure [148], which we refer to below as the "liquid phase permethylation" procedure, and applied it for the first time for profiling glycan nodes in cell lysates and in blood plasma, and compared it to the widely used solid phase permethylation procedure that was adapted by Borges et al [100]. We found that the liquid phase permethylation procedure offers higher sensitivity for detection of glycan nodes in complex cell lysate samples. The permethylation efficiency for the liquid phase permethylation method is shown, and it is compared to the permethylation efficiency of the solid phase permethylation procedure. Both methods offer ≥99 % percent permethylation efficiencies. Analytical reproducibly of both permethylation methods is

shown in blood plasma and in HepG2 cell lysates, and it was found that the liquid phase permethylation procedure offers better overall precision (%CVs) for some of the glycan nodes than the solid phase permethylation procedure.

4.2 Experimental Procedures

4.2.1 Materials

HepG2 cells (Cat. No. HB-8065), THP-1 cells (TIB-2020), and Eagle's Minimum Essential Medium (EMEM) (Cat. No. 30-2003) were purchased from ATCC. K562 cells were generously provided by Dr. Karen Anderson's laboratory (School of Life Sciences, Arizona State University). Trima residuals (RE202), which are whole blood products collected by Trima apheresis that enhance PBMC collection per donor, were purchased from Blood Center of the Pacific. Fetal bovine serum (FBS) (Cat. No. FB-11) was purchased from Omega Scientific. Sterile 1X PBS pH 7.4 1L (Cat. No. 101642-262) and trypsin 0.25 % 1X (Cat. No. 16777-166) were purchased from VWR. Density gradient medium Ficoll-Paque (GHC-17-1440-02) was purchased from GE Healthcare. Spin columns (0.9 ml) with plugs and polyethylene frits (Cat. No. 69705) were purchased from Thermo Fisher Scientific. HEPES (Cat. No. H3375-250G), DMSO (Cat. No. D8418-1L), sodium hydroxide beads (Cat. No. 367176-2.5KG), acetonitrile (Cat. No. 539996-1KG), iodomethane (Cat. No. I8507-500G), chloroform (Cat. No. 650498-4L), sodium chloride (Cat. No. S7653-1KG), sodium phosphate dibasic (Cat. No. S7907-500G), sodium phosphate monobasic (Cat. No. S8282-500G), trifluoroacetic acid (TFA) (Cat. No. 299537-500G), ammonium hydroxide (Cat. No. 320145-50ML), glacial acetic acid (Cat. No. 27225-1L-R), and acetic anhydride (Cat. No. 539996-1KG), were purchased from MilliporeSigma. Sodium borohydride (Cat. No. 71321-100G) was purchased from Fluka). Methanol (Cat. No. A452SK-4) and dichloromethane (Cat. No. D143SK-4) were purchased from Fisher

Chemical. GC-MS autosampler vials (Cat. No. 03-377K) were purchased from VWR. Teflon-lined pierceable caps, 9mm (Cat. No. C500-51G) were purchased from Thermo Fisher Scientific. GC consumables were purchased from Agilent (Santa Clara, Ca), and MS consumables were acquired from Waters (Milford, MA).

4.2.2 Cancer Cell culture

HepG2 cells were cultured in EMEM (ATCC) media supplemented with 10% FBS. K562 cells were cultured in RPMI media with 10% FBS. THP-1 cells were cultured in RPMI media ATCC treated supplemented with 10% FBS. HepG2, K562, and THP-1 cells were cultured in T75 flasks at 37°C in 5% CO_2 (daily care and maintenance of these cells were done following ATCC guidelines for cell culture).

4.2.3 PBMC Isolation

Peripheral blood mononuclear cells (PBMCs) were isolated by density gradient centrifugation from Trima Residuals. Trima Residuals or whole blood products were diluted by half with 1X PBS supplemented with 2% FBS. Twenty-five milliliters of the diluted Trima Residuals were added to 50-ml SepMate tubes containing 14 ml of Ficoll Paque density gradient medium. Then tubes containing Trima Residuals in density medium were centrifuged at 1200 g for 20 minutes at 15 °C. Then the top layer (which contained all the mononuclear cells) was poured off into new conical 50 ml tubes, and it was diluted with 25 ml of 1X PBS in 2% FBS. Then the tubes were centrifuged at 330 x g for 8 minutes. Supernatant was removed, and the bottom layer was reconstituted in 25 ml 1X PBS in 2% FBS, then centrifuged at 120 x g for 10 minutes to remove platelets. Supernatant was removed, and PBMCs were resuspended in a final volume of 25 ml 1X

PBS in 2% FBS. From this stock multiple aliquots were made and stored in the vapor phase of liquid nitrogen until they were used for cell lysis, as described below.

4.2.4 Sample Preparation

Cell lysis: The following cell lysis protocol was modified and adapted from Bio-Rad laboratories. HepG2 cells were detached with 3 ml of 0.25% trypsin at 37 ^{o}C for 10 minutes, and trypsin was neutralized with 6 ml of media, then cells were centrifuged at 200 x g for 3 minutes to remove media. Suspension cells K562 and THP-1 were also centrifuged at 200 x g for 3 minutes to remove media. All cell pellets were washed three times with 1 X PBS. PBMCs were thawed in a water bath at 37°C, reconstituted in 5 ml of serum free X-VIVO 10 media, and centrifuged at 330 x g for 8 minutes to remove FBS and washed three times with 1X PBS. All cell pellets were reconstituted in 0.6 ml of lysis buffer (5 M NaCl, 1 M Tris-HCl pH 7, and 1% NP-40). Cell lysates were incubated in ice for 20 minutes with constant mixing with pipette, then centrifuged at 5,000 x g for 10 minutes at room temperature to remove cell debris (Bio-Rad laboratories protocol; see: https://www.bio-radantibodies.com/western-blot-protocol-cell-lysis-mammalian cells.html). Supernatant containing soluble as well as membrane proteins was concentrated to a final concentration of about 20 mg/ml using a Speed Vac. Then detergent and salts were removed by the methanol/chloroform method.

Methanol/Chloroform Method: cell lysate supernatants were precipitated using the methanol/chloroform method to remove detergents and salts from lysates, as previously done by Wessel & Flugge [151]. One hundred microliters of cell lysate supernatant at 20 mg protein/ml was placed into a 1.5 ml Eppendorf tube. To this was added 400 µl of methanol, 100 µl of chloroform, and 300 µl of DI water, with vortexing every time a reagent

was added. Then samples were centrifuged at 14,000 x g for 1 minute, during which three layers formed; a top aqueous layer (polar phase), an interface layer (membrane and soluble proteins), and a bottom layer (non-polar phase). The top aqueous layer was removed without touching the interface layer and bottom layer. Then 600 µl of methanol were added, vortexed, and centrifuged at 17,000 x g for 5 minutes. At this point a white precipitate forms at the bottom of the tube and on the walls of the tube, and an organic liquid layer is on top. The organic liquid layer was removed completely without disturbing the white precipitate. Then the precipitate was completely dried in a Speed Vac for 10 minutes and solubilized in 40 µl of 8 M urea solution pH 8, this gave a final protein concentration of about 40 mg/ml (determined using a BCA assay kit with albumin as the standard, as described below). Then 10 µl aliquots were made for glycan node analysis, with at least 6 replicates per cell lysate.

BCA Assay: all cell lysate protein concentrations were determined using a BCA assay kit with bovine serum albumin (BSA) as the standard. One microliter of cell lysate sample was aliquoted and diluted in 79 µl of water. One microliter of 8 M urea was diluted in 79 µl of water to use as a solvent blank to subtract any signal caused by the urea from that of protein samples. Color reagents and BSA standard were prepared as described in assay kit, then added 200 µl of color reagent to 96 well plate. To this were added 25 µl of diluted lysate or solvent blank and 25 µl of BSA standard into a separate well. Incubated plate for 25 minutes in an oven at 37 °C. Then absorbance was measured at 562 nm. Final protein concentrations were determined using the BSA standard curve.

4.2.5 Permethylation Procedures

Liquid phase permethylation procedure: the following liquid phase permethylation procedure was adapted from Anumula and Taylor [148]. An aqueous 50% (w/v) sodium hydroxide solution was freshly prepared using sodium hydroxide beads and water. To prepare the permethylation base, 100 µl of the 50% sodium hydroxide solution were dissolved in 200 µl of methanol, followed by addition of 4 ml of DMSO. Then permethylation base was centrifuged briefly and supernatant discarded. This DMSO wash procedure was repeated a total of 6 spin throughs. The gelatinous base was then reconstituted in 2 ml of DMSO and gently mixed it (this was used as the "permethylation base"). Ten microliters of crude biological sample solution or cell lysate were added to a 1.5 ml polypropylene test tube, and to this were added 200 µl of DMSO and 230 µl of liquid permethylation base, incubated for 4 minutes at room temperature, and immediately added 100 µl of iodomethane. Samples were vortexed and incubated for 11 minutes at room temperature. Immediately after, samples were transferred to a silanized glass tube containing 3.5 ml of 0.2 M sodium phosphate buffer, pH 7 containing 0.5 M NaCl. To this was added 1.2 ml of chloroform. L/L extractions were done 3 times with the sodium phosphate buffer, saving the chloroform layer every time. Chloroform was dried under a nitrogen stream.

Solid phase permethylation procedure: ten microliters of crude biological solution or cell lysate were added to a 1.5 ml polypropylene test tube. To this was added 270 µl of dimethylsulfoxide (DMSO) and 105 µl of iodomethane. This solution was mixed and added to a plugged 1 ml spin column containing sodium hydroxide beads, which were preconditioned with acetonitrile and two rinses with DMSO. Samples were gently mixed with the sodium hydroxide beads 3 times for 11 minutes. Then columns were unplugged and centrifuged at 10000 g for 15 sec to collect sample, leaving any NaOH residues

behind. Immediately after, 300 µl of acetonitrile were added to the columns to wash off any sample left on the column. Samples were transferred to a silanized glass tube containing 3.5 ml of 0.2 M sodium phosphate buffer, pH 7 containing 0.5 M NaCl. To this was added 1.2 ml of chloroform. L/L extractions were done 3 times with the sodium phosphate buffer, saving the chloroform layer every time. Chloroform was dried under a nitrogen stream.

4.2.6 Glycan Linkage Analysis

Permethylation of glycans (which includes release of O-glycans): Permethylation was carried out following either one of the procedures described above.

Hydrolysis, reduction, and acetylation of glycans: After permethylation, 2 M Trifluoroacetic acid (TFA) was used to hydrolyze all glycans to single monosaccharide units. Hydrolysis was done as follows; 325 µl of the 2 M TFA solution were added to each sample, which were tightly capped to prevent evaporation, then samples were heated at 120° C for 2 hours. Then TFA was removed by drying sample under nitrogen stream. Reduction was carried out as follows; 475 µl of 10 mg/ml sodium borohydride in 1 M ammonium hydroxide were added to each tube and allowed to react for 1 hour. Sixty three microliters of methanol were added to each sample to remove any residual borate, followed by 125 µl of 9:1 methanol: acetic acid. Each time samples were dried under nitrogen, and a final drying step for 20 minutes in a vacuum desiccator. After drying, 18 µl of DI water were added to each sample, followed by 250 µl of acetic anhydride, mixed thoroughly, and sonicated for 2 minutes. Samples were incubated at 60° C for 10 minutes, followed by addition of 230 µl of TFA, and incubating again at 60°C for 10 minutes. 1.8 ml of dichloromethane and 2 ml of DI water were added to each sample. Then L/L extraction

was done twice with water, saving the dichloromethane layer. The dichloromethane layer was transferred to silanized autosampler vials and dried under nitrogen. Samples were reconstituted with 50 µl of acetone and placed on to the GC-MS autosampler rack.

Gas Chromatography-Mass Spectrometry**:** A gas chromatograph coupled to a time of flight mass spectrometer was used. One microliter of the sample was injected in split mode (1:10) onto a silanized glass liner held at a temperature of 280ºC. Using helium as the carrier gas, samples were transferred onto the GC column, which is maintained in an oven at an initial temperature of 165 ºC, followed by ramping the temperature at 10 ºC per minute to 265 ºC, then ramping at 30 ºC per minute to 325 ºC and holding for 3 minutes. Samples eluting from the column were transferred to a mass spectrometer where they were ionized by a beam of 70 eV electrons, and analyzed by TOF.

Data Analysis: Identification of each glycan node was made by comparing retention times with data obtained by Borges et al., (29-31) and mass spectra were verified through comparison with the mass spectral library of PMAAs at the University of Georgia's Complex Carbohydrate Research Center website (https://www.ccrc.uga.edu/databases/index.php#). Each glycan node was quantified by integrating extracted ion chromatogram peak using QuanLynx software. Integrated peaks were exported to an Excel spreadsheet to normalize the area of each glycan node by dividing each individual hexose glycan node by the sum of all hexoses, and each individual HexNAc glycan node by the sum of all HexNAcs. Normalized values were exported to GraphPad to calculate significant differences between cell lines using the two-stage linear set up procedure of Benjamini, Krieger and Yekutieli, with Q = 1 %.

Permethylation efficiencies: Permethylation efficiencies for each glycan standard were calculated as previously done by Hu and Borges, using as much of the ion current for each PMAA as possible. Low abundance ions from each PMAA were only omitted when it was necessary to do so to prevent signal interferences. The summed XIC peak area of the glycan node representing the fully permethylated form was divided by this same value plus the sum of areas of all the undermethylated fractions. For example, the area of t-GalNAc, representing the fully permethylated HexNAc, was divided by this same area plus the sum of all of its undermethylated forms, such as 3-GalNAc, 4-GalNAc, 6-GalNAc, and 3,6-GalNAc.

4.3 Results

4.3.1 Optimization of Permethylation Reagent Volumes for the Liquid Phase Permethylation Procedure

The optimal total volume of water in the original sample was assessed to identify permethylation efficiencies in the liquid phase permethylation procedure. The volumes of iodomethane and DMSO were held constant, and sample-water volume on permethylation efficiencies were investigated at total water volumes of 10 µl, 20 µl, and 30 µl. It was observed that at aqueous volumes greater than 40 µl, the permethylation solution precipitated. The glycan standard 2-Acetamido-2-deoxy-D-lactose (Gal-4-GlcNAc, a.k.a. N-acetylactosamine or LacNAc) was used to assess permethylation efficiency. Five micrograms of LacNAc were reconstituted into the volumes of water described above (n = 6 each), and samples were processed by liquid phase permethylation, followed by hydrolysis, reduction, and acetylation steps. As shown in **Figure 4.1**, permethylation efficiencies decrease as water volume increases. For samples with 10 µl total volume, approximately 1.4% of hexose and 0.2% of HexNAc residues were undermethylated.

However, for samples with a total volume greater than 10 µl, the undermethylated fractions were significantly higher. Therefore, 10 µl total original sample volume was determined to be the optimal volume to use for subsequent experiments.

4.3.2 Permethylation Efficiency of the Liquid Phase Permethylation Procedure Compared to the Solid Phase Permethylation Method.

The permethylation efficiency of the LP procedure was validated by comparing it with the spin column permethylation procedure, which was developed by Kang et al [98], Goetz et al [99], and further adapted and modified by Borges et al [96]. LacNAc and 3-O-(2-acetamido-2-deoxy-β-D-galactopyranosyl)-D-galactopyranose (GalNAc-3-Gal) were used as the glycan standards to determine permethylation efficiencies. Five micrograms of each glycan standard were processed with each permethylation procedure in parallel. Then with all samples in the same batch, hydrolysis, reduction, and acetylation steps were performed. Permethylation efficiencies were calculated as described in the experimental procedures section. Results were evaluated with individual two tailed t-tests. Results showed that both permethylation methods have similar permethylation efficiencies. For instance, for HexNAcs, the undermethylation fraction by the liquid phase permethylation procedure was 0.19 % for 4-GlcNAc and 0.24 % for t-GalNAc. With the solid phase permethylation procedure was 0.25 % for 4-GlcNAc and 0.26 % for t-GalNAc. For hexoses, the undermethylation factions with both methods were about 1%. (**Figure 4.2A, B, C, & D**). As shown here, both methods give ≥99% permethylation efficiencies for both hexoses and HexNAcs. We then evaluated the yield ratio of HexNAcs to hexoses by comparing the ratio of peak areas of HexNAcs and hexose residues. As with the assessment of permethylation efficiencies, peak areas were obtained using the extracted ion chromatograms (XICs) of hexose and HexNAc used by Hu & Borges [112]. Results

showed that both permethylation methods give similar relative yields of HexNAcs residues, as shown by the HexNAc/hexose ratios (**Figure 4.2E & F**).

4.3.3 Application and Improvement of the Liquid Phase Permethylation Procedure to Membrane Glycoproteins

HepG2, THP-1, K562, and PBMC cell pellets were washed three times with 1X PBS to remove any FBS related proteins. Then cell lysis was performed as described in experimental procedure section. Because we observed that detergents and salts can negatively interfere with permethylation procedures giving low overall yield/signal, lysis buffer and detergent were removed from each cell lysate by precipitation using the methanol/chloroform method (see experimental procedure section). Precipitates containing membrane glycoproteins and soluble glycoproteins were solubilized in 8 M urea pH 8 at a final concentration of 38-43 mg/ml. The LP and SP permethylation procedures were then applied to each cell lysate in parallel, n = 6 for LP and n = 6 for SP, plus two blood plasma samples to use as procedural and instrumental quality controls. Ten microliters of sample containing the membrane/soluble glycoproteins were processed by either LP or SP permethylation procedure, followed by hydrolysis, reduction, acetylation and GC-MS analysis steps. Two blank samples (8 M urea) were analyzed per every batch of samples to verify GC-MC signal was coming from biological sample. An example of extracted ion chromatograms from biological sample and blank processed by the liquid phase approach is shown in **Figure 4.3** for membrane glycoproteins/glycolipids derived from PBMCs. No significant background was observed for any of the biological matrices tested using the two permethylation methods (**Figure 4.3**). After verifying background and signal to noise, data were processed as described in the experimental section, and the XIC peak area for each glycan node was normalized to protein concentration. Results

showed that the LP permethylation procedure provided stronger overall signals than the SP procedure for nearly all cell lysate derived glycan nodes. For every cell derived membrane and soluble glycoprotein matrix peak intensities were significantly higher for the LP procedure than the SP procedure. For example, the signal for 4-GlcNAc node was about 50% higher with the LP procedure than with the SP procedure (**Figure 4.4**). This suggested that better reproducibility might be obtained with the LP procedure than with the SP procedure in membrane glycoprotein samples, especially for the glycan nodes with the lowest signal to noise. To determine intra- and inter-assay reproducibility in membrane/soluble glycoprotein samples using the two methods, six 10-µl aliquots of HepG2 cell membrane glycoproteins were processed and analyzed on three different days using the two permethylation methods in parallel. One experiment was performed two weeks apart. For the LP method, the average intra-assay reproducibility was 5.5%, and the average inter-assay reproducibility was 6.9%. For the SP method, average intra-assay reproducibility was 7.2 % and average inter-assay reproducibility 12.1 % (**See Table 4.1**).

Using glycan node analysis with the two different permethylation procedures, we found consistently different glycosylation profiles among the membrane and soluble glycoproteome in three cancer cell lines and PBMCs. Every cell-derived hexose glycan node was normalized to the sum of all hexoses, and every HexNAc was normalized to the sum of all HexNAcs. After normalization, glycan nodes were compared across cell lines. Statistically significant differences were found in multiple glycan nodes between the three cancer cell lines and PBMCs (**Figures 4.5 & 4.6**). For instance, 4-linked glucose (4-Glc), 3,4-linked galactose (3,4-Gal), 4,6-linked glucose (4,6-Glc), and 4-GlcNAc residues were most strikingly elevated in THP-1, K562, and PBMC cells relative to HepG2 cells (**Figures 4.5 & 4.6**). On the other hand, the relative abundance of terminal fucosylation (t-fuc), 2-

linked mannose (2-Man), α2,6-sialylation (6-Gal), β1,6-branching (2,6-Man), β1,4-branching (2,4-Man), 3,6-linked mannose (3,6-Man), and 3,4-GlcNAc were found to be elevated in HepG2 cells relative to K562 cells, THP-1 cells, and PBMCs (**Figures 4.5 & 4.6**). Additionally, the relative abundance of 4-Glc, 3,4-Gal, and 4,6-Glc were significantly elevated in THP-1 cells and K562 cells relative to PBMCs (**Figures 4.5 & 4.6**).

Using glycan node analysis, we identified an unknown hexose residue that is present in membrane glycoproteins derived from cells. This unknown hexose residue has a retention time of 7.31 min (**Figure 4.7 A & B**), and a mass spectrum that is similar to the mass spectra of 3,4,6-Man, which had a retention time of 7.26 min. These similarities in retention time and mass spectra strongly suggest that the unknown hexose is 3,4,6-linked and is therefore mostly likely 3,4,6-Gal or 3,4,6-Glc. Besides possible undermethylation, the origins of these nodes are unclear. Notably, the 3,4,6-Man node was barely detectable by GC-MS in HepG2 cells, PBMCs, and THP-1 cells, and the %CV for this particular glycan node was not acceptable (>20%).

It was found that for cell lines that had similar glycan profiles or for which the differences between glycan nodes were not strikingly different, the permethylation methods varied in their results only for certain hexoses. For instance, it was found that 3,4-Gal and the unknown hexose were elevated in THP-1 cells relative to K562 cells using the SP method. However, the LP method suggested that there was not a significant difference between these glycan nodes (**Figures 4.5 & 4.6**). The differences in results for these particular glycan nodes between the two methods might be because of the different ratios among 3-Gal, 3,4-Gal, 6-Gal, and unknown hexose to 3,4,6-Man in the two methods (**Figure 4.7**). For example, it was found that the signal for 3,4-Gal was similar to the signal

for 3-Gal in K562 cell derived membrane glycoprotein using the solid phase permethylation method. However, the signal of 3,4-Gal was higher than the signal for 3-Gal using the liquid phase method. The signal for 3-Gal was about the same as the signal for the unknown hexose using the liquid phase approach. However, the signal for 3-Gal was higher than the signal for the unknown hexose, using the solid phase approach (see **Figure 4.7 A & B**). Even though the overall yield/signal obtained from these glycan nodes are significantly higher using the liquid phase approach than the solid phase, their ratios differed. The explanation for these differing ratios is not immediately clear, but it may have something to do with variability in the solubility of different glycopolymers (from which these nodes are derived) in the two different permethylation mediums. Notably, 3,4-Gal and the unknown hexose have the worst precision in both methods (**Table 4.1**) and are unacceptable (>20%) for the solid-phase permethylation procedure applied to this biomatrix—suggesting that significant differences in these nodes revealed by the solid phase method may be false discoveries. Importantly however, with the exception of these glycan nodes, the ratio for all the other glycan nodes was similar among the two methods. Notably, it was interesting to see that both permethylation methods produced the same results for all HexNAcs. For example, both permethylation methods revealed that 3,4-GlcNAc is elevated in THP-1 cells relative to K562 cells (**Figures 4.5 & 4.6**).

4.3.4 Application of the Liquid Phase Permethylation Approach to Human Blood Plasma

The solid phase (SP) permethylation procedure has been previously applied to quantify glycan nodes in whole blood plasma, with potential clinical implications in cancer [34, 35, 97], and the reproducibility of the SP procedure has already been established [100]. To determine the reproducibility of the liquid phase (LP) procedure as applied to EDTA blood

plasma, 10 μl aliquots of an EDTA blood plasma sample from an individual donor were processed by LP procedure, followed by hydrolysis, reduction, acetylation, and analysis by GC-MS. Six 10 μl blood plasma aliquots were processed and analyzed on three different days to determine reproducibility. Table 4.2 shows the % CVs for all glycan nodes that contribute to more than 1% of the total hexose or HexNAc signal with the LP method and the SP method. For the LP method, the average %CV for all glycan nodes per day (intra-assay reproducibility) was 5.6 %, and for all three days (inter-assay reproducibility) was 7.5 %. For the SP method, average intra-assay reproducibility was 5.9 % and average inter-assay reproducibility 8.2 % (**See Table 4.2**). Notably, of the 16 glycan nodes detected in plasma samples, all of them had intra- and inter-assay reproducibility of less than 20 % with both methods. The glycan nodes with %CVs greater than 10% are the ones with lower signal to noise ratios.

4.4 Discussion

Glycan structures of membrane glycoproteins have been assumed to vary between cell types and in cancer [152]. Glycan analysis provides a basis for investigating the function of glycans in tumor development [153]. However, glycan analysis remains challenging, and there is a need for new glycomics methods that can provide reliable and reproducible results. Although there are various methods for intact glycan analysis in cell culture cell lines such as liquid chromatography mass spectrometry (LC-MS) [154], MALDI technologies [155], and glycan microarrays [156], up to this day no one has employed a GC-MS methodology to study the membrane glycome. Here we have applied for the first time a GC-MS glycan linkage methodology (glycan node analysis) to profile specific glycan features in cancer cell lines and in PBMCs. Two different permethylation procedures were used for glycan node analysis; a solid phase permethylation procedure and a liquid phase

permethylation procedure. This is the first time a liquid phase permethylation procedure has been applied to whole, complex biospecimens. Anumula & Taylor developed this procedure in 1992, which they refer to as the NaOH/DMSO and iodomethane suspension for permethylation of carbohydrates. They implemented this procedure with pre-isolated glycoproteins, such as ovalbumin and fetuin. However, up to this day no one has implemented this procedure to whole biospecimens using GC-MS methodologies. We found that this liquid phase approach makes the glycan node analysis procedure easier/more streamlined for higher sample throughput, and it gives better overall yield/signal than the conventional solid phase approach. Both permethylation procedures were found to be consistent and reproducible for most of the glycan nodes observed in cell lysates. Moreover, in this study, a new important biological matrix was analyzed by glycan node analysis that provides access to the glycans of membrane glycoproteins and glycolipids, and significant differences in glycan nodes were found among four different cell types. Specific tumor antigens were found to be elevated in hepatocellular carcinoma cells (HepG2 cells) relative to other cancer cell lines and PBMCs. For example, 3,4-GlcNAc was found to be consistently elevated in HepG2 cells relative to THP-1 cells, K562 cells, and PBMCs. 3,4-GlcNAc represents antennary fucosylation, and this particular glycan feature has been found to be elevated in hepatocellular carcinoma patients by other groups and using different methods [116]. Additionally, our glycan node analysis results revealed that HepG2 cells have elevated β1,6-branching (2,6-Man), β1,4-branching (2,4-Man) relative to PBMCs, THP-1 cells, and K562 cells. These features are indicative of increased N-glycan branching, which is another documented unique glycan feature in the tissue of hepatocellular carcinoma patients [157]. While this study didn't compare primary cells to cancer cells of the same tissue, these results suggest that glycan node analysis

can be used to identify particular glycan features that are commonly found elevated in cancer cells relative to normal cells.

Glycolipids constitute a major portion of glycans in membrane glycoproteins [11]. Our glycan node analysis method allowed us to capture specific glycan features that correspond to glycolipids. For example, 4-Glc, and 3,4-Gal glycan nodes are found predominately on glycolipids. Results revealed that these glycan nodes are elevated in THP-1 cells and K562 cells relative to primary PBMCs. Other studies have observed dysregulated expression of glycolipids in different types of cancer cells that promote tumor development [158]. Among the many forms of glycolipids, changes in the expression of gangliosides, which are heavily sialylated and ubiquitously distributed on membrane proteins, have been observed in cell proliferation, differentiation, and tumor development [159]. Therefore, the clinical utility of glycolipids as biomarkers of cancer has been suggested, and glycan node analysis shows the potential to be a valuable tool to identify certain dysregulated lipid glycosylation changes in cancer.

Additionally, as compared to other biological matrices that have been studied using glycan node analysis, the 4,6-Glc node was detected in the four cell matrices. 4,6-Glc represents glycogen, and it was found to be elevated in in THP-1 cells and K562 cells relative to primary PBMCs. Studies have found that cancer cells are metabolically stressed, and that increased accumulation of glycogen is important for maintenance of ATP levels during bioenergetic stress [160].

4.5 Conclusion

Glycan node analysis is a process by which pooled glycans within complex biological samples are chemically deconstructed in a way that facilitates the analytical quantification of uniquely linked monosaccharide units ("glycan nodes"). Using this approach, we implemented a liquid phase permethylation procedure to perform glycan node analysis. Liquid phase permethylation procedure was applied for the first time to whole, complex biospecimens, such as blood plasma and membrane glycoproteins. In this study, a new important biological matrix was analyzed by glycan node analysis that provides access to the glycans of membrane glycoproteins and glycolipids, and we demonstrated that glycosylation profiling of membrane glycoproteins and membrane glycolipids by glycan node analysis and GC-MS is sufficiently reproducible and consistent. The liquid phase permethylation procedure was compared to our conventional solid phase permethylation procedure, and we found that by avoiding the use of expensive spin columns that are commonly used in solid phase permethylation, the liquid phase approach makes the glycan node analysis procedure easier/more streamlined and cheaper for higher sample throughput than the solid phase approach. It was also found that the liquid phase approach gives better overall yield/signal and better precision (%CVs) for some of the glycan nodes derived from membrane glycoproteins/glycolipids than our usual solid phase approach. Both permethylation methods revealed several differences in glycan nodes among the three cancer cells studied and among the PBMCs. Particularly, specific glycan features such as antennary fucosylation, N-glycan branching, and α2,6-sialylation were found to be particularly elevated in hepatocellular carcinoma cells relative to the other two cancer cells and PBMCs. The relative abundance of 4-Glc, 3,4-Gal, and 4,6-Glc were found to be elevated in THP-1 cells and K562 cells, but in HepG2 cells and PBMCs, the relative abundance of these glycan nodes was significantly downregulated, especially for HepG2 cells.
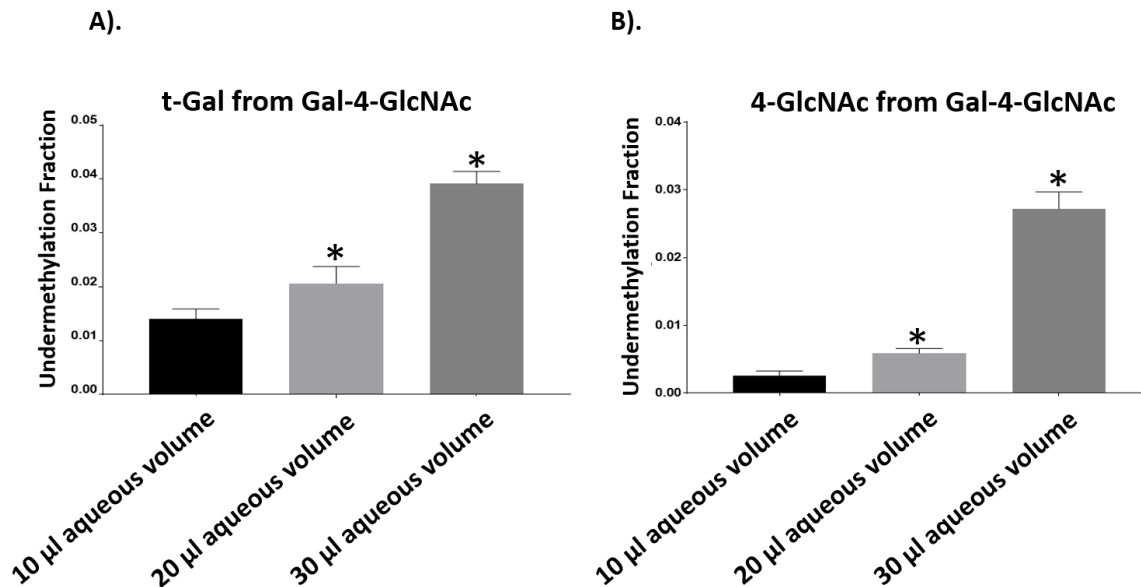
Figure 4.1. Effect of aqueous sample volume on permethylation efficiency using glycan standard Gal-4-GlcNAc. A) Distribution of the undermethylated fraction for t-Gal. B) Distribution of undermethylated fraction for 4-GlcNAc. N = 5 for each volume. Undermethylation for each linkage-based monosaccharide was calculated as described in methods section. * Indicates statically significant differences in the degree of undermethylation at the tested volumes (p<0.001). Statistical significance determined using one-way ANOVA with Turkey posthoc test. n = 5 per group. Error bars represent standard deviation.
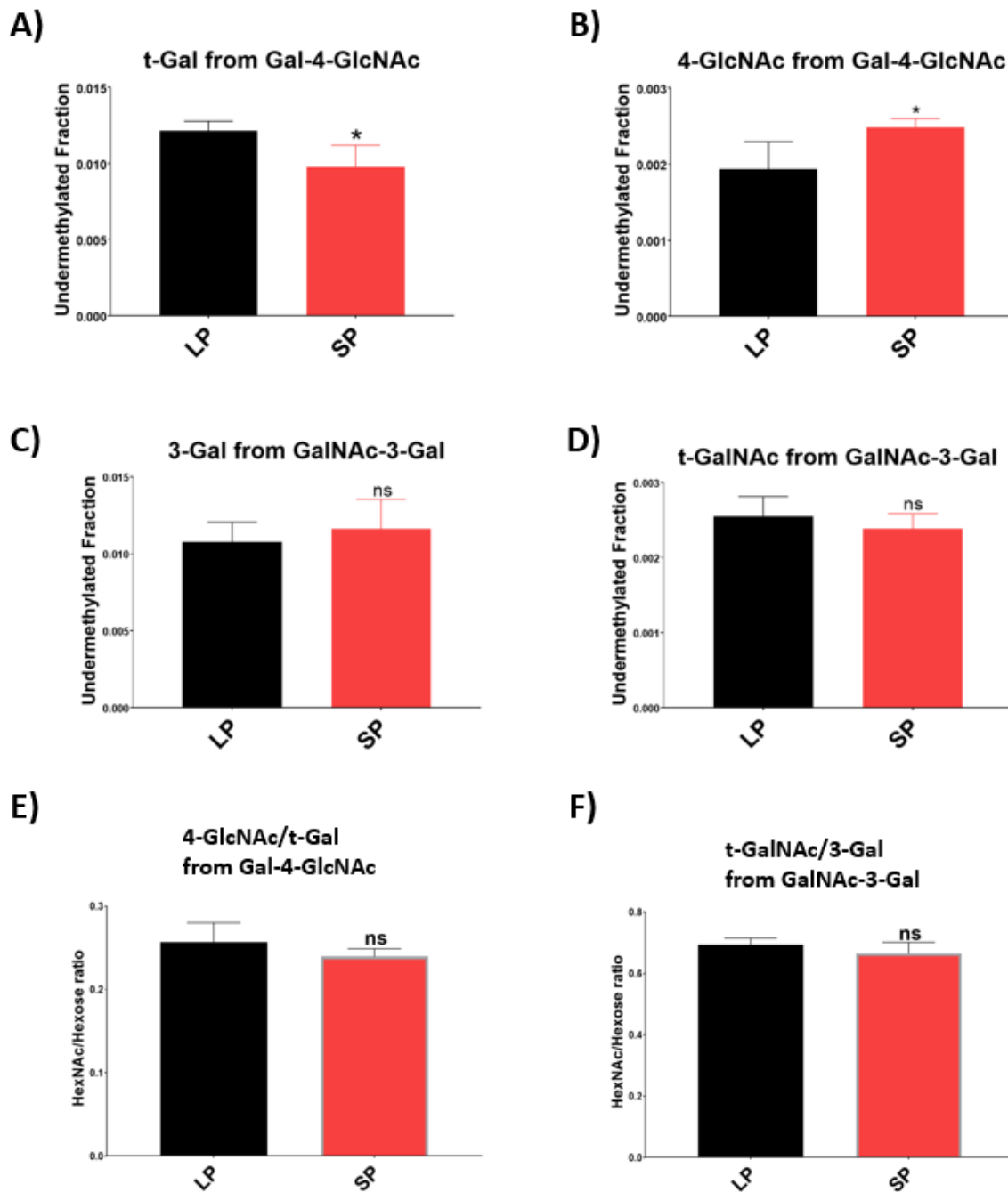
Figure 4.2. Permethylation efficiencies of solid phase (SP) and liquid phase (LP) permethylation procedures compared. A) Undermethylated fractions for t-Gal from Galactopyranosyl-β-1,4-N-acetyl-D-glucosamine (Gal-4-GlcNAc or LacNAc). B) Undermethylated fraction for 4-GlcNAc from Gal-4-GlcNAc. C) Undermethylated fraction for 3-Gal from 3-O-(2-acetamido-2-deoxy-b-D-galactopyranosyl)-D-galactopyranose (GalNAc-3Gal). D) Undermethylated fraction for t-GalNAc from GalNAc-3-Gal. E) The ratios of the peak areas under the summed extracted ion chromatograms (XICs) of HexNAc to hexose were compared for both glycan standards. Both permethylation procedures showed highly similar permethylation efficiencies (≥99 %). Statistical significance determined using a two-tailed t-test. ns indicates no statistically significant

difference. * indicates a statistically significant difference (p<0.001). N = 6 per group. Error bars represent standard deviation.
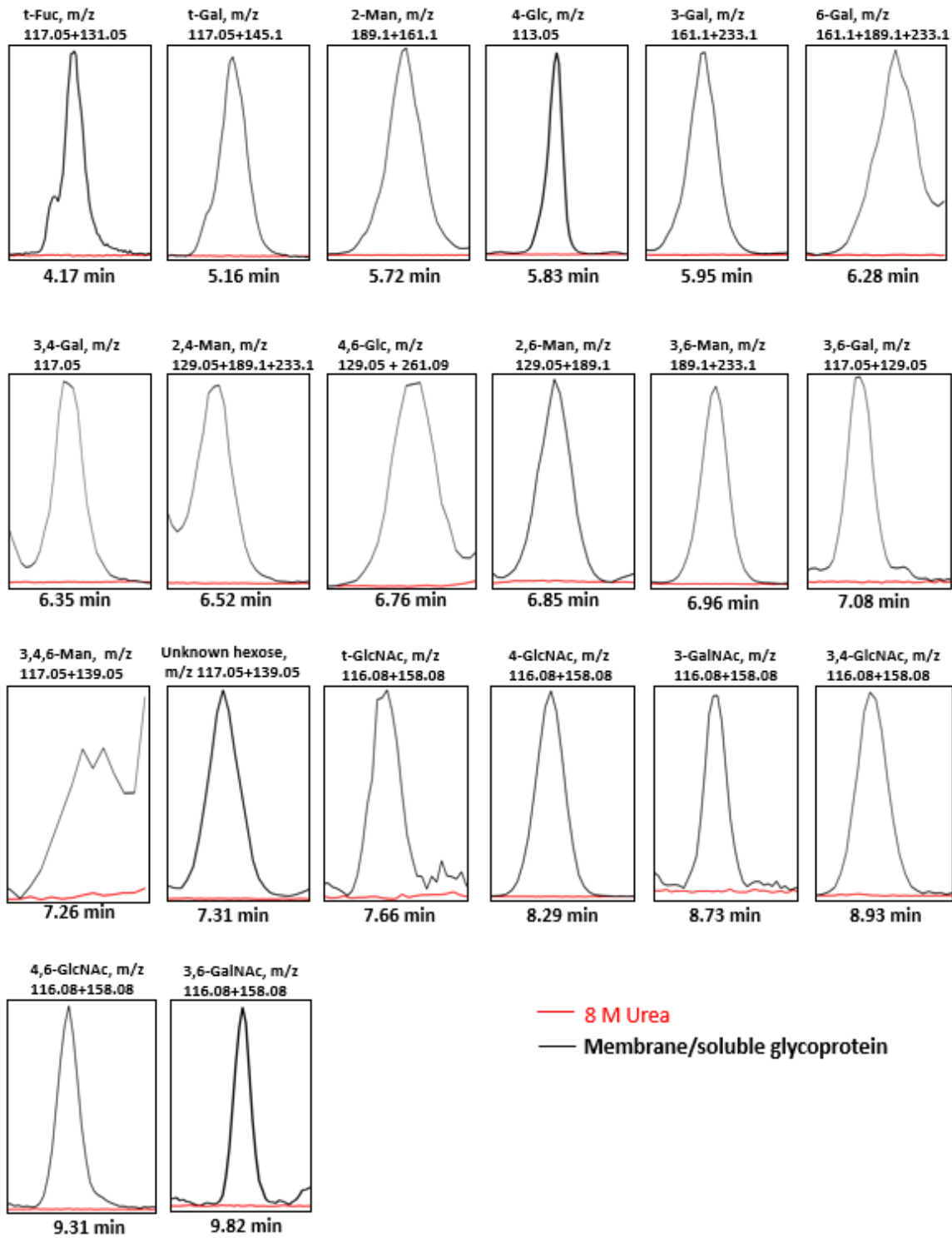
Figure 4.3. Summed extracted ion chromatograms (XICs) for the 20 glycan nodes found in "normal" donor PBMC cell membrane glycoproteins using the liquid phase permethylation procedure. Raw XIC traces for 8 M urea blank samples that were

processed by glycan node analysis using the liquid phase approach are shown in red (i.e., "8 M urea"); raw XIC traces for glycan nodes derived from membrane/soluble glycoprotein processed by the liquid phase approach (see experimental procedure section) are shown in black (i.e., "Membrane/soluble glycoprotein"). Retention times listed correspond to the XIC peak apex. For XIC traces, a mass window of ± 0.15 Da is taken around the indicated m/z value.
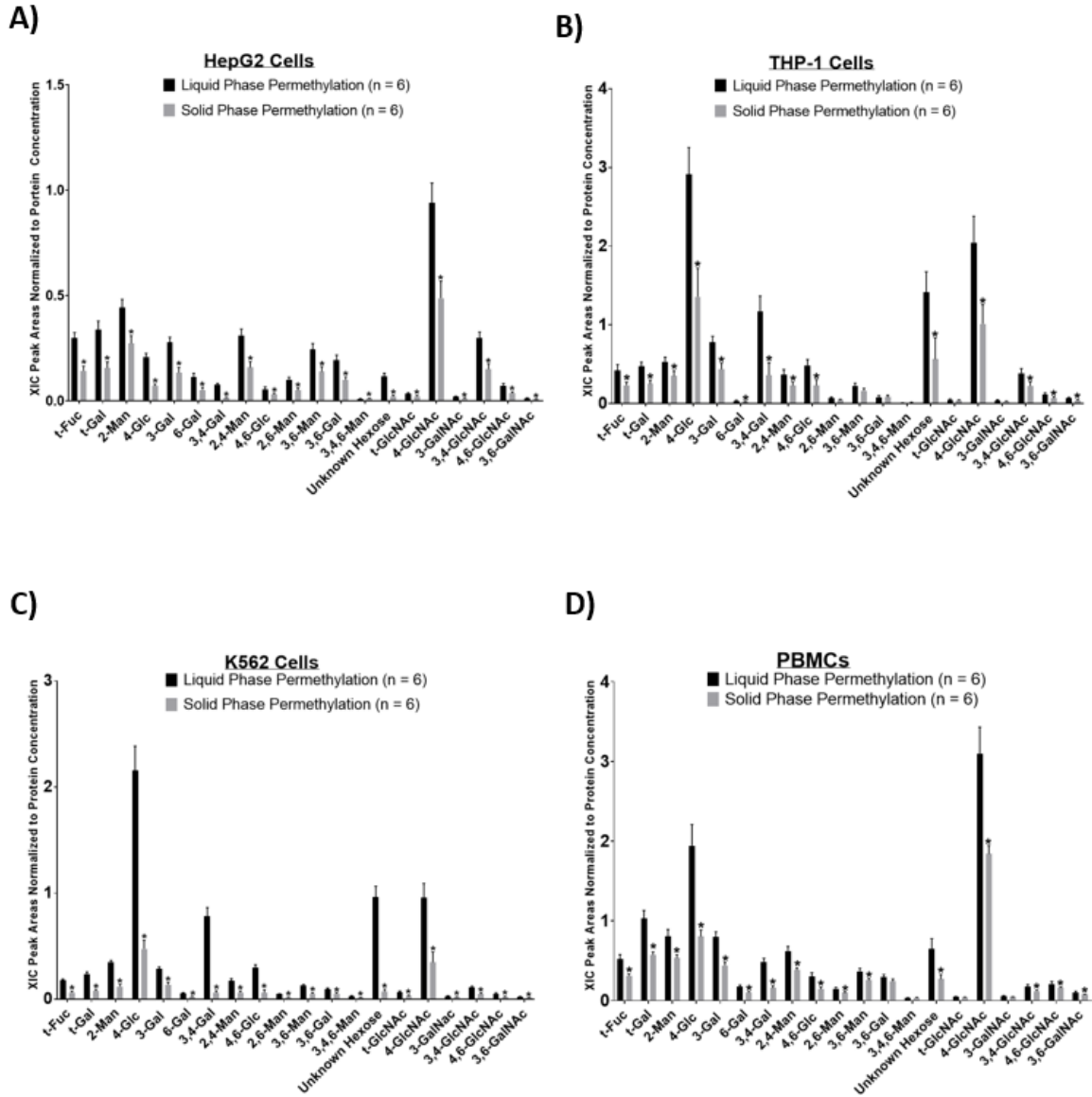
Figure 4.4. Improved total signals obtained from the liquid phase procedure Detergents were removed from each cell lysate using the methanol/chloroform method, and precipitates were reconstituted in 8 M urea pH 8, as described in the experimental procedure section. Data represent extracted ion chromatogram (XIC) peak areas for each hexose or N-acetylhexosamine (HexNAc) within each sample. The analytical signal for each glycan node was compared for the two methods using peak areas. Extracted ion chromatogram peak areas corresponding to each glycan node were normalized to total

amount of protein used for glycan node analysis in A) HepG2 cells B) THP-1 cells, C) K562 cells, and D) Peripheral blood mononuclear cells (PBMCs). The peak areas were generally much higher with the liquid phase permethylation procedure than with the solid phase permethylation procedure for each biological cell matrix. Statistical significance determined using multiple tests with the Holm–Sidak method for multiple comparisons correction (GraphPad v8.2). * indicates a statistically significant difference (p<0.001). N = 6 per group. Error bars represent standard deviation.
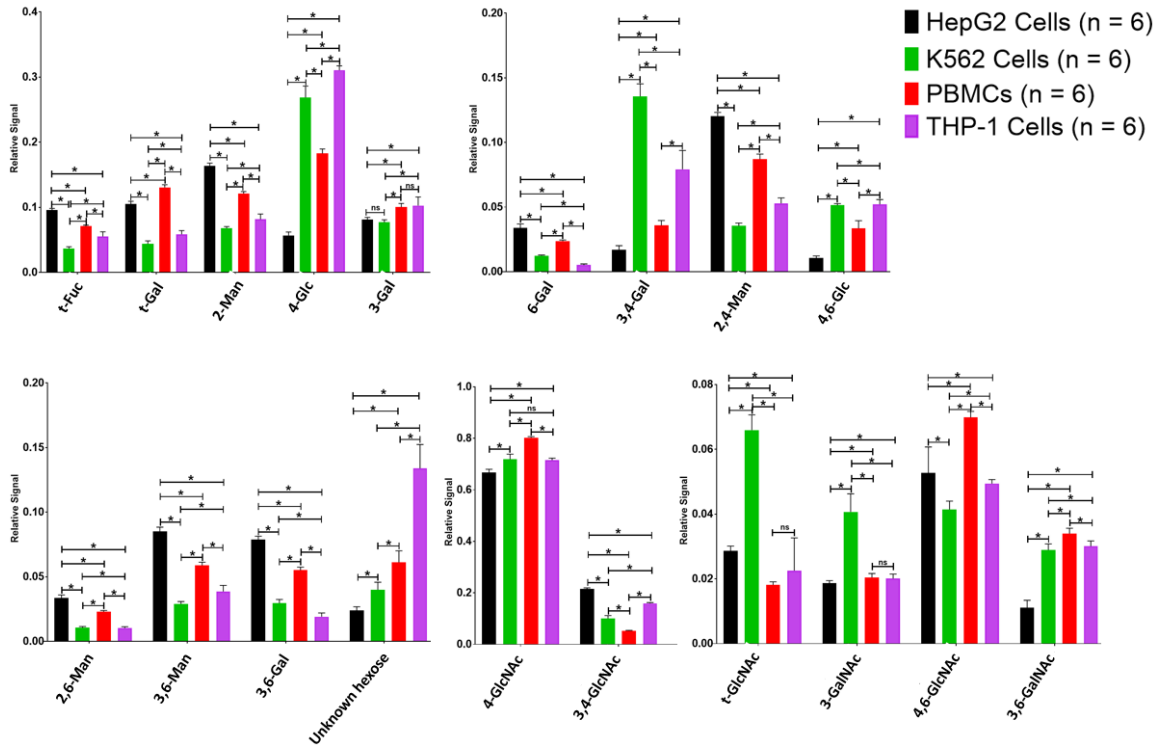
Figure 4.5. Comparison of glycan node profile from three cancer cells and "normal" donor PBMCs using the _solid_ phase permethylation procedure. Data represent extracted ion chromatogram (XIC) peak areas for each hexose or HexNAc within each sample. Extracted ion chromatogram peak areas corresponding to each glycan node were normalized to the summed area of all hexoses or HexNAcs (as appropriate per that particular glycan node). Error bars represent standard deviation. * Indicates statistically significant differences between cells (p < 0.001). Statistical significance determined using multiple one-way ANOVAs with Tukey test (GraphPad v8.2).

96
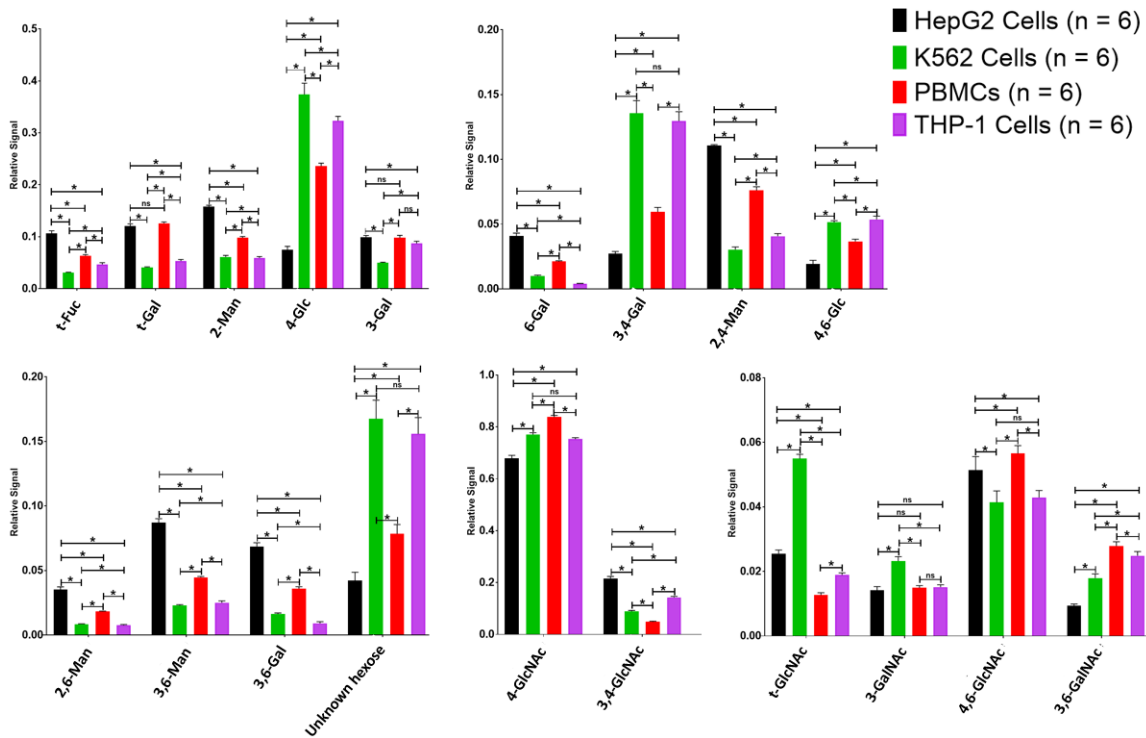
Figure 4.6. Comparison of glycan node profile from three cancer cells and "normal" donor PBMCs using the _liquid_ phase permethylation procedure. Data represent extracted ion chromatogram (XIC) peak areas for each hexose or HexNAc within each sample. Extracted ion chromatogram peak areas corresponding to each glycan node were normalized to the summed area of all hexoses or HexNAcs (as appropriate per that particular glycan node). Error bars represent standard deviation. * Indicates statistically significant differences between cells (p < 0.001). Statistical significance determined using multiple one-way ANOVAs with Tukey test (GraphPad v8.2).
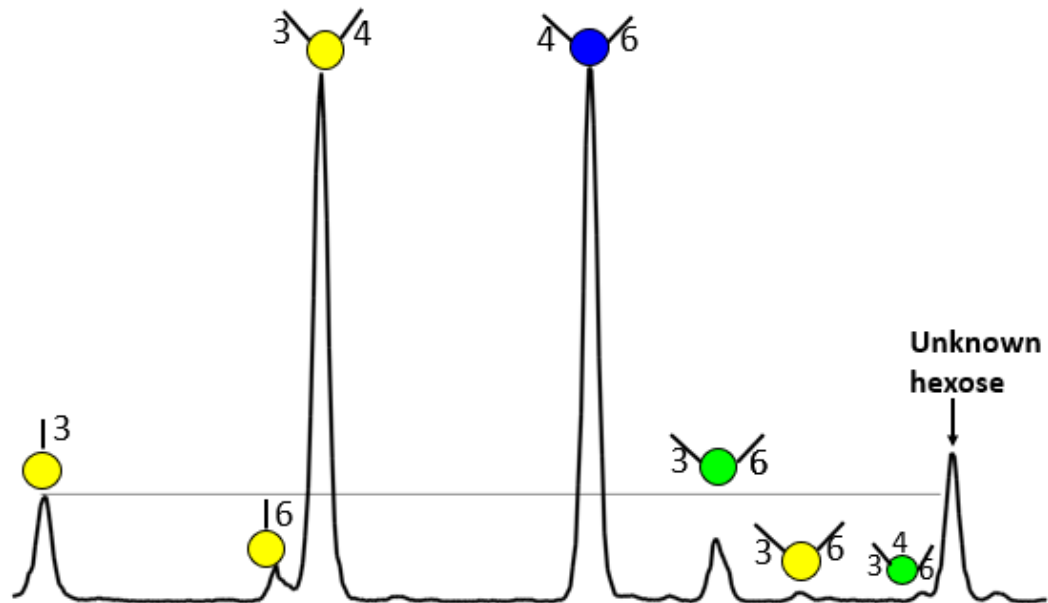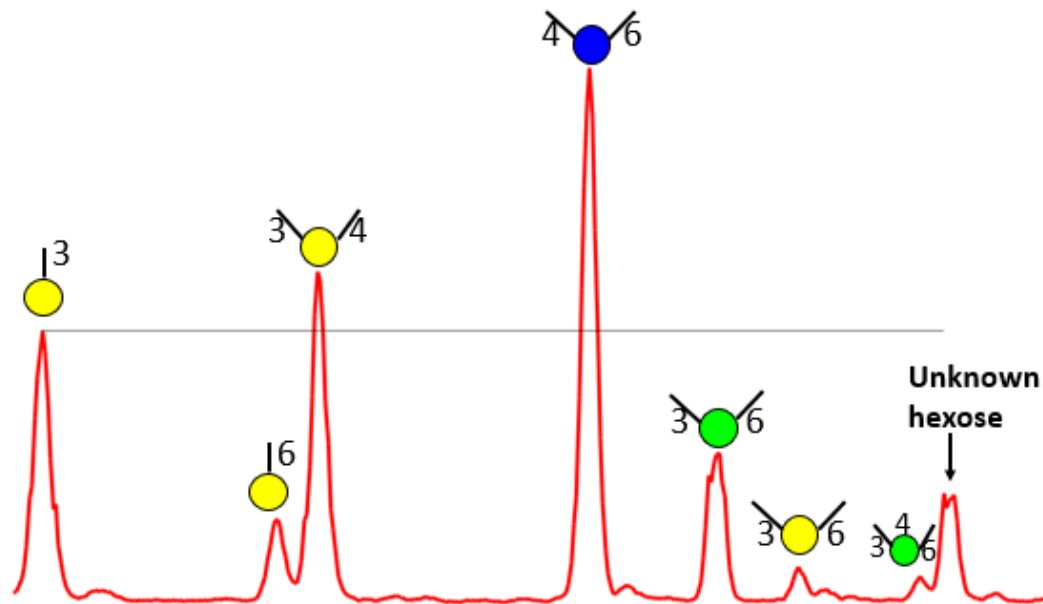
Figure 4.7. Extracted ion chromatograms (XICs) of glycan nodes derived from K562 cells showing different ratios among glycan nodes in the two methods. A & B show XIC at m/z 117.05 using the liquid phase permethylation procedure (A) or the solid phase permethylation procedure (B). The grey horizontal line is used to show the different ratios among glycan nodes in each method. The 3-Gal node was selected as a reference point

to check for undermethylation of 3-Gal in the two methods. The overall signal/yield is higher using the liquid phase approach for the eight glycan nodes shown.

Table 4.1. Analytical Reproducibility of Glycan Nodes in HepG2 Membrane Glycoproteins

Glycan Node	Day 1 CV[a]		Day 2 CV[a]		Day 3 CV[a]		All three days CV[a]		F-Test[b]
	LP	SP	LP	SP	LP	SP	LP	SP	
t-Fuc	8	2	5	2	5	4	7	3	0.0081
t-Gal	4	4	1	5	3	2	3	4	0.69
2-Man	3	4	2	5	1	2	2	5	0.00051*
4-Glc	6	9	4	8	9	9	6	10	0.35
3-Gal	3	4	3	4	3	6	4	6	0.17
6-Gal	4	6	3	4	5	6	5	5	0.90
3,4-Gal	12	18	3	26	6	18	16	32	0.55
2,4-Man	2	5	1	3	0.5	3	1	5	1.9E-05*
4,6-Glc	12	14	9	8	14	13	14	50	1.9E-05*
2,6-Man	6	7	3	2	6	4	6	16	2.2E-05*
3,6-Man	5	4	4	2	3	6	6	6	0.70
3,6-Gal	3	4	2	3	4	4	5	7	0.064
Unknown Hexose	6	12	13	17	15	23	14	27	0.71
t-GlcNAc	5	9	4	10	4	8	5	9	0.0038
4-GlcNAc	2	1	1	4	2	2	2	3	0.046
3-GalNAc	6	4	8	9	8	9	9	7	0.51
3,4-GlcNAc	3	2	3	4	3	4	3	10	1.2E-05*
4,6-GlcNAc	11	13	7	6	8	5	9	9	0.98
3,6-GalNAc	11	20	9	6	5	2	13	12	0.37

[a]%CV of total hexose or total HexNAc-normalized individual glycan nodes in HepG2 membrane glycoproteins. All glycan nodes contributing at least 1% of the total hexose or HexNAc signal are listed. Data were acquired on three different days using the liquid phase (LP) permethylation procedure (n = 6 per day) or the solid phase permethylation procedure (n = 6 per day).

[b]The F-test was used to compare inter-assay precision between the two methods for each glycan node. To correct for multiple comparisons the Bonferroni correction was used (0.05/n where n = 19). * Indicates statistically significance ($p < 0.003$).

Table 4.2. Analytical Reproducibility of Glycan Nodes in Blood Plasma

Glycan Node	Day 1 %CV[a]		Day 2 %CV[a]		Day 3 %CV[a]		All three days %CV[a]		F-Test[b]
	LP	SP	LP	SP	LP	SP	LP	SP	
t-Fuc	6	2	6	3	5	5	7	7	0.72
t-Gal	6	6	2	5	6	6	5	7	0.11
2-Man	3	3	7	1	3	5	5	4	0.48
3-Gal	11	7	5	5	10	10	10	7	0.063
6-Gal	2	4	2	1	7	8	6	8	0.21
2,4-Man	4	5	3	3	5	4	4	5	0.84
2,6-Man	4	4	2	3	5	9	12	13	0.61
3,6-Man	5	7	3	3	5	8	5	8	0.11
3,6-Gal	13	10	13	7	10	11	13	14	0.0094
3,4,6-Man	4	6	3	3	5	11	7	9	0.16
t-GlcNAc	2	3	5	5	5	5	4	7	0.0067
4-GlcNAc	0.8	2	3	2	2	2	2	2	0.50
3-GalNAc	4	8	3	4	5	4	9	6	0.14
3,4-GlcNAc	3	5	3	5	5	7	6	6	0.86
4,6-GlcNAc	6	5	11	13	6	6	10	9	0.84
3,6-GalNAc	8	9	15	13	7	13	12	18	0.29

[a]%CV of total hexose or total HexNAc-normalized individual glycan nodes in blood plasma. All glycan nodes contributing at least 1% of the total hexose or HexNAc signal are listed. Data were acquired on three different days using the liquid phase (LP) permethylation procedure (n = 6 per day) or the solid phase permethylation procedure (n = 6 per day).

[b]The F-test was used to compare inter-assay precision between the two methods for each glycan node. To correct for multiple comparisons, the Bonferroni correction was used, in which a significant difference p must be < 0.003 (0.05/n where n =19, the number of glycan nodes).

CHAPTER 5

ROLE OF BLOOD PLASMA SIALYLATION IN CANCER IMMUNITY AND

ANTICANCER IMMUNOTHERAPY

5.1 Introduction

Among the immunotherapy methods being considered for anticancer therapy, adoptive transfer of lymphokine-activated killer (LAK) cells is one of the biotherapy approaches that has been translated into clinical studies [64, 161–164]. In vitro culture of peripheral blood mononuclear cells (PBMCs) with interleukin-2 (IL-2) for several days results in a population of LAK cells with upregulated cytotoxicity against cancer cells and IFN-γ production [165]. LAK cells are composed mostly of NK cells (CD3$^-$CD56$^+$) and NKT cells (CD3$^+$CD56$^+$), and unlike cytotoxic T cells, LAK cells do not require the major histocompatibility complex (MHC) pathway to perform their antitumor activities [166]. This feature makes LAK cells an important anticancer biotherapy for those cancer cells that lack MHC and can't be targeted by T cells. The pathway through which LAK cells target and kill transformed cells is through the Natural Killer Group 2D (NKG2D) receptor [167]. The NKG2D receptor is expressed on both NK cells and NKT cells, and it acts as an activation signal when it recognizes its ligands on cancer cells [168]. When NK cells and NKT cells are activated through the NKG2D receptor, they secrete apoptosis inducing effectors that kill the cancer cells. Ligands for NKG2D include MICA, ULBP4, and ULBP1, which are implicated in NKG2D mediated recognition of multiple cancers [167, 168].

Several clinical trials have successfully activated and expanded LAK cells using IL-2 [64, 66, 161, 166, 169, 170]. When LAK cells were first introduced by Rosenberg et al in 1985 [66, 169], eleven of 25 patients showed significant cancer reduction, with one showing complete tumor regression. Recent studies have shown that the effectiveness of

IL-2/LAK immunotherapy can be improved with locoregional administration, rather than by systemic administration of LAKs [170]. However, the cytotoxicity activity of LAK cells is ephemeral after they are administered to patients. Studies have shown that LAK cell immunotherapy is more effective with the continuous administration of IL-2 [171]. After LAK cell administration to patients, LAK cells need to be continuously activated to work. IL-2 activates LAK cells, but it can also inhibit them by inducing the expansion of regulatory T cells [172]. Moreover, administration of IL-2 can cause adverse effects on patients, such as vascular leak syndrome [67]. Additionally, there are inhibitory factors that inhibit the antitumor functions of LAK cells such as MHC [173], and sialic acid overexpression on cancer cells [71, 72].

Although there are many factors that might be involved in lymphocyte cell inhibition, studies suggest that low-density lipoproteins, free cholesterols, and lipids, can also affect lymphocyte antitumor functions [89–91, 174, 175]: Low-density lipoprotein uptake inhibits the antitumor functions of γδT cells, which express NK receptors that determine their antitumor cytotoxicity [90]. Inhibition of cholesterol esterification increases CD8$^+$ T cell cytotoxic functions [174]. NK cells with increased intracellular lipid accumulation display decreased cytotoxicity effects [89, 175]. Oxidation of low-density lipoprotein by polymorphonuclear leukocytes inhibits NK activity [91]. Oxidation and desialylation of LDL are two important features in the development of atherosclerosis that appear to facilitate the increase of LDL uptake by macrophages [81, 82], smooth muscle cells [176], fibroblasts [177], and aorta cells [178]. In vitro studies have shown that oxidized-desialylated LDL samples induce an increase in intracellular accumulation of triglycerides, free cholesterol, and cholesterol esters in these cells, as compared to native LDL samples [178]. In vivo studies suggest that desialylation of LDL appears to be an

early event that leads to smaller, denser, more electronegative, and oxidized LDL particles, all of which are referred to as multiple modified LDL, which appear to be a hallmark of atherosclerosis [78, 80]. Although the link between multiple modified LDL and cancer immunity remains unclear, several studies have suggested that increased lipid accumulation and increased LDL uptake lead to the impairment of lymphocyte cytotoxic functions against cancer cells [179]. However, to our knowledge, there is still no evidence on whether multiple modified LDL affects LAK cell antitumor activity.

In this study, we found that the oxidized and/or desialylated forms of LDL modulate LAK cell cytotoxicity towards leukemia cells (K562 cells). We found that LAK cells take up oxidized-desialylated LDL to a greater extent than native LDL, and it causes them to be less cytotoxic against cancer cells. Moreover, oxidized-desialylated LDL uptake drives the downregulation of cytotoxicity associated proteins CD56 and NKG2D, as well as impairment of IFNγ production.

Oxidized-desialylated LDL becomes abundant under the conditions that foster atherosclerosis. Atherosclerosis shares multiple pathways with cancer, and it has been suggested that atherosclerosis promotes tumor development [180]. Here we found that oxidation and desialylation are two important posttranslational modifications on LDL that make it an important inhibitor of LAK cell antitumor activity. Thus, the results presented in this chapter provide a link between factors involved in atherosclerosis and the progression of cancer.

5.2 Experimental Procedures

5.2.1 Cell Culture and Cytotoxicity Assay

For LAK cell culture and expansion, peripheral blood mononuclear cells (PBMCs) were isolated by density gradient centrifugation (Ficoll-Paque-GHC-17-1440-02; GE Healthcare) from Trima Residual Apheresis collection kits (RE202-Blood Centers of the Pacific). Trima residuals were centrifuged at 1200 g for 20 minutes at 15 ^{0}C. Isolated PBMCs were cultured in serum free X-VIVO 10 medium with Gentamicin L-Gln and Phenol Red (04-380Q; Lonza) for 5 days in the presence of interleukin-2 (IL-2, 589102; BioLegend) at 0.1 µg/ml. At day 5, fresh media was added along with fresh IL-2, and LAK cell populations were cultured for 72 hours in the presence or absence of native low-density lipoprotein (LDL, 12-16-120412; 50 µg/ml, Athens Research & Technology) or oxidized-desialylated low-density lipoprotein, and LAK cell cytotoxicity was evaluated in an *in vitro* killing assay. Cells were counted via hemocytometer and Trypan blue solution (0.4 %). K562 leukemia cells were cultured in RPMI medium supplemented with 10% fetal bovine serum (FBS, SER-500, Zen-Bio). For the *in vitro* killing assays, about 800,000 LAK cells were washed three times in 2 ml serum free X-VIVO 10 media and seeded in a V-bottom 96 well plate. K562 cells were washed two times with 5 ml 1X PBS and stained with CFSE green dye (0.25 µmol/L in 1X PBS; Thermo Scientific) for 10 minutes at room temperature. Eighty microliters of target K562 cells at 10^6 cells/ml were added to a V-bottom 96 well plate containing 100 µl of the LAK cells at a 10:1 effector to target ratio, and incubated for 4 hours at 37 ^{0}C and 5% CO_2. Immediately afterward cells were centrifuged at 800 x g for 10 minutes and reconstituted in 700 µl of 1X PBS, and to this was added 2 µl of a 1 mg/ml propidium iodide solution (P3566; Thermo Scientific) which was incubated for 20 minutes and subsequently analyzed by flow cytometry.

5.2.2 Desialylation of Low-Density Lipoprotein and Glycan Node Analysis

In vitro desialylation of native low-density lipoprotein (LDL) was performed by incubating 50 µl of a 7.11 mg/ml LDL stock with 100 µl of 0.1M sodium acetate buffer pH 5, plus 50 µl of neuraminidase enzyme from Clostridium perfringens (1 U/ml, 11585886001; SIGMA) or 50 µl of water for the control. Total volume was brought up to 250 µl with water, and samples were incubated at 37 ^{0}C for 24 hours. pH was brought back to 7 with 20 µl of 0.5 M sodium bicarbonate solution. To remove neuraminidase enzyme, samples were spin filtered using Amicon Ultra-0.5 Centrifugal 100 kD spin filter devices (UFC510024; Fisher Scientific). Samples were reconstituted in 450 µl of 10 mM HEPES in 0.15 M NaCl pH 7 buffer each time for a total of 4 spin throughs. To verify complete desialylation of LDL, the glycan node analysis method [34, 96, 97, 100, 181, 182] was used. Glycan node analysis is a procedure based on glycan methylation analysis by which pooled glycans within whole biological samples are deconstructed in a way that conserves their monosaccharide and linkage information [96]. For this procedure, 60 µg of LDL were aliquoted, and to this was added 270 µl of DMSO and 105 µl of iodomethane. Then samples were added to sodium hydroxide beads for 11 minutes to drive permethylation. The rest of the steps for glycan linkage analysis of intact, complex biospecimens are described elsewhere [34, 96, 97, 100, 181, 182]. An increase in the relative abundance of terminal galactose and a near-complete loss of 6-linked galactose signals (which arise solely due to terminal sialylation of glycans) were used to verify desialylation of LDL [96].

5.2.3 Oxidation of Desialylated Low-Density Lipoprotein and TBARS Assay

A 200 µM copper(II) chloride solution was prepared using acetic acid pH 4. Desialylated LDL and/or native LDL at 1.7 mg/ml was incubated with 10 µM copper(II) chloride overnight at 4 ^{0}C to generate oxidized-desialylated and/or oxidized only LDL. For the control, native LDL was incubated with a blank acetic acid solution pH 4 at 4 ^{o}C overnight.

Oxidation was verified with the thiobarbituric acid reactive substances (TBARS) assay, as described by Aguilar Diaz de leon & Borges [88]. Briefly, to 100 µl of an LDL sample (60 µg) or calibration standards were added 200 µl of 8.1% sodium dodecyl sulfate, 1.5 ml of 20 % acetic acid solution adjusted to pH 4 with NaOH, and 1.5 ml of 0.8 % aqueous solution of thiobarbituric acid. Final volume was brought up to 4 ml with water. The mixture was heated at 95 ^{0}C for 1 hour and centrifuged at 1600 g at 4 ^{0}C. One hundred fifty microliters of supernatant was transferred to a 96 well plate, and the absorbance was measured immediately at 532 nm.

5.2.4 Flow-Cytometry Analysis

For antibody staining, LAK cells and PBMCs were labeled with monoclonal antibodies: anti-CD3, anti-CD56, and APC anti-human CD314 (NKG2D) (1D11, BioLegend). The percentage of CD3, CD56, and NKG2D positive cells was evaluated by flow cytometry in a ThermoFisher Attune NxT flow cytometer and FlowJo software. For LDL uptake measurements, 900,000 LAK cells were seeded in a 96 well plate with 225 µl X-VIVO 10 media and incubated with either native or oxidized-desialylated pHrodo Green LDL (L34355, Thermo Scientific) at 10 µg/ml for 1, 2, 8, 16, 32, and 72 hours. LAK cells were washed three times with 2 ml serum free X-VIVO 10 media, reconstituted in 700 µl 1X PBS, and immediately analyzed by flow cytometry.

5.2.5 Enzyme Linked Immunosorbent Assay (ELISA) of Interferon Gamma (IFNγ)

IFNγ was quantitatively measured in undiluted samples of LAK culture supernatant. The wells of a high binding flat bottom 96-well plate (Costar, Washington, D.C.) were first coated overnight at 4 °C with 100 µl of 1 µg/mL solution of α-Human IFNγ monoclonal antibody (Clone 1-D1K, Mabtech, Sweden) diluted in bicarbonate buffer (1 to 100 dilution),

pH 9.8. The wells were then washed 5 times with 200 µl PBS-T buffer. Next, 200 µl of 5% milk in PBS-T blocking buffer was incubated in each well for 1 hour at room temperature. Standards were diluted in PBS-T containing 5% powered milk and ranged from 2 ng/mL to 34 pg/mL of recombinant human IFNγ (R&D Systems, Minneapolis, MN). One hundred microliters of cell culture supernatants were plated in triplicate at dilutions of 1:10, 1:100, and 1:500 in 200 µl PBS-T 5% milk and incubated for 2 hours at room temperature. Samples were washed 5 times with 200 µl PBS-T. Biotinylated, secondary α-Human IFNγ monoclonal antibody (Clone 7-B6-1, Mabtech, Sweden) was diluted to 1 µg/mL in PBS-T containing 5% powered milk and 100 µl was incubated in each well overnight at 4 °C. Samples were once again washed 5 times with PBS-T, after which Precision Protein StrepTactin-HRP Conjugate (Bio-Rad, Hercules, CA) was diluted 1:250 in PBS-T containing 5% powered milk and 100 µl incubated in each well for 30 minutes at room temperature. After 5 more washes with PBS-T, 100 µl of TMB substrate (Thermo Scientific, Waltham, MA) was added to each well and allowed to incubate until a visible gradient developed in the standards, which was about 5 minutes. Subsequently, 100 µl of 2N sulfuric acid stop solution was added and the plate was read at 450 nm immediately.

5.2.6 Data Analysis

Statistical analysis was performed using two-way ANOVA with multiple comparison test for comparison of experimental groups with cytotoxicity assays, TBARS assays, and flow cytometry analysis. For glycan linkage analysis, each uniquely linked monosaccharide was quantified by integrating extracted ion chromatogram peak using QuanLynx software. Integrated peaks were exported to an Excel spreadsheet. Statistical significance between glycan nodes was determined using two-tailed t-tests. Statistical analysis was performed using GraphPad.

5.3 Results

5.3.1 Initial Hypothesis

It is well established that increased sialylation is a mechanism by which cancer cells evade an immune response [76], and now days there are sialic acid-based targeting strategies for cancer therapy [183]. Increased cell surface sialylation on cancer cells allows the inhibition of natural killer cells and Tumor infiltrating lymphocytes by engaging the inhibitory Siglec receptors on NK cells or T-cells [184, 185]. By following such well-established principles on aberrant sialylation in cancer, we hypothesized that increased sialylation of blood plasma glycoproteins would also enhance inhibitory Siglec binding, causing NK cell and T-cell inhibition. To test this hypothesis, we incubated PBMCs with IL-2 overnight to generate NK cells. We then induced *in vitro* desialylation of human serum glycans by incubating human serum with neuraminidase enzyme overnight, removed sialidase enzyme with a 100 kD molecular weight (MW) cutoff spin filter, and then incubated IL-2 stimulated-PBMCs with the high MW components (>100 kD) of the filtered sialylated serum or desialylated serum to see how this affected the cytotoxicity of PBMCs against K562 cells in a 4-hour killing assay. However, the results were unexpected; desialylation induced a significant inhibition of PBMC cytotoxicity against target cancer cells (K562 cells) (**Figure 5.1**). Hence, there appeared to be a human serum factor, that when desialylated, induced a significant inhibition of PBMC cytotoxicity. We knew that this desialylated human serum factor that caused PBMC inhibition had to be >100 kDa because the desialylated high molecular weight components (>100 kD) of the human serum had been incubated with PBMCs overnight. Alpha-2-macroglobulin is a protein with a MW greater than 100 kD, however, we had already previously tested the inhibitory capacity of this protein in PBMC cytotoxicity. Alpha-2-macroglobulin was deglycosylated with PNGase F enzyme. Both native and deglycosylated alpha-2-macroglobulin were

incubated with IL-2-stimulated-PBMCs, but glycosylation on alpha-2-macroglobulin had no effect on PBMC cytotoxicity (data no shown). Hence we inferred that desialylation of alpha-2-macroglobulin would have no effect on PBCM cytotoxicity either. . We then tested IgGs. Pre-isolated IgG was desialylated with neuraminidase enzyme overnight. Then, neuraminidase enzyme was removed by spin filtration using a 100 kD MW cutoff spin filter, then incubated overnight with IL-2 stimulated-PBMCs, and cytotoxicity was evaluated in a 4-hour killing assay with K562 cells. Even though both native IgG and desialylated IgG caused a significant inhibition in PBMC cytotoxicity against K562 cells (data no shown), there was no significant difference in cytotoxicity between native IgG and desialylated IgG (data no shown). Hence, IgG wasn't the desialylated factor in human serum that caused PBMC inhibition. At this point it was nearly impossible to test every single protein and antibody in human serum. Therefore, first we wanted to know if these phenomena was even biologically relevant in human serum. We searched the literature to see if desialylation was a biologically relevant feature in biology, and we came across "desialylated" low-density lipoprotein (LDL) [80]. Desialylated LDL is a hallmark of atherosclerosis because it promotes atherosclerosis [80]. Therefore, we decided to test LDL. Pre-isolated LDL was desialylated with neuraminidase enzyme overnight, spin filtered with a 100 kD filter device, and incubated with IL-2-stimulated PBMCs overnight. Results showed that LDL was a desialylated human serum factor responsible for PBMC cytotoxicity inhibition (pilot data not shown). Therefore, we decided to pursue these experiments with LDL further to investigate the role of desialylated LDL in cancer immunity. For the following experiments with LDL, we decided to incubate PBMCs with IL-2 for 5 days instead of 1 day to generate lymphokine activated killer cells. The reason for using LAK cells is that LAK cells offered greater cytotoxicity against K562 cells—and cytotoxicity assays with LAK cells were more consistent and reproducible.

5.3.2 Oxidized-Desialylated LDL Inhibits LAK Cell Cytotoxicity *In Vitro.*

This study was initiated by investigating the capacity of desialylated LDL to inhibit LAK cell cytotoxicity. For this purpose, PBMCs were activated and expanded *in vitro* for 8 days in the presence of IL-2 to generate lymphokine activated killer (LAK) cells. LAK cells are composed of NK cells (CD3$^-$CD56$^+$) and NKT cells (CD3$^+$CD56$^+$). Analysis of IL-2 treated PBMCs by flow cytometry revealed an induced population of cells of which about 6% were NK cells and another 4% were NKT cells (**Figure 5.2**). This population of cells, referred to as LAK cells, were optimally cytotoxic against K562 cells in a 4-hour killing assay at a 10:1 effector to target ratio (**Figure 5.3**). Native LDL was desialylated with neuraminidase enzyme and added to the LAK cells at day 5 at 50 µg/ml and incubated for 72 hours. Our glycan node analysis procedure [34, 96, 97, 100, 181, 182] was used to verify LDL desialylation prior to adding the LDL samples to the LAK cells. An increase in the relative abundance of terminal galactose, a decrease in 3-linked galactose, and a near-complete loss of 6-linked galactose revealed a major decrease in the number of terminal sialic acid residues present on LDL (**Figure 5.4**). Only a small inhibition of LAK cell cytotoxicity was observed every time we performed a K562 killing assay after having exposed the LAK cells to desialylated LDL (**Figure 5.5**). Because previous research has demonstrated that desialylation of LDL appears to be an early event that leads to its oxidation in atherosclerosis [83], we induced oxidation of desialylated LDL with Cu(II) ions. A thiobarbituric acid reactive substances (TBARS) assay revealed that Cu(II)-treated native and desialylated LDL were approximately 50% more oxidized than their untreated LDL counterparts (**Figure 5.6**). Desialylated and oxidized LDL was then added to the LAK cells at 50 µg/ml (5 mg/dL) and incubated for 72 hours to see how LDL with both modifications affected the cytotoxicity of LAK cells. Significant inhibition of LAK cell cytotoxicity was observed when LDL was both oxidized and desialylated (**Figure 5.5**). A lesser degree of

inhibition was observed when LAK cells were treated with merely desialylated LDL. Oxidation alone did not induce a significant inhibition of LAK cell cytotoxicity (**Figure 5.5**). To ensure that inhibited K562 cell killing was not simply due to loss of LAK cells, LAK cell viability was checked by incubating the LAK cells with oxidized-desialylated LDL for 72 hours and labeling with Sytox Blue. Cell viability was determined using flow cytometry. Results revealed that treatment of LAK cells with oxidized-desialylated LDL induced a small toxic effect (about 4 %) (**Figure 5.7**). By comparison, the magnitude of the inhibition effect observed in Fig. 1 suggests that the inhibition of K562 cell killing by pre-treating LAK cells with oxidized-desialylated LDL is not simply due to the toxicity of oxidized-desialylated LDL toward LAK cells.

5.3.3 Enhanced Uptake of Oxidized-Desialylated LDL by LAK Cells

pHrodo Green-labeled LDL was desialylated with neuraminidase enzyme and oxidized with 10 µM Cu(II) ions. LAK cells were then incubated with native and oxidized-desialylated forms of pHrodo green LDL (**Figure 5.8**). During the first two hours of incubation, LAK cells took up native LDL faster than oxidized-desialylated LDL. After 8 hours of incubation, the uptake of native and oxidized-desialylated LDL was the same, with no significant difference. However, after 16, 32, and 72 hours, oxidized-desialylated LDL was taken up to a greater extent than native LDL in a time-dependent manner. After 72 hours, a clear increase in oxidized-desialylated LDL uptake was observed (**Figure 5.8B**). Non-significant differences in uptake were observed for oxidized LDL and, separately, desialylated LDL compared to native LDL (data not shown).

5.3.4 Oxidized-Desialylated LDL Downregulates the Cytotoxicity Receptors CD56 and NKG2D

LAK cells express the surface markers CD56, CD3, and NKG2D. CD56 and NKG2D are cytotoxicity associated receptors expressed on both NK cells and NKT cells, and CD3 is an activating receptor expressed on NKT cells and T cells [186]. Because LAK cell anti-cancer (anti-K562) activity was reduced in the 4-hour killing assay upon LAK cell uptake of oxidized-desialylated LDL over a 72-hour period, we tested whether the expression levels of these receptors were also affected. After gating all the live cells and plotting them against CD3 and NKG2D, a decrease in the proportion of CD56$^+$ cells and CD3$^+$CD56$^+$ cells was observed (**Figure 5.9A-C**). Interestingly, it was observed that as the number of CD3$^-$CD56$^+$ cells and CD3$^+$CD56$^+$ cells decreased, the number of CD3$^+$-only cells increased (**Figure 5.9D**). This inverse relationship implies that oxidized-desialylated LDL causes LAK cells to differentiate into CD3$^+$-only rather than CD56$^+$ cells, making them less cytotoxic against K562 cancer cells. It was also observed that native LDL induced a small increase in the number of CD56$^+$ cells, although in the 4-hour killing assay no change in cytotoxicity was observed.

Additionally, it was observed that native LDL induced a small increase in the expression of NKG2D receptor (**Figure 5.10A-C**). However, oxidized-desialylated LDL downregulated the percentage of CD3$^-$NKG2D$^+$ cells while slightly increasing the percentage of CD3$^+$NKG2D$^+$ cells (**Figure 5.10A-C**). A small increase in the number of CD3$^+$ only cells was also observed in the oxidized-desialylated treated samples (**Figure 5.10D**).

5.3.5 Oxidized-Desialylated LDL Impairs Interferon Gamma (IFN-γ) Production

Interferon gamma (IFN-γ) is a pleiotropic cytokine with antitumor functions. IFN-γ is secreted by NK cells and NKT cells, and it is often considered the major effector of

immunity [187]. Because oxidized-desialylated LDL caused an inhibition of LAK cell cytotoxicity and downregulation of the cytotoxicity receptors, we investigated whether production of IFN-γ was altered during the process. An ELISA was performed to quantitively measure soluble IFN-γ in LAK cell supernatants that had been treated with native LDL or oxidized-desialylated LDL. Results showed that oxidized-desialylated LDL decreased the production of IFN-γ. Previous research has shown that native LDL downregulates the production of IFN-γ in γδT cells [90]—prompting expectations of a similar result. Unexpectedly, however, native LDL significantly enhanced the production of IFN-γ in LAK cells (**Figure 5.11)**.

5.4 Discussion

Cancer and atherosclerosis are distinct diseases that share several molecular pathways, with some studies suggesting that atherosclerosis can lead to cancer development [180]. Characteristic features of both diseases include inflammation, uncontrolled cell proliferation, and oxidative stress [188]. Atherosclerosis is characterized by chronic inflammation, diabetes, hypertension, dyslipidemia, and obesity, all of which are predisposing risk factors for cancer [188]. At the molecular level, inflammation leads to the production of inflammatory cytokines, such as IL-6, IL-1β, and TNF, which have been associated with cardiovascular disease and several different types of cancer [189]. High concentrations of biomarkers for reactive oxygen species such as oxidized LDL and myeloperoxidase (MPO), have been found in the blood plasma of cancer patients and atherosclerosis patients, and the origin of both diseases is associated with oxidative stress [190, 191]. Additionally, it has been found that the metabolism of unstable atherosclerotic plaques is similar to that of cancer cells [192].

Oxidation and desialylation of low-density lipoprotein are hallmark modifications of LDL in atherosclerosis that contribute to the initiation and progression of the disease [80]. These modifications are believed to be needed to facilitate increased LDL uptake by atherosclerotic cells and cause them to have increased intracellular triglycerides, free cholesterol, and cholesterol esters [78, 80]. Although little is known about oxidized-desialylated LDL in cancer, literature suggests that this type of LDL is involved in tumor development [85]. Long term exposure of human vascular smooth muscle cells (hVSMC) to chemically oxidized LDL promotes the overexpression of osteopontin, a glycoprotein involved in cancer metastasis [193]. Inflammation is a characteristic feature of both atherosclerosis and cancer, and studies have shown that oxidized LDL triggers inflammation. Macrophages take up oxidized LDL via scavenger receptors which, once inside the cell, induce cholesterol crystals that ultimately activate the inflammasome to release IL-1β and TNF cytokines, which are mediators of inflammation in both cancer and atherosclerosis [194–197].

Although it has been suggested that oxidized-desialylated LDL plays a role in cancer development [198], little is known about the role that LDL plays in antitumor immunity. It has been previously shown that accumulation of native LDL in γδ T cells leads to reduced antitumor function [90]. A different study showed that when LDL becomes oxidized by polymorphonuclear lymphocytes, it inhibits NK cell cytotoxicity [91]. However, to our knowledge the role of LDL that is both oxidized and desialylated on the cytotoxicity of LAK cells has been unknown until now. Oxidation and desialylation are characteristic features of LDL in atherosclerosis [80]; the meaning of this in cancer immunity is still not well understood. We found that oxidized-desialylated LDL is taken up by LAK cells more

114

extensively than native LDL after 16 hours of incubation, which leads to reduction of LAK cell cytotoxicity.

The data presented here showed that the expression of the cytotoxicity-associated receptors CD56 and NKG2D, which determine the ability of LAK cells to mediate cancer cell lysis [199], was downregulated upon exposure of LAK cells to oxidized-desialylated LDL. This occurred in pre-expanded LAK cells that were kept on IL-2 stimulation during the incubation with oxidized-desialylated LDL. Thus IL-2 stimulation was not able to compensate for the inhibitory effect of oxidized-desialylated LDL. We also found an impairment in the production of IFNγ, a pleiotropic cytokine secreted by LAK cells. These results, however, differ according to the use of different cytotoxic lymphocytes. For instance, a different study found that native LDL can lower the expression of CD56 and NKG2D cytotoxicity receptors and IFN-γ in γδT cells [90]. However, we observed the opposite in that native LDL induced a small increase in the expression of CD56, NKG2D, and IFN-γ in LAK cells. Nevertheless, previous studies and our work show that enhanced uptake of LDL by cytotoxic immune cells can impair their antitumor capacity.

Multiple modified LDL has been extensively studied in the context of atherosclerosis, and how it can contribute to the development of this disease [79]. Although it is unknown how LDL becomes multiply modified in atherosclerosis, our findings suggest that the desialylated and oxidized LDL that is produced as a byproduct of atherosclerosis may at least partially inhibit the ability of the immune system to effectively surveil against cancer cells. Thus, the data presented here suggests at least one particular mechanistic link between atherosclerosis and cancer. Future research investigating the

link between multiple modified LDL and cancer immunity will help establish additional details on the complex connection between these two devastating chronic diseases.

5.5 Conclusion

LDL is a human serum factor that when it becomes desialylated inhibits LAK cell antitumor activity. It was observed that inducing oxidation of LDL along with its desialylation, the magnitude of the inhibition effect was much greater. However, the cytotoxicity assays showed that oxidization alone is not enough to inhibit LAK cell cytotoxicity since non-significant inhibition was observed. The reduced cytotoxicity of LAK cells was further corroborated by a reduction in the number of CD56$^+$ and Natural Killer Group 2D (NKG2D) receptor positive cells, as well as impairment of IFN-γ production. pHrodo Green LDL was used to measure the rate at which LAK cells take up both native and oxidized-desialylated LDL for a period of 72 hours. It was observed that during the first two hours native LDL is taken up faster than oxidized-desialylated LDL. However, after 16, 32 and 72 hours, oxidized-desialylated LDL is taken to a significantly greater extent than native LDL. In summary, these results suggest that oxidization and desialylation facilitate LDL uptake by LAK cells and inhibit their antitumor functions.
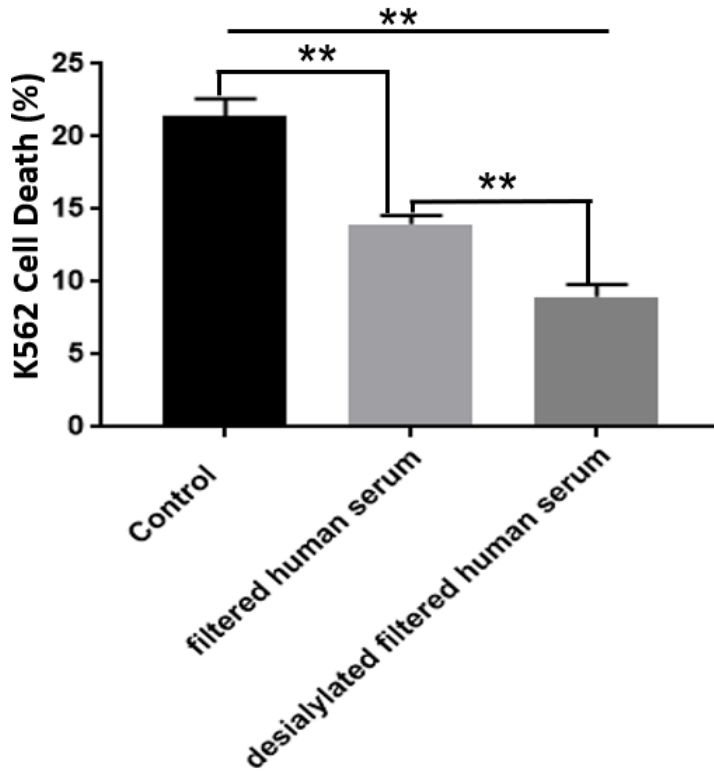
Figure 5.1. Desialylation of human serum inhibits NK cell cytotoxicity. Human serum was heat inactivated by heating at 56 ^{0}C for 25 minutes. Heat inactivated human serum was incubated with neuraminidase enzyme pH 5 for 24 hours at 37 ^{o}C. Then serum was filtered using a spin filter with a 100 kDa MW cutoff ("filtered human serum"). The high molecular weight components (>100 kD) of the filtered human serum (desialylated and sialylated) were incubated with IL-2 overnight induced PBMCs for 24 hours. ** Indicates statically significant differences between groups (p<0.001). Statistical significance determined using one-way ANOVA with Turkey posthoc test. n = 4 per group. Error bars represent standard deviation.
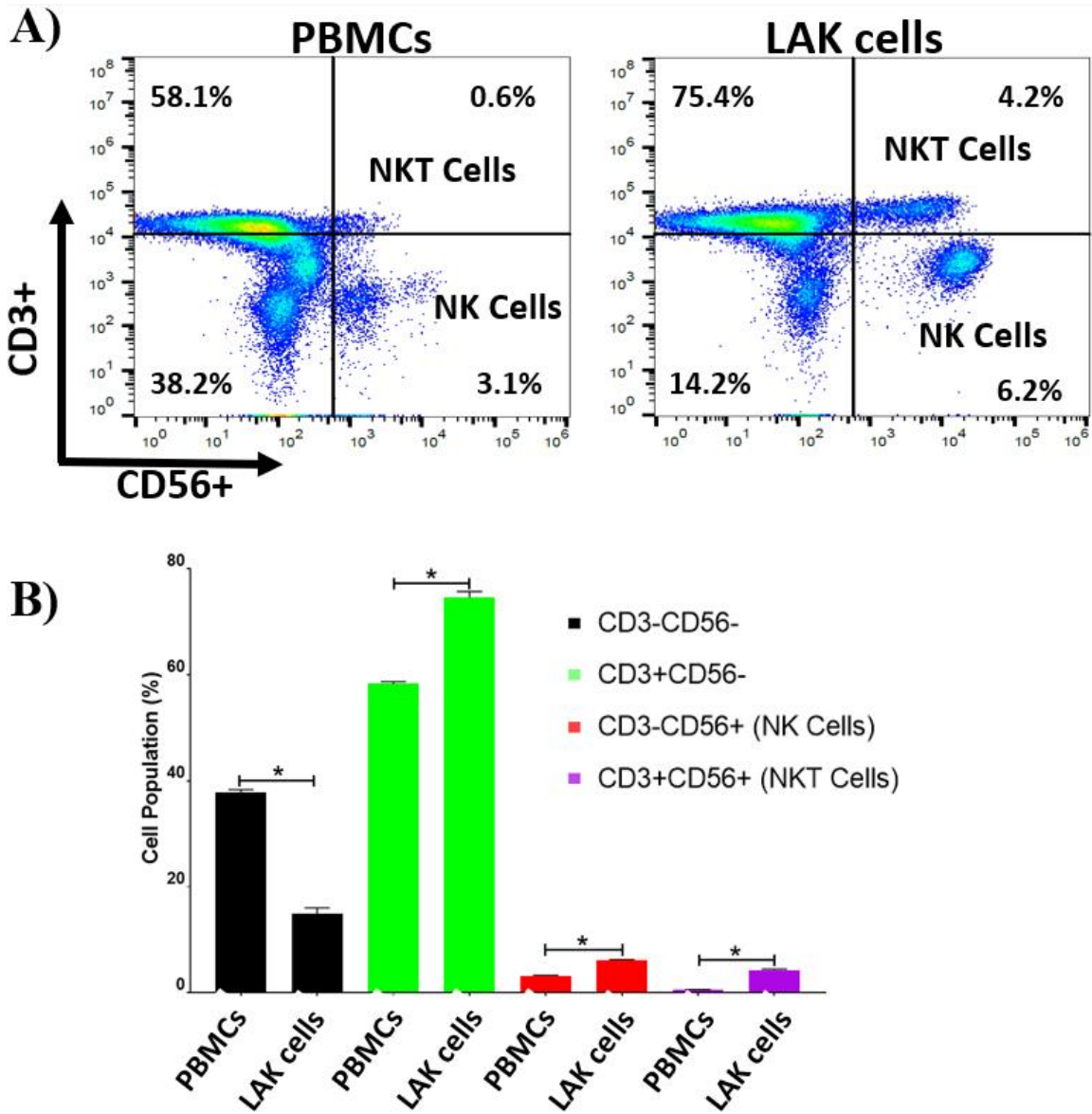
Figure 5.2. LAK cell phenotype. **A)** Lymphokine Activated Killer (LAK) cells (**right**), induced by exposure of PBMCs (**left**) to IL-2 for 8 days are composed of NK cells (CD3⁻ CD56⁺) and NKT cells (CD3⁺ CD56⁺). **B)** CD3 and CD56 marker expression on PBMCs vs. LAK cells. n = 4 per group. * indicates a statistical significance (p<0.001). Error bars represent standard deviation. Statistical significance determined using individual two tailed t-tests.

Cytotoxicity assay with LAK cells
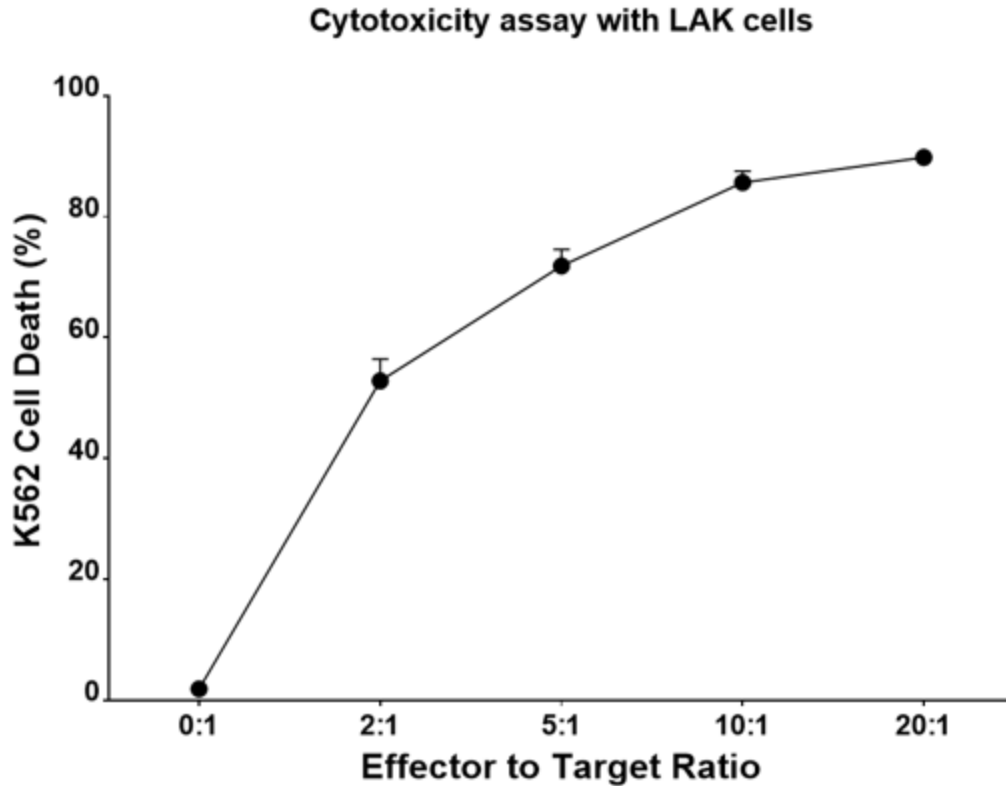
Figure 5.3. Cytotoxicity assay effector cell ratio optimization. Lymphokine Activated Killer (LAK) cells were optimally cytotoxic against K562 cells at a 10:1 effector to target ratio. PBMCs were incubated with 0.1 µg/ml IL-2 for 8 days to generate LAK cells. K562 cells were labeled with CFSE green dye and co-incubated with unlabeled LAK cells for 4 hours at different effector to target ratios. Error bars represent standard deviations. n = 4 per group.
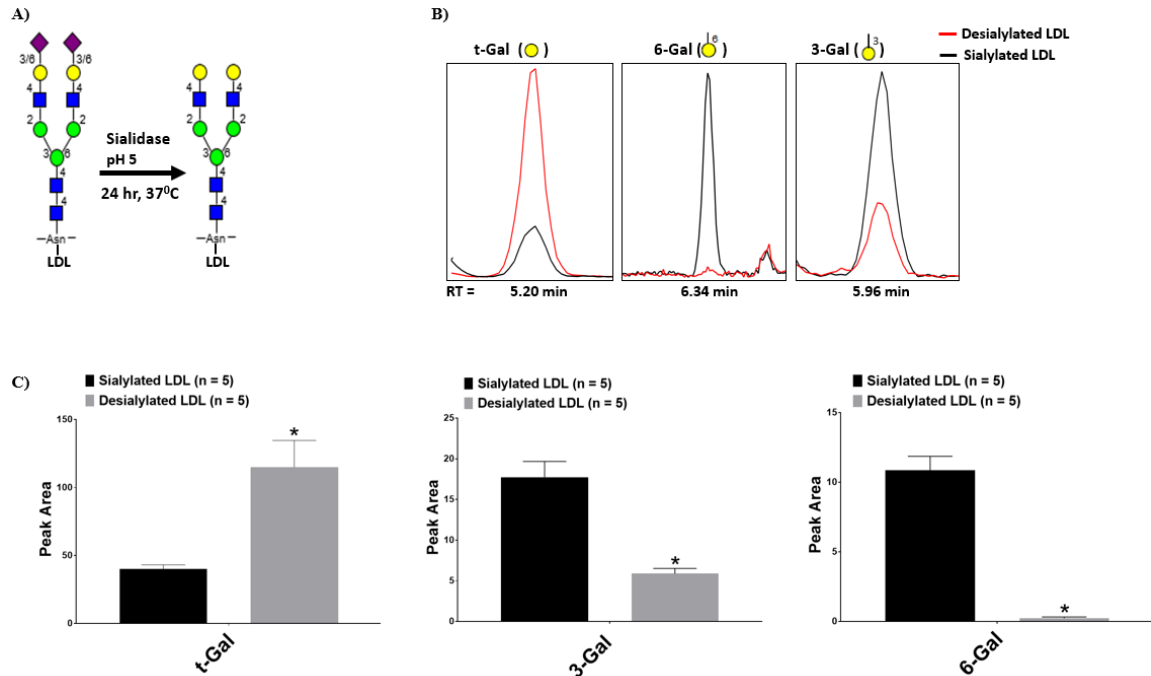
Figure 5.4. In vitro LDL desialylation and glycan node analysis. A) LDL samples were desialylated with neuraminidase enzyme (1 U/ml) in 0.1 M sodium acetate buffer pH 5 at 37 ^{0}C for 24 hours. Representative molecular changes are illustrated. **B)** Summed extracted ion chromatograms at m/z 117.05+ 145.1 for terminal galactose (t-Gal), m/z 161.1 + 233.1 + 189.1 for 6-linked galactose (6-Gal), and 161.1 + 233.1 for 3-linked galactose (3-Gal) show a significant decrease in terminal sialylation, as determined by glycan node analysis [34, 96, 97, 100, 181, 182]. **C)** Quantitative summary of illustrative data shown in B that reveal a major increase in terminal galactose residues, a decrease in 3-linked galactose residues, and a near-complete loss of 6-linked galactose residues, indicating an overall decrease in terminal neuraminic acid residues. Statistical significance determined using a two tailed t-test. n = 5 per group. * indicates a statistically significant difference (p<0.001). Error bars represent standard deviation.
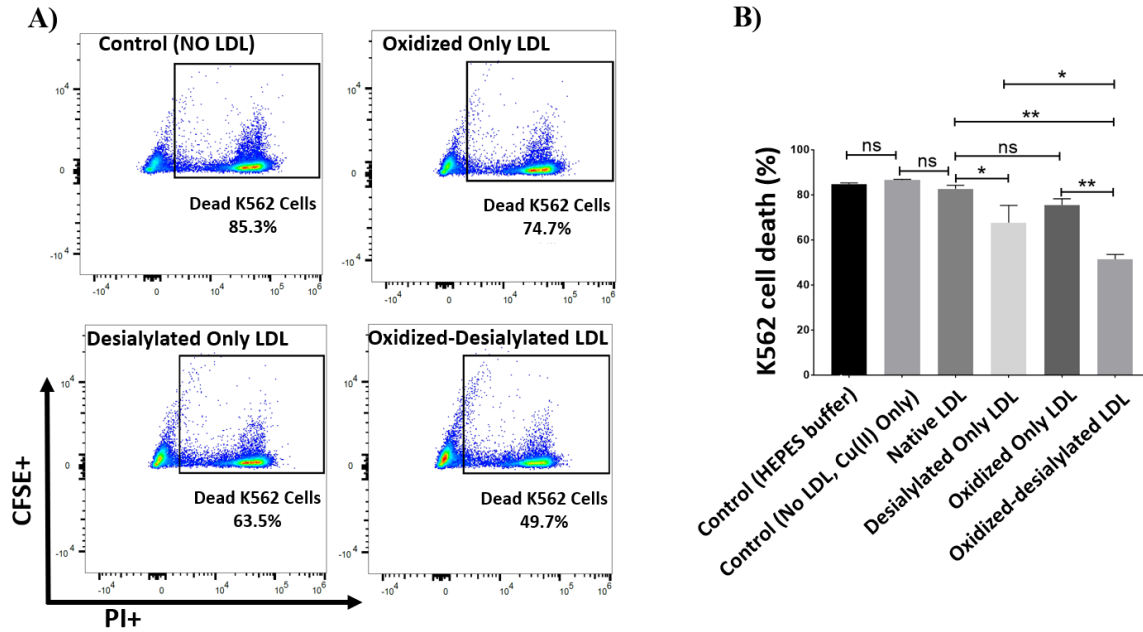
Figure 5.5. Oxidized-desialylated LDL inhibits LAK cell cytotoxicity in vitro. A) Activated and expanded LAK cells were cultured in serum free X-VIVO 10 media in a 24 well plate with 0.1 µg/ml IL-2 in the absence or presence of native LDL, oxidized only LDL, desialylated only LDL, or oxidized-desialylated LDL at 50 µg/ml for 72 hours. Then LAK cells were washed three times with X-VIVO 10 serum free media to remove residual external LDL and incubated in a 4-hr killing assay with K562 cells at a 10:1 effector to target ratio. Percent cytotoxicity was determined by flow cytometry. **B)** Quantification of K562 cell death. **indicates a statically significant difference between native LDL (control) and oxidized-desialylated LDL treated LAK cells, and oxidized only LDL vs oxidized-desialylated LDL treated LAK cells (p<0.0001).* indicates significant difference between native LDL and desialylated only LDL, and desialylated only LDL vs oxidized-desialylated (p <0.001) treated LAK cells, n = 5 per group. ns indicates not statistically significant. Statistical significance determined using two-way ANOVA with Tukey posthoc test. Error bars represent standard deviation.
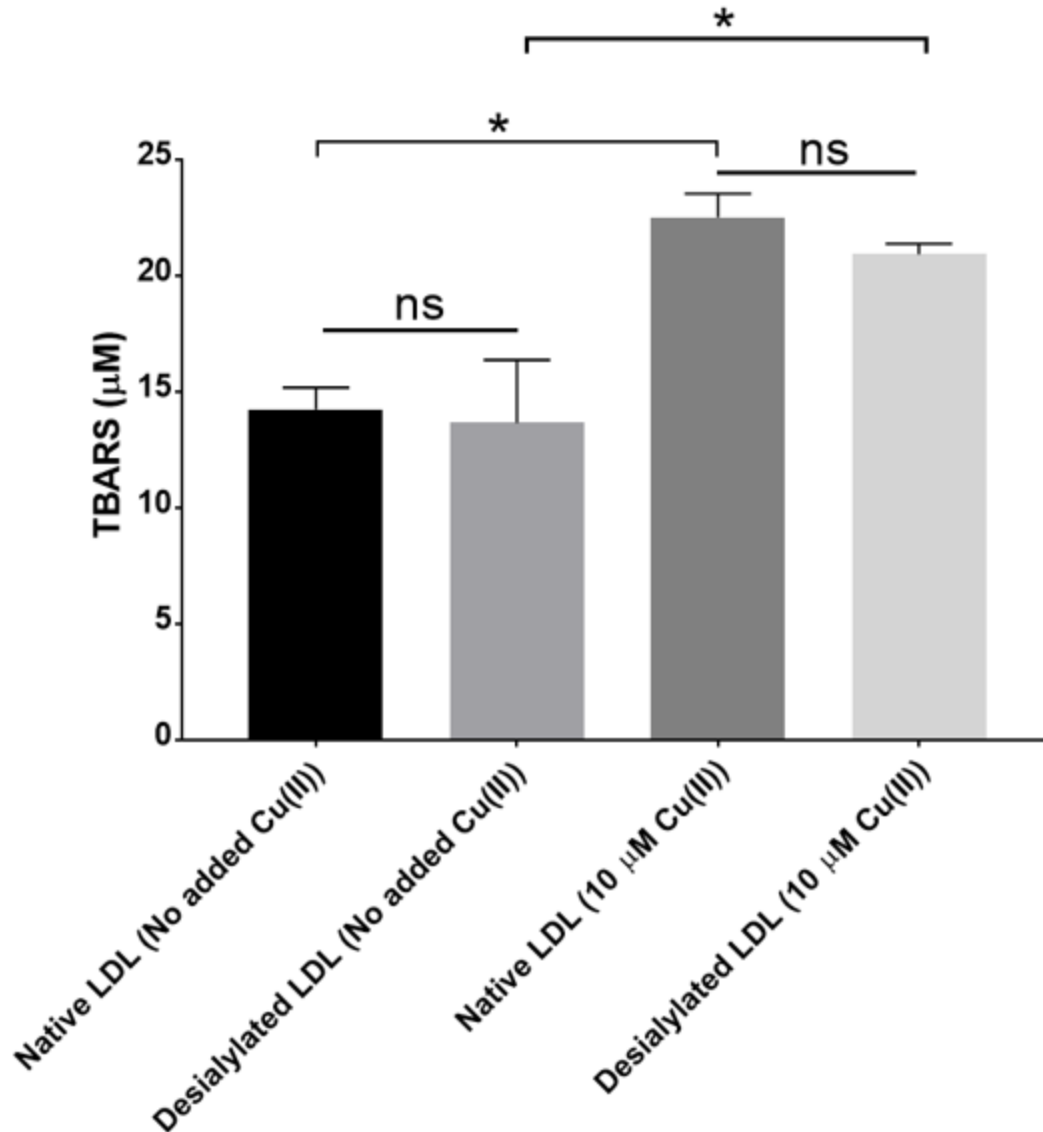
Figure 5.6. In vitro LDL oxidation. After desialylation, samples were incubated with 10 µM Cu (II) ions for 24 hours at 4 ^{0}C to drive oxidation of LDL. Levels of LDL oxidation were verified by measuring the production of thiobarbituric acid reactive substances (TBARS) [88]. Error bars represent standard deviation. * indicates statistically significant differences between samples (p<0.001) and ns indicates no significant difference. n = 5 per group. Statistical significance determined using a two-way ANOVA test with Tukey posthoc test.
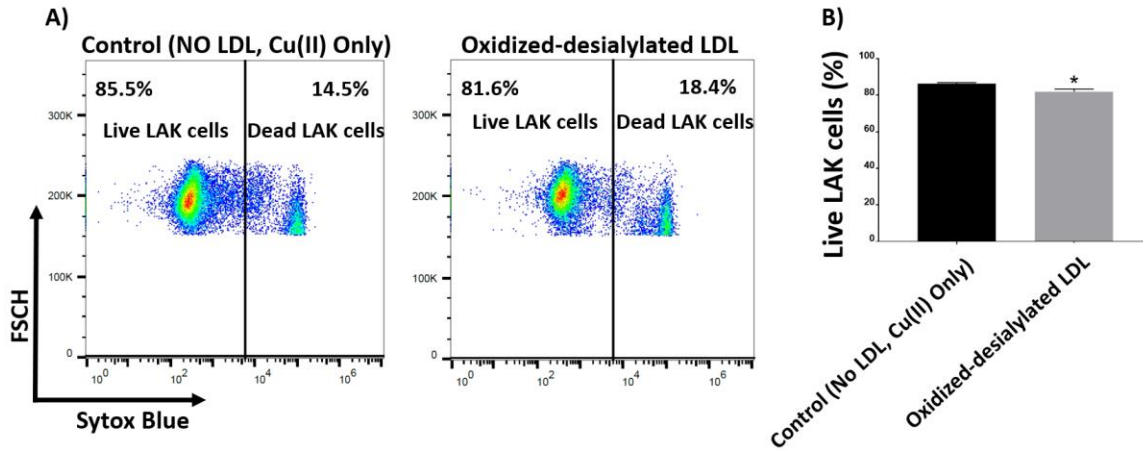
Figure 5.7. LAK cell viability. A) LAK cells were incubated with oxidized-desialylated LDL for 72, then LAK cells were stained with Sytox blue and analyzed by flow cytometry to determine LAK cell viability. FSCH stands for forward scatter cell signal height which facilitates selection of single cells. **B)** Oxidized-desialylated LDL was slightly toxic to the LAK cells. n = 4 per group. Statistical significance determined using a two-tailed t-test. * indicates a statistically significant difference (p = 0.028). Error bars represent standard deviation.
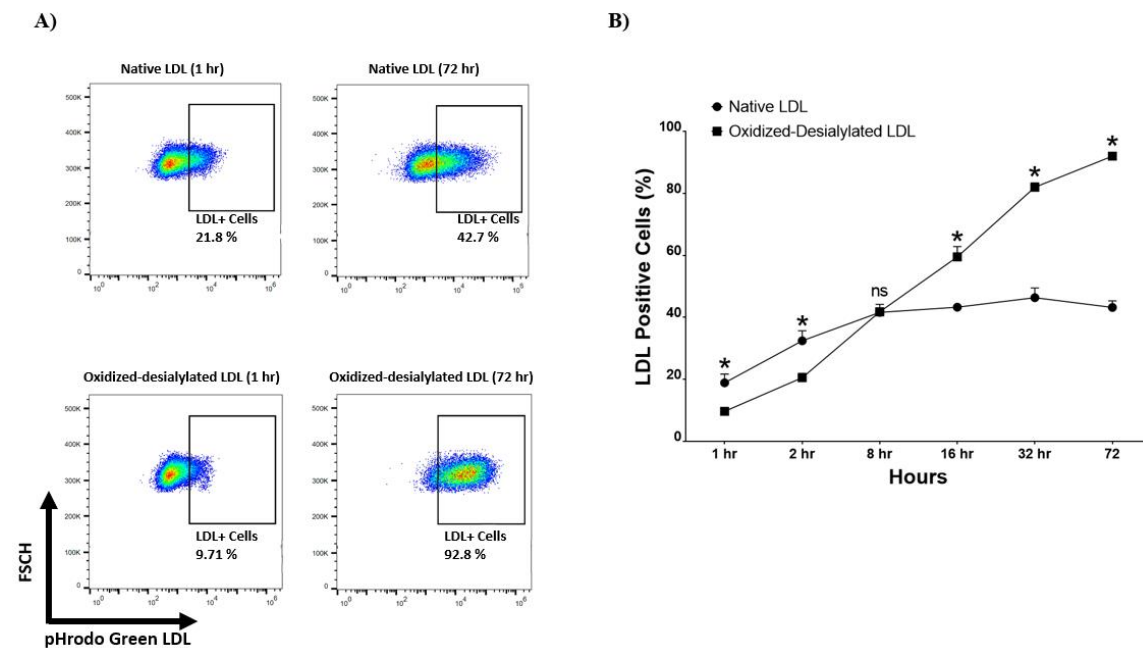

Figure 5.8. Enhanced uptake of oxidized-desialylated LDL by LAK cells. LAK cells were cultured in serum free X-VIVO 10 media in a V-bottom 96 well plate with IL-2 in the absence or presence of native pHrodo Green Conjugate LDL or oxidized-desialylated pHrodo Green Conjugate LDL at 10 µg/ml for 1, 2, 8, 16, 32, and 72 hours. The percentage of LDL positive cells was measured by flow cytometry. **A)** Qualitative flow data showing uptake of oxidized-desialylated LDL and native LDL, which shows the differences in uptake between the two forms of LDL. FSCH stands for forward scatter cell signal height

123

which facilitates selection of single cells. **B)** Time course of native LDL and oxidized-desialylated LDL uptake by LAK cells. * Indicates statically significant differences between native LDL (control) and oxidized-desialylated LDL treated LAK cells (p<0.001). Statistical significance determined using multiple t-tests (one per group) and corrected for multiple comparisons using the Holm-Sidak method. n = 3 per time point. Error bars represent standard deviation. For some points, errors bars are shorter than the symbol, and error bars are not shown.
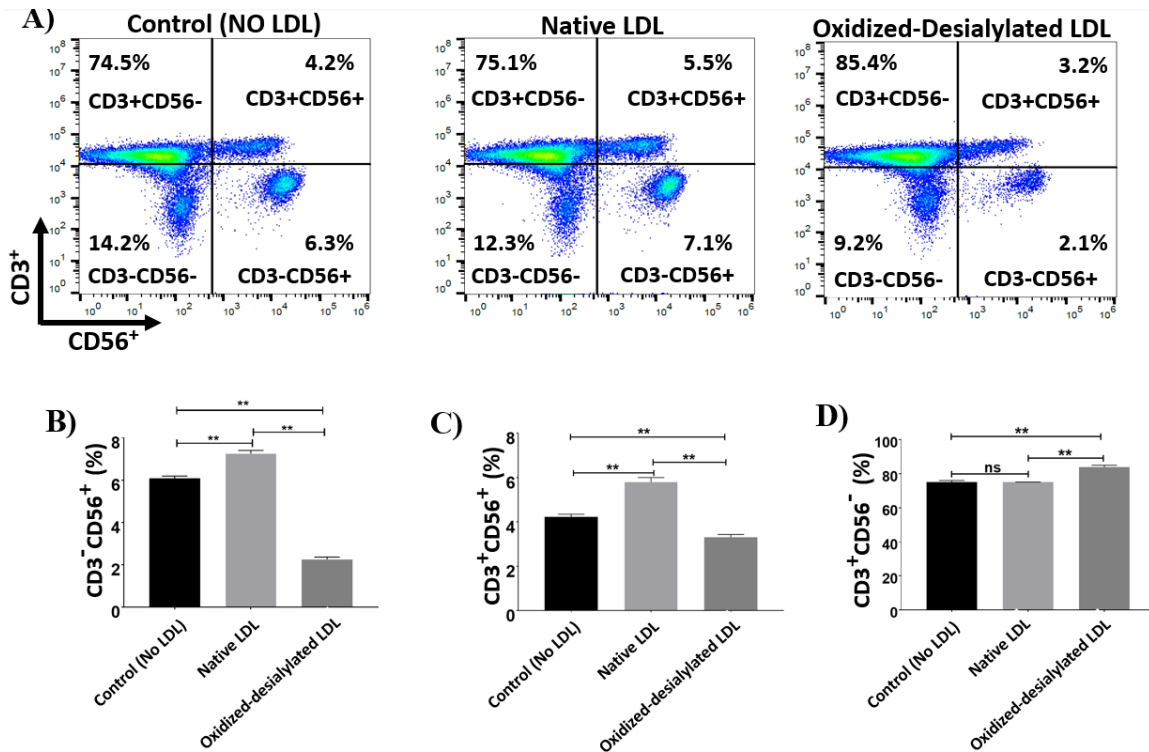
Figure 5.9. Oxidized-desialylated LDL downregulates cytotoxicity receptor CD56 and upregulates the CD3 receptor. Activated and expanded LAK cells were cultured in serum free X-VIVO 10 media in a V-bottom 96 well plate with IL-2 in the absence or presence of native LDL or oxidized-desialylated LDL at 50 μg/ml for 72 hours. Then LAK cells were washed three times with X-VIVO 10 serum free media, reconstituted in PBS, and labeled with anti-CD56 antibodies, as well as with the dead staining dye SytoxBlue. **A)** Live cells were gated and plotted against CD3 and CD56. **B)** Oxidized-desialylated LDL decreased the number of CD3⁻CD56⁺ cells. **C)** The number of NKT cells (CD3⁺ CD56⁺) also decreased significantly. **D)** The number of CD3 positive cells increased significantly upon oxidized-desialylated LDL treatment of LAK cells. n = 5 per group. Error bars represent standard deviation. ** indicates statically significant differences (p<0.0001), determined using one-way ANOVA with Tukey posthoc test.
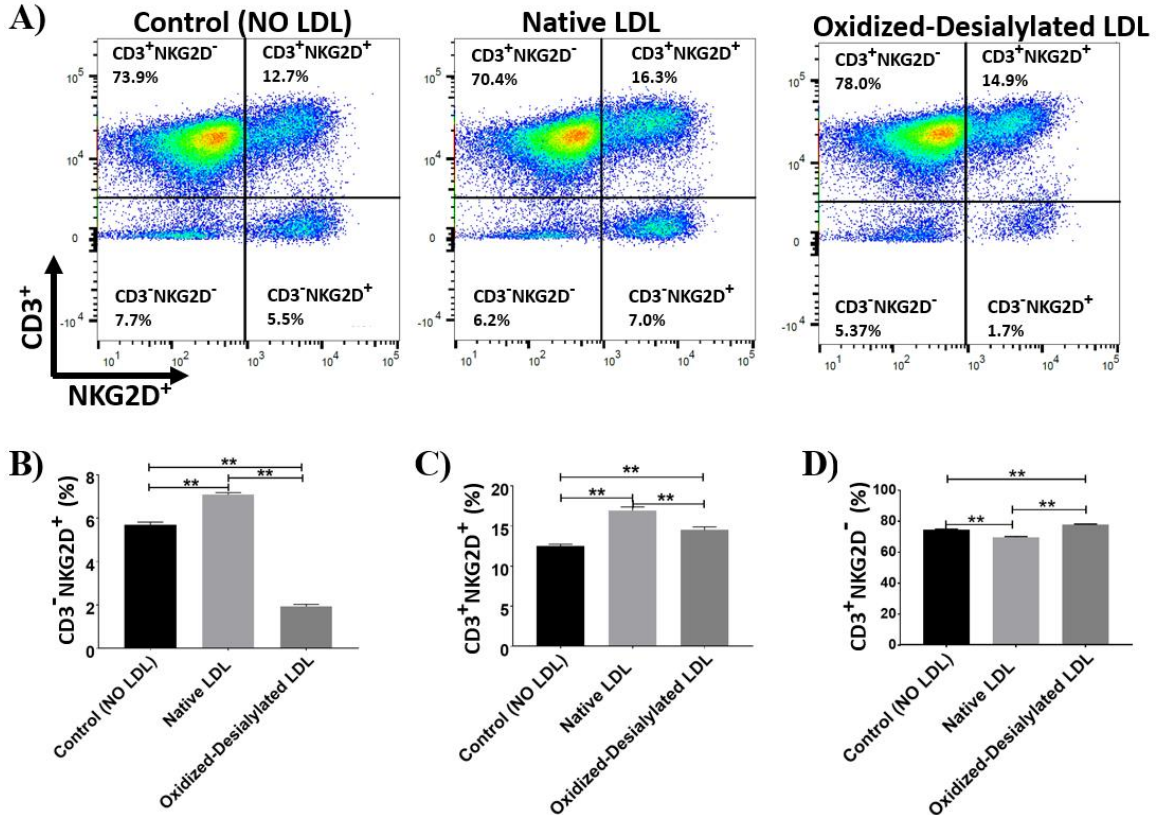
Figure 5.10. Oxidized-desialylated LDL downregulates activating receptor NKG2D.
LAK cells were cultured and washed as described in Fig. 3. Then LAK cells were labeled
with anti-NKG2D antibodies, as well as with the dead staining dye SytoxBlue. A) Live cells
were gated and plotted against CD3 and NKG2D. B) Oxidized-desialylated LDL decreased
the number of CD3⁻NKG2D⁺ cells. C) Oxidized-desialylated LDL increased the number of
CD3⁺ cells relative to the LDL-free control, but decreased them relative to treatment with
native LDL. D) Oxidized-desialylated LDL increased the percentage of CD3⁺NKG2D⁻ cells
relative to both other groups. n = 5 per group. ** indicates statistically significant
differences (p<0.0001), determined using one-way ANOVA with Tukey posthoc test. Error
bars represent standard deviation.
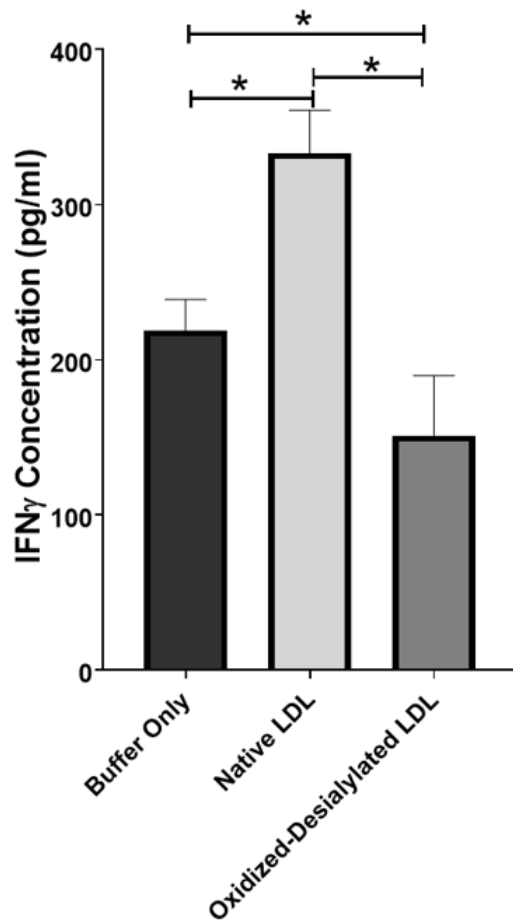
Figure 5.11. Oxidized-desialylated LDL impairs IFNγ production. LAK cells were cultured in serum free X-VIVO 10 media with 0.1 µg/ml IL-2 in the presence or absence of native LDL or oxidized-desialylated LDL for 72 hours. After 72 hours, cell supernatants were removed, centrifuged at 330 g for 8 minutes. Soluble IFNγ was measured in undiluted cell supernatants by ELISA. * Indicates statically significant differences between native LDL (control) and oxidized-desialylated LDL treated LAK cells (p<0.001). Statistical significance determined using one-way ANOVA with Turkey posthoc test. n = 4 per group. Error bars represent standard deviation.

CHAPTER 6

OXIDATIVE STRESS AND THIOBARBITURIC ACID REACTIVE SUBSTANCES

ASSAY

6.1 Introduction

Oxidation of low-density lipoprotein is an important mediator in the development of atherosclerosis [200]. Additionally, as it was discussed in chapter 5, oxidation of desialylated LDL enhances LDL uptake by LAK cells and inhibits their cytotoxicity against cancer cells. Therefore, a rapid, reliable, cheap, and reproducible method to determine the oxidative modification of LDL is needed for studies of LDL in cancer immunity. The most commonly used and preferred method for measuring oxidation on LDL is the thiobarbituric acid reactive substances (TBARS) assay. However, there are no detail TBARS assay protocols available in the literature, and they are only available as an expensive, impractical kit. For studies of LDL in regulating LAK cell activity we needed to perform multiple TBARS assays to determine levels of oxidation of LDL prior to doing experiments with LAK cells, and purchasing an expensive TBARs assay kit every time was impractical. For these reasons we decided to put together our own TBARs assay for studies of oxidation on LDL samples. In doing so, we determined the reproducibility of the TBARS method in other biological matrices, such as cell lysates and blood serum.

Lipid peroxidation is a process in which free radicals, such as reactive oxygen species and reactive nitrogen species, attack carbon-carbon double bonds in lipids, a process that involves the abstraction of a hydrogen from a carbon and insertion of an oxygen molecule. This process leads to a mixture of complex products including, lipid peroxyl radicals and hydroperoxides as the primary products, and malondialdehyde (MDA) and 4-hydroxynonenal as the predominant secondary products [87].

MDA has been widely used in biomedical research as a marker of lipid peroxidation due to its facile reaction with thiobarbituric acid (TBA). The reaction leads to the formation of MDA-TBA$_2$, a conjugate that absorbs in the visible spectrum at 532 nm and produces a red-pink color [201]. Other molecules derived from lipid peroxidation besides MDA can also react with TBA and absorb light at 532 nm, contributing to the overall absorption signal that is measured. Similarly, MDA can react with most other major classes of biomolecules, potentially limiting its accessibility for reaction with TBA [202]. As such, this traditional assay is simply considered to measure "thiobarbituric acid reactive substances" or TBARS [203].

When correctly applied and interpreted, the TBARS assay is generally considered a good indicator of the overall levels of oxidative stress in a biological sample [204]. Unfortunately, as documented by Khoubnasabjafari and others, the TBARS assay is often conducted and interpreted in ways that facilitate dubious conclusions [202, 205–209]. The causes for this are rooted primarily in sample-related pre-analytical variables and a lack of assay ruggedness that prohibits seemingly minor variations in assay protocol without substantial changes in assay results [87, 205, 210, 211].

Pre-analytical variables related to biospecimen handling and storage (e.g., blood plasma kept even temporarily at -20 °C) [212, 213] can have a major impact on TBARS assay results [214, 215]—so much so, that in our opinion, TBARS assay results should not be compared across different laboratories unless such a comparison is warranted by explicit inter-laboratory analytical validation data. This recommendation is akin to how western blots are commonly used and interpreted: comparisons of band densities are valid

for within-blot and perhaps within-laboratory studies, but comparing band densities between laboratories is generally considered an invalid practice.

Some researchers have suggested that MDA as measured by the TBARS assay simply does not meet the analytical and/or clinical criteria required of an acceptable biomarker [208, 209, 216–218]. Indeed, if the assay had not been developed over 50 years ago, it probably would not have gained the widespread use and tacit acceptability that it enjoys today. Although there are other assays with greater analytical sensitivity, specificity and ruggedness used for the determination of oxidative stress in biological samples, because of its ease of use the TBARS assay based on absorbance at 532 nm still remains by far one of the most commonly used assays for the determination of lipid peroxidation [219], and thereby assessment of oxidative stress in general.

The TBARS assay can only be found as an expensive kit (over $400 U.S dollars), in which the instructions do not provide detailed information on most of the concentrations of the reagents used. Additionally, the reagents provided can only be used for one experiment because only one colorimetric standard curve can be made per kit. This can be problematic for researchers who intend to determine levels of oxidation within a few samples at different time points because the same standard curve cannot be used at multiple times. Hence, multiple kits need to be purchased for multiple experiments. Currently, unless an expensive kit is purchased, there is not a detailed protocol available for how to perform a TBARS assay. Some researchers in the past have vaguely described how to perform a TBARS assay [220, 221], but neither a fully detailed protocol or comprehensive video on how to conduct the TBARS assay without an expensive kit is available in the literature.

Here we report a detailed, analytically validated for-purpose methodology on how to perform a TBARS assay in a simple, reproducible and inexpensive way. Changes in the lipid peroxidation of human serum, HepG2 lysates, and low-density lipoproteins upon treatment with Cu(II) ions are demonstrated as illustrative applications for the TBARS assay. Results demonstrate that this TBARS assay is consistent and reproducible on a day-to-day basis.

6.2 Experimental Procedures

6.2.1 Materials

Thiobarbituric acid (TBA) (T5500-100G), malondialdehyde bis (dimethyl acetal) (8207560250), sodium dodecyl sulfate (436143-100G), sodium hydroxide beads (367176-2.5KG), sodium chloride (S7653-1KG), HEPES (H3375-250G), glacial acetic acid (27225-1L-R), and copper(II) chloride (222011-250G) were purchased from Sigma. Non-treated clear bottom 96 well plate (280895) and caps for glass tubes (14-930-15D) were purchased from Thermo Fisher Scientific. 13 x 100 mm glass tubes (53283-800) were purchased from VWR.

6.2.2 Sample Preparation

Cell lysate preparation; HepG2 cells were seeded at $10X10^6$ cells/ml in 16 T75 flasks with 14 ml of EMEM media supplemented with 10 % FBS and grown for 2 days. Then, media was removed, and cells were washed twice with 5 ml of cold sterile 1X PBS. One ml of lysis buffer (5 M NaCl, 1 M Tris-HCl pH 7, 1 % NP-40, and 100X protease inhibitor solution) were added to the T75 flask containing the cells and incubated for 10 minutes at room temperature with constant swirling. Cell lysates were collected into snap-cap polypropylene tubes, incubated on ice for 10 minutes, and centrifuged at 5,000 x g for 10

minutes at room temperature to collect cell debris. Cell lysate supernatants were collected into a single 15 ml tube and concentrated 4-fold using a Speed Vac at 50 °C and 3 mbar. Aliquots of 94 µl were made, and samples were stored at -80 °C until they were used for *in vitro* oxidation and/or TBARS assay. For the *in vitro* oxidation of cell lysates, a 35 mM CuCl$_2$ stock solution was prepared in acetic acid pH 4 to prevent precipitation of copper hydroxide. Then, 6 µl of the 35 mM CuCl$_2$ stock solution were added to 6 samples containing 94 µl of cell lysate to make the final CuCl$_2$ concentration of about 2 mM. Six µl of an acetic acid solution pH 4, that did not have CuCl$_2$, were added to 6 samples containing 94 µl cell lysate to use as control. Samples were incubated in an oven at 37 °C for 2 hours, and a TBARS assay was performed immediately after.

Low density lipoprotein (LDL) sample preparation; because LDL samples used here contained 0.01 % EDTA, and EDTA can inhibit *in vitro* Cu(II) mediated oxidation of LDL, EDTA was removed from LDL samples by spin filtration. Twenty-four µl of a 5.51 mg/ml LDL stock (protein concentration determined by Modified Lowry Method using BSA as a standard) were diluted in 476 µl of a 10 mM HEPES buffer in 0.15 M NaCl pH 7 to bring the final volume to 500 µl. Then, diluted LDL samples were added to 0.5 ml centrifugal spin filter device with a 100K molecular weight cutoff. Samples were centrifuged at 14,000 x g for 10 minutes at room temperature, leaving a final retentate volume of about 30 µl. Samples were reconstituted in 480 µl of the 10 mM HEPES buffer in 0.15 M NaCl pH 7 and centrifuged again at 14,000 x g for 10 minutes. This last step was repeated a total two more times for a total of 4 spin throughs. Spin filter device was placed upside down into a new snap-cap polypropylene tube and centrifuged at 1000 x g for 2 minutes to collect LDL sample in a final volume of about 30 µl. Twenty µl of water were added to each LDL sample to bring final volume to 50 µl. For the *in vitro* oxidation of

131

LDL, 2.7 µl were aliquoted from a 200 µM CuCl$_2$ stock solution that was prepared in acetic acid pH 4 and added it to six samples containing 50 µl of LDL to make a final CuCl$_2$ concentration of about 10 µM. For the control samples, 2.7 µl of an acetic acid solution pH 4 were added to six samples containing 50 µl of LDL. Then, LDL samples with or without CuCl$_2$ incubated for 2 hours in an oven at 37 °C. After 2 hours, final volume was brought to 100 µl with 10 mM HEPES buffer in 0.15 M NaCl pH 7, and immediately after a TBARS assay was performed.

Human serum sample preparation; aliquots of 94 µl each were made from a human serum stock, and samples were kept at -80 °C. For the oxidation of human serum, a 35 mM CuCl$_2$ stock solution was prepared in acetic acid pH 4. Then, 6 µl of the 35 mM CuCl$_2$ stock solution were added to 6 samples containing 94 µl of cell lysate to make the final CuCl$_2$ concentration of about 2 mM. Six µl of an acetic acid solution pH 4, that did not have CuCl$_2$, were added to 6 samples containing 94 µl cell lysate to use as control. Samples were incubated in an oven at 37 °C for 2 hours. A TBARS assay was performed immediately after.

6.2.3 TBARS Color Reagent Preparation

An 8.1 % (w/v) sodium dodecylsulfate (SDS) solution was prepared by dissolving 32.4 grams of SDS in a final water volume of 400 µl. A 3.5 M sodium acetate buffer pH 4 was prepared as follows; one hundred ml of glacial acetic acid were diluted in 350 ml of DI water, to this was added 46 ml of a 6.5 M NaOH solution, which brought the pH of the solution to 4. Then, final volume of sodium acetate buffer was brought to 500 ml with DI water.

An 0.8 % aqueous solution of thiobarbituric acid adjusted to pH 4 was prepared as follows; four grams of thiobarbituric acid were added into a beaker containing 450 ml of DI water. To this was added a total volume of 3 ml of a 5 M NaOH solution in 100 µl increments, which causes the thiobarbituric acid particles to dissolve. pH of thiobarbituric acid solution was determined to be around 4 with a pH paper. Then, final volume of solution was brought to 500 ml with DI water.

6.2.4 Malondialdehyde Standard Sample Preparation

Malondialdehyde (MDA) is unstable and it is not commercially available. However, there are different chemical forms of MDA that are commercially available, such as MDA tetrabutylammonium salt, MDA bis (dimethyl acetal), and MDA bis (diethyl acetal). Of these three chemical forms we used MDA bis (dimethyl acetal) because the vast majority of studies have used this same standard[21,22]. A 550 µM MDA bis (dimethyl acetal) stock solution was prepared by diluting 92 µl of pure MDA bis (dimethyl acetal) in 1 L of water. A 200 µM MDA bis (dimethyl acetal) solution was prepared by diluting 726 µl from the 550 µM MDA bis (dimethyl acetal) stock in 1274 µl of DI water. This 200 µM MDA bis (dimethyl acetal) solution was prepared fresh every time a TBARS assay was performed.

For the standard curve preparation, a total of eight 2-ml snap-cap polypropylene tubes were labeled A-H, and MDA bis (dimethyl acetal) was added to each tube from the 200 µM stock and diluted in water as described in Table 1. Eight glass tubes (13 x 100 mm) were labeled A-H and added 100 µl of each diluted standard to corresponding glass tube. A total of six replicates for the blank standard (sample A) were performed to calculate limits of detection of the TBARS assay.

133

6.2.5 Thiobarbituric Acid Reactive Substances Assay

One hundred µl of prepared sample (cell lysate, LDL, or serum) were added to a 13 x 100 mm glass tube. To this was added 200 µl of 8.1 % SDS to each sample and standard, followed by 1.5 ml of the 3.5 M sodium acetate buffer pH 4 and 1.5 ml of the aqueous 0.8 % thiobarbituric acid solution pH 4. Final volume was brought to 4 ml for each sample and standard by adding 700 µl of DI water. Each glass tube was tightly capped and incubated at 95 °C for 1 hour. Then samples were incubated in ice for 30 minutes. Samples and standards were centrifuged at 1500 x g for 10 minutes at 4 °C. Immediately after centrifugation, 150 µl of supernatant were aliquoted from each tube and placed it into a separate well of a 96-well plate. Absorbance was taken at 532 nm, and average absorbance reading of the blank samples was subtracted from all other absorbance readings. Unknown sample concentrations were calculated using linear regression obtained from standard curve.

6.3 Results

Under acidic conditions (pH 4) and at 95 °C, malondialdehyde (MDA) bis (dimethyl acetal) yields MDA [222]. MDA and closely related chemical congeners react with two molecules of thiobarbituric acid (TBA) to produce compounds called thiobarbituric acid reactive substances (TBARS), which give a red-pink color and have an absorbance λ_{max} at 532 nm (**Figure 6.1 & Figure 6.2**). Using MDA bis (dimethyl acetal) as the standard, standard curves were generated (**Figure 6.3 & Table 6.1**) to determine the limits of detection and sensitivity of the assay and the levels of oxidation in three different types of biological samples. A total of nine TBARS assays were performed to determine the levels of oxidation in the three different samples on different days. Hence, a total of nine standard curves were generated, as shown in **Figure 6.3**. The least-squares procedure [223] was

used to determine the standard deviations of the slope and the y-intercept, which were

8.67 x 10⁻⁶ and 5.66 x 10⁻⁴, respectively.

The limits of detection of the TBARS assay were determined according to standard

analytical procedures [224] by measuring the absorbance of the blank samples (6

experimental replicates with 2 technical replicates per experimental replicate) on three

different days. The minimum distinguishable analytical signal (S_m) was determined by

summing the mean of the blank signal ($\bar{S}_{bl}$) plus a multiple k of the standard deviation of

the blank (ks_{bl}), where k = 3. That is; $S_m = \bar{S}_{b_l} + ks_{bl}$. Using S_m and the slope of the

standard curve (m), the detection limit (c_m) was calculated as; $c_m = (S_m - \bar{S}_{bl}) / m$. The

resulting data of the blank samples on three different days shows that the minimum

concentration of TBARS substance needed to give a detectable non-noise absorbance

signal is 1.1 µM (**Table 6.2**). The sensitivity of the TBARS assay is about 0.00160

absorbance units/µM, which is the ability of the assay to distinguish differences in analyte

concentration (**see Table 6.2**).

To illustrate the applicability of the TBARS assay in detecting changes in lipid

peroxidation in various biological matrices, CuCl$_2$ was used to induce the *in vitro* oxidation

of human serum, HepG2 cell lysates, and low-density lipoproteins. These biological

samples used here are prototypes of biological matrices. For example, based on the

results presented here for HepG2 cell lysates, it is reasonable to expect that this assay

will work with other types of cell lysate—but it would need to be analytically validated for

this purpose. Also, of the three biological matrices used here, it is common for certain

types of samples to exhibit low endogenous concentrations of TBARS. For example,

TBARS for HepG2 cell lysates that were not treated with CuCl$_2$ were just above the limit

of detection of the assay (about 2 μM) (**Figure 6.4**). As would be expected in the presence of low signal-to-noise ratios, the standard deviation and coefficient of variation for this particular sample is relatively high (**see Table 6.3**). However, as the signal increases as a result of Cu(II) mediated oxidation, the coefficient of variation becomes lower. In general, as the absorbance increases beyond the detection limit, assay reproducibility improves (**Table 6.3**).

Four our purposes, we don't want to use antioxidants to mask the *in vitro* Cu(II) mediated oxidation of biological samples. Commercially prepared low-density lipoproteins (LDL) may contain 0.01 % EDTA. EDTA will prevent Cu(II) mediated oxidation of LDL, but not necessarily other metal-mediated oxidation reactions [225, 226]. A TBARS assay was performed on LDL samples containing EDTA, and the levels of TBARS did not change between the Cu(II)-treated and untreated LDL samples (**Figure 6.5A**). However, after EDTA was removed by spin filtration (see step 1.2.3 to 1.2.5), LDL underwent Cu(II) mediated oxidation, as detected by the TBARS assay (**Figure 6.5B**).

The normal range of lipid peroxidation products in the human serum from healthy donors expressed in terms of MDA is between 1.8-3.94 μM [227]. To illustrate the dynamic range of the TBARS assay in human serum, a concentration of 2 mM Cu(II) ions was added to the samples, followed by incubation for 24 hours at 37 ºC. This resulted in a 6-7x increase in TBARS (**Figure 6.6**).

6.4 Discussion

Despite its limitations [202, 205, 206, 208–213, 216, 218, 228] and, in our opinion, lack of suitability for comparison between laboratories, the TBARS assay is one of the oldest

[229, 230] but still most widely used assays to measure oxidative stress in biological samples. The TBARS assay is a straightforward method that only takes about two hours to perform once all the required reagents have been prepared. Here we have described in detail how this assay, including standard curve, can be performed many times in an economical way (about $3.50 USD for 96 samples), that is, without having to buy an expensive kit for every batch of samples.

All the steps of the assay are critical, but there are some steps that require extra attention. For instance, the pH of the thiobarbituric acid should not be higher than 4. Precautions should be taken when adding the sodium hydroxide solution to the thiobarbituric acid and avoid having a pH greater than 4. An acidic environment is required for the reaction between MDA and TBA to occur, and the MDA standard is released from MDA bis (dimethyl acetal) by acid-catalyzed hydrolysis. Hence, a high pH may lead to unpredictable and highly variable results [231]. Also, while this may be obvious to some readers, it is also critical to remove any bubbles in the 96 well plate before measuring the absorbance. The presence of bubbles will give high absorbance values and differences between replicates, leading to high % CVs. Additionally, after the 1-hour incubation at 95 ^{o}C, samples should not be incubated longer than 30 minutes on ice since this will precipitate the entire sample and collecting a precipitate-free supernatant will be difficult to accomplish. Notably, there are no good stopping points once the TBARS assay has been started; it should be taken through completion once it has been initiated. Finally, there are a great many possible methodological variations that could be applied to this assay. The general protocol described here can be further adapted (and validated) for specific applications—including those for which the addition of radical scavengers or other types of antioxidants prior to analysis is appropriate or mandated.

137

While the TBARS assay is popular, it is important for practitioners of it to realize that it is not a molecularly specific assay; numerous chemically reactive carbonyl-containing organic molecules, including those derived from oxidized biomolecules other than lipids, can react with TBA and therefore are counted as TBARS [213, 228, 232, 233]. In addition, the limits of detection of the absorbance-based TBARS assay do not get much better than about 1.1 µM, as determined by our method. However, the limits of detection can be improved by using other detection methods. For instance, spectrofluorometry with excitation at 520 nm and emission at 550 nm offer higher sensitivity and better limits of detection, as previously suggested by Jo and Ahn [234]. Mass spectrometry-based methods can dramatically improve both specificity and limits of detection. For example, a GC-MS/MS with electron-capture negative-ion chemical ionization (ECNICI) method has been used to detect the pentafluorobenzyl derivative of MDA in human serum and urine samples, with limits of detection of 2×10^{-18} mol MDA on column [235]. Here, the chromatographic separation, in combination with tandem mass spectrometry, dramatically improves the molecular specificity of the assay as well.

Nevertheless, as with other measurements of oxidative processes within biological samples [236, 237], pre-analytical sample handling is critical to the outcome of TBARS measurements. For example, blood plasma storage at -20 °C results in slow but dramatic increases in MDA concentrations [238, 239]. Thus, exposure of biological samples to thawed or even partially thawed conditions for anything but a minimal amount of time should, in the absence of contrary evidence, be assumed to cause artifactual elevation of TBARS levels. This means that even modest variability in the pre-analytical handling and storage of biospecimens that are to be compared to one another using the TBARS assay must be avoided.

Given these caveats related to pre-analytical variability as well as limited sensitivity and specificity, we recommend that the absorbance-based TBARS assay only be used for intra-laboratory general assessment or range-finding experiments in which relative TBARS levels are directly compared between one or more groups of biologically similar samples that were processed and/or stored together and separated by only a single variable that was fully controlled by the researchers.

6.5 Conclusion

Despite its limited analytical specificity and ruggedness, the thiobarbituric acid reactive substances (TBARS) assay has been widely used as a generic metric of lipid peroxidation in biological fluids; and it is often considered a good indicator of the levels of oxidative stress within a biological sample—provided that the sample has been properly handled and stored. The assay involves the reaction of lipid peroxidation products, primarily malondialdehyde (MDA), with thiobarbituric acid (TBA) which leads to the formation of MDA-TBA$_2$ adducts called TBARS. TBARS give a red-pink color that can be measured spectrophotometrically at 532 nm. The TBARS assay is performed under acidic conditions (pH 4) and at 95 ^{o}C. Pure MDA is unstable, but these conditions allow the release of MDA from MDA bis (dimethyl acetal), which is used as the analytical standard in this method. The TBARS assay is a straightforward method that can be completed in about 2 hours. Preparation of assay reagents are described in detail here. Budget-conscious researchers can use these reagents for multiple experiments at low cost (about \$3.50 USD for 96 samples) rather than having to buy an expensive TBARS assay kit that only permits construction of a single standard curve and therefore can only be used for one experiment. The applicability of this TBARS assay is shown in human serum, low-density lipoproteins,

and cell lysates. The assay is consistent and reproducible on a day-to-day basis and limits

of detection of 1.1 µM can be reached.
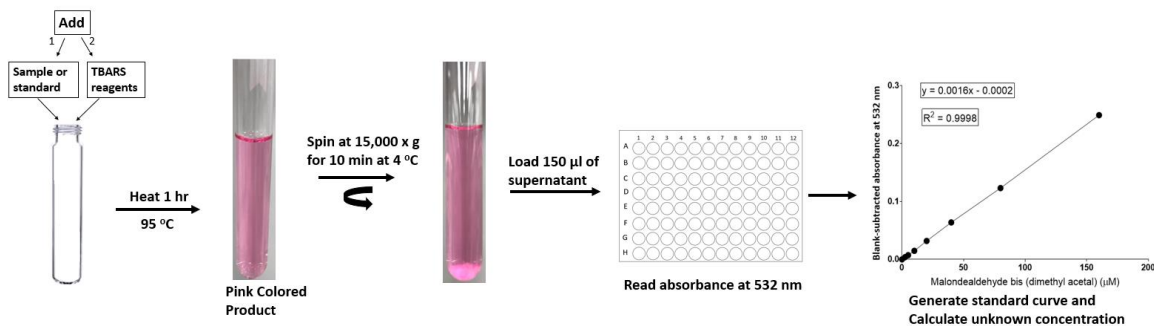
Figure 6.1. Thiobarbituric Acid Reactive Substances Assay Schematic. One hundred microliters of sample or standard are added to a 13x100 mm glass tube, followed by addition of thiobarbituric acid reactive substances (TBARS) reagents. After incubation at 95 °C for 1 hour, samples and standards are incubated in ice for 30 minutes, then centrifuged at 1500 x g for 10 minutes at 4 °C. One hundred fifty microliters of sample or standard supernatant are loaded onto a 96-well plate, and absorbance is measured at 532 nm. Unknown sample concentration is calculated using the equation of the standard curve.
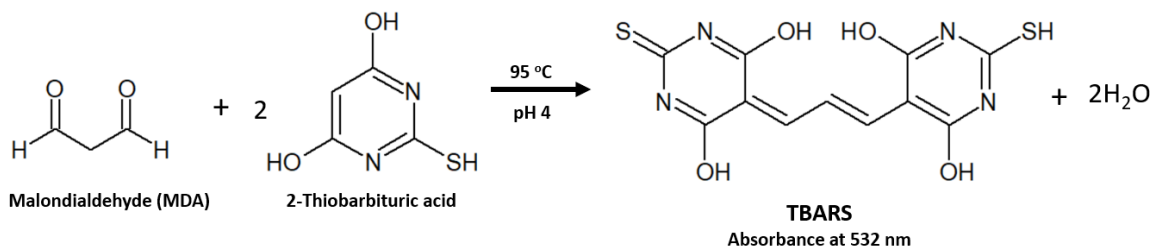
Figure 6.2. Archetype Thiobarbituric Acid Reactive Substances reaction. Malondialdehyde bis (dimethyl acetal) yields malondialdehyde under acid-catalyzed hydrolysis [228]. Released Malondialdehyde (MDA) then reacts with two molecules of 2-thiobarbituric acid (TBA) at pH 4 and 95 °C to form MDA-TBA_2 adducts that give a red-pink color and can be measured spectrophotometrically at 532 nm. Because other molecules besides MDA that are derived from oxidized lipids can also react with TBA, the absorbance measurement at 532 nm is simply referred to as a measurement of thiobarbituric acid reactive substances or TBARS.

140
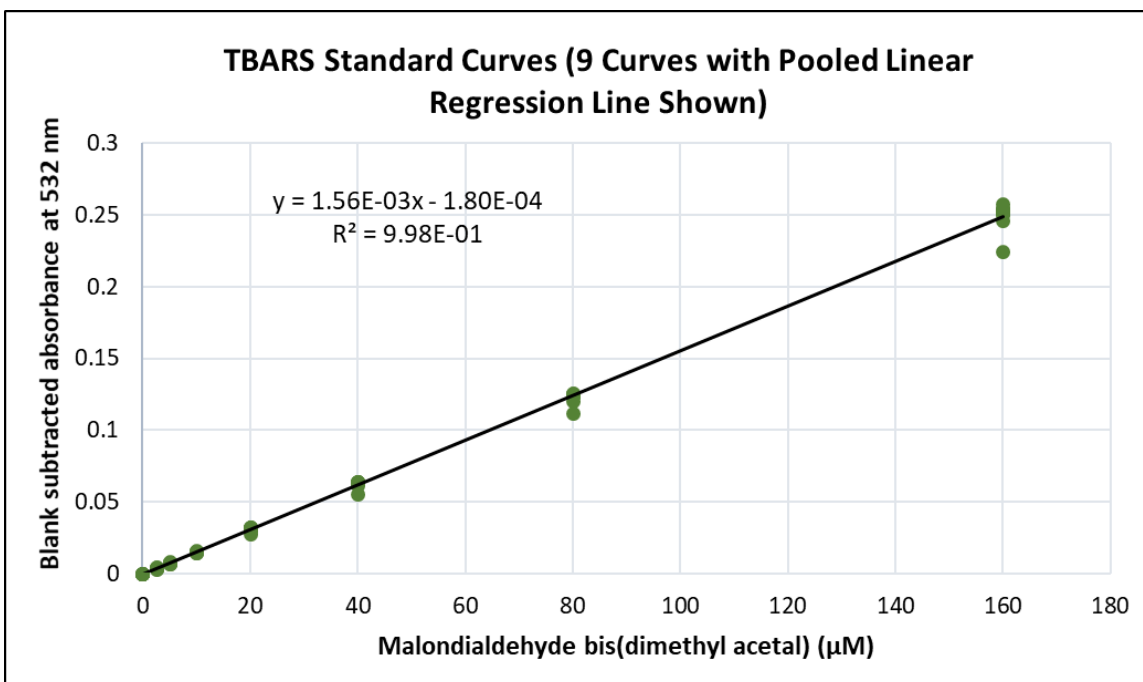
Figure 6.3. Malondialdehyde bis (dimethyl acetal) Colorimetric Standard Curves. Figure shows nine standard curves as created on different days. Some points overlap and cannot be distinguished from one another. Malondialdehyde bis (dimethyl acetal) was fortified into calibrator samples at 0, 2.5, 5, 10, 20, 40, 80, and 160 μM (as shown in Table 1; n = 1 per concentration point per day). Absorbance was measured at 532 nm with the average absorbance of the blank samples subtracted from all measurements in that batch, including unknowns. Each day, the equation generated by least-squares linear regression was used to determine TBARS in biological samples. For all nine standard curves combined, the standard deviation of the slope was 8.67×10^{-6}, and the standard deviation of the y-intercept was 5.66×10^{-4}. Standard deviations of the slope and y-intercept were calculated using the least-squares procedure [223].
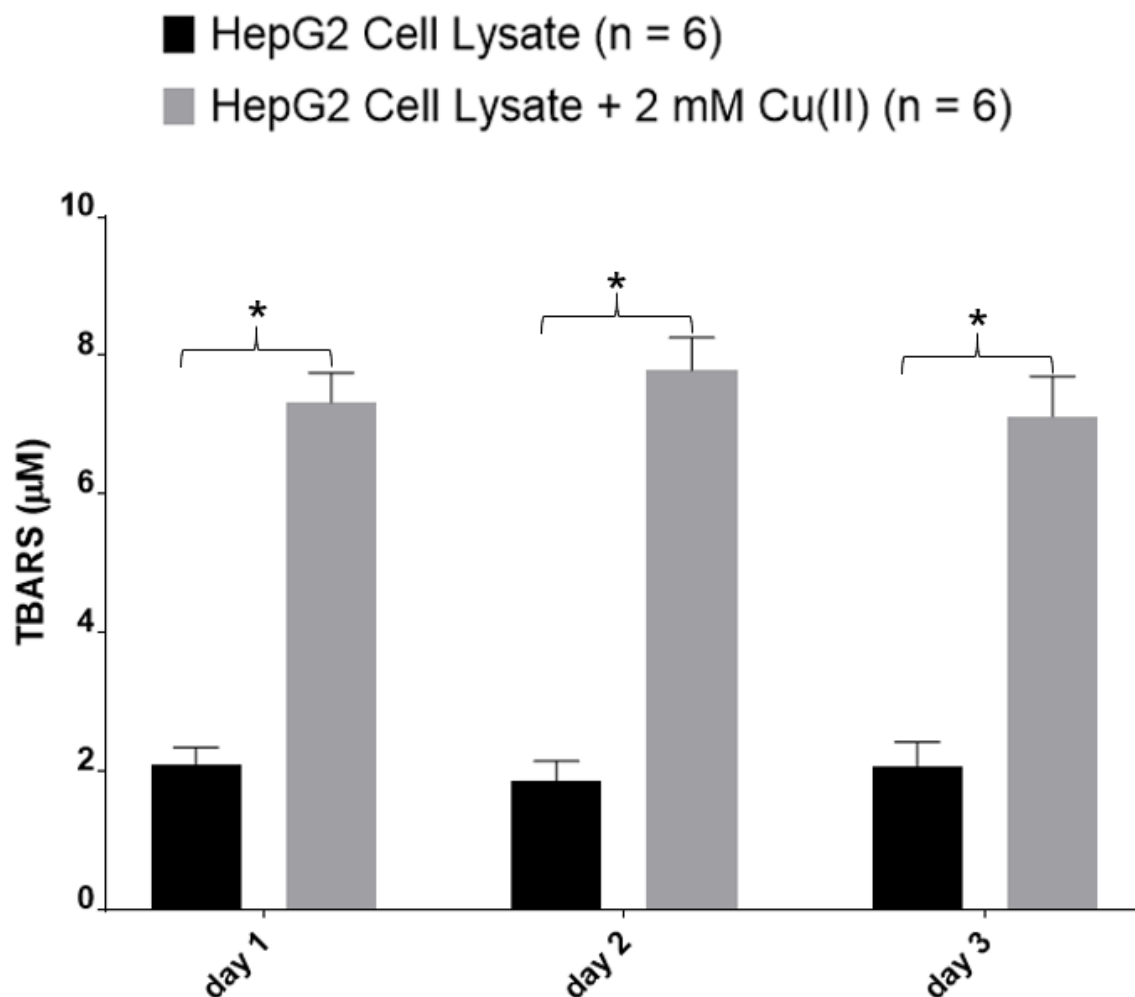
Figure 6.4. Oxidation in HepG2 lysates detected by TBARS. Six HepG2 cell lysate samples were incubated with 2 mM CuCl$_2$ (HepG2 cell lysate + 2 mM Cu(II)) and six samples were incubated in a solution without CuCl$_2$ (HepG2 cell lysate) for 24 hours at 37 ^{o}C. After incubation, the TBARS assay was performed on the 12 samples. This procedure was repeated two more days for a total of three different days. Error bars represent standard deviation. * Indicates statistically significant differences between control and Cu(II)-treated lysates (p<0.001). Statistical significance was determined using a Mann Whitney U test in GraphPad.

142
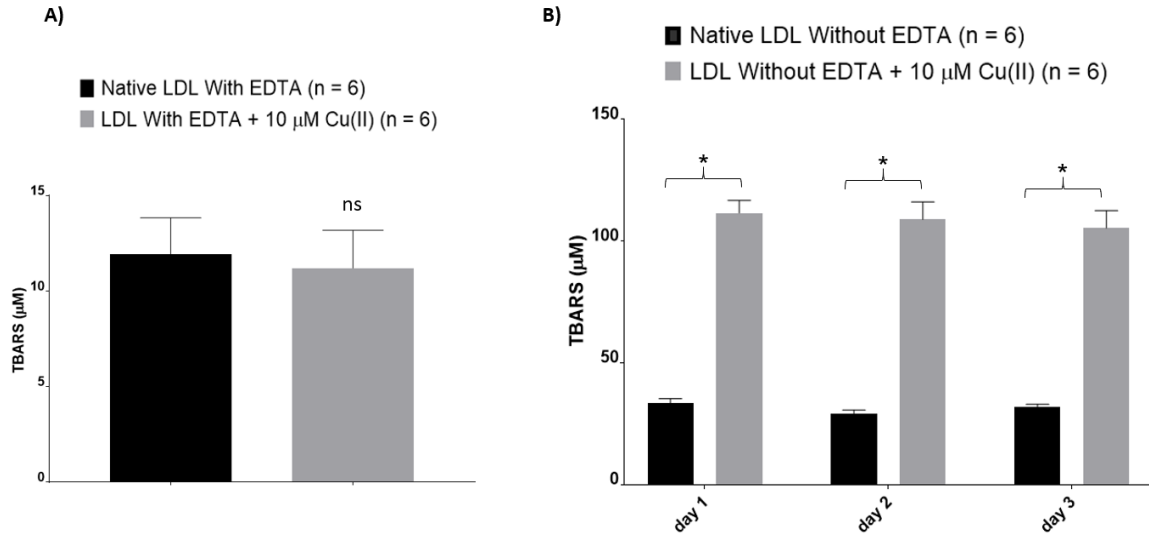
Figure 6.5. Oxidation in Low density lipoprotein detected by TBARS. A) TBARS assay conducted in LDL samples containing 0.01% EDTA (as prepared by Athens Research & Technology company). Six LDL samples were incubated with 10 µM CuCl$_2$ (LDL + 10 µM Cu(II)) and six samples were incubated with a control solution that did not have any CuCl$_2$ added (Native LDL) for 2 hours at 37 °C. Then a TBARS assay was performed on the 12 samples. *ns* represents no statistical significance. **B)** LDL was spin filtered using an Amicon Ultra-0.5 100 KDa MWCO centrifugal spin filter device to remove EDTA. Then, incubation with and without added Cu(II) was performed again as described for A). The TBARS assay was performed immediately afterward. This same procedure was repeated on two more days for a total of 3 days. Error bars represent standard deviation. * Indicates statistically significant differences between control and Cu(II)-treated LDL samples (p<0.001). Statistical significance was determined using the Mann Whitney U test in GraphPad.
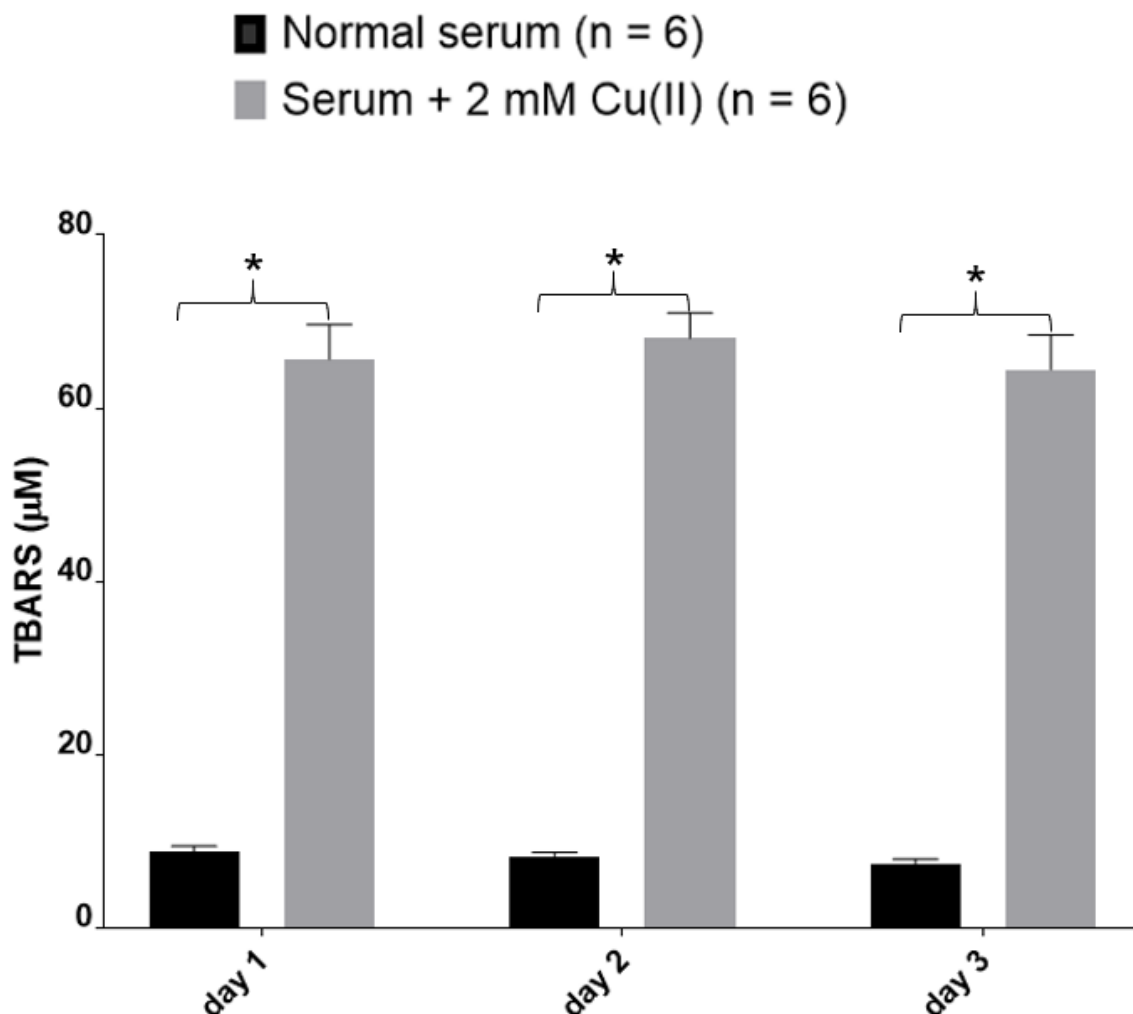
Figure 6.6. Lipid peroxidation in human serum samples detected by TBARS. Six human serum samples were incubated with 2 mM $CuCl_2$ (serum + 2 mM Cu(II)) and six samples were incubated with a solution that did not have any added $CuCl_2$ (normal serum) for 24 hours at 37 °C. After incubation, the TBARS assay was performed on the 12 samples. This procedure was repeated on two additional days. Error bars represent standard deviation. * Indicates statistically significant differences between control and Cu(II)-treated serum samples ($p < 0.001$). Statistical significance was determined using the Mann Whitney U test in GraphPad.

Table 6.1. Malondialdehyde bis(dimethyl acetal) standard sample preparation[a]

Glass Tube	200 µM MDA bis (dimethyl acetal) (µl)	Water (µl)	MDA bis (dimethyl acetal) Final Concentration (µM)
A[b]	0	1000	0
B	12.5	987.5	2.5
C	25	975	5
D	50	950	10
E	100	900	20
F	200	800	40
G	400	600	80
H	800	200	160

[a]From the freshly prepared 200 µM malondialdehyde bis (dimethyl acetal), aliquot the suggested volumes to reach the final concentration for the standard curve.

[b]It is recommended to perform at least six replicates of the blank sample (A) per day to determine the limits of detection of the method.

Table 6.2. Detection limits of the TBARS assay

Day	Absorbance [a]	S_{bl} [b]	S_m [c]	Sensitivity (absorbance units/μM) [d]	c_m (μM) [e]
1 (n = 6)	0.0412	0.000612	0.0430	0.00160	1.14
2 (n = 6)	0.0415	0.000632	0.0433	0.00160	1.18
3 (n = 6)	0.0413	0.000605	0.0431	0.00160	1.13
All three days (n = 18)	0.0413	0.000589	0.0431	0.00160	1.10

[a]Absorbance of the blank samples on three different days with 6 replicates per day.

[b]S_{bl} = Standard deviation of the absorbance of the blank samples.

[c]S_m = Minimum distinguishable analytical signal, which was determined by summing the mean of the blank signal ($\bar{S}_{bl}$) plus a multiple k of the standard deviation of the blank (ks_{bl}), where k = 3. That is; $S_m = \bar{S}_{bl} + ks_{bl}$.

[d]Sensitivity of the TBARS assay, which is the slope of the standard curve.

[e]c_m = Limits of detection, which was calculated as; $c_m = (S_m - \bar{S}_{b_l})/m$, where m = the slope of the standard curve.

Table 6.3. Analytical reproducibility of the TBARS in three different biological samples

Low density lipoprotein		Human Serum		HepG2 Cell Lysate	
Day	% CV	Day	% CV	Day	% CV
1 (n = 6)	5.6	1 (n = 6)	7.9	1 (n = 6)	12.6
2 (n = 6)	5.4	2 (n = 6)	7.2	2 (n = 6)	15.8
3 (n = 6)	3.9	3 (n = 6)	7.0	3 (n = 6)	17.7
All three days (n = 18) [a]	7.4	All three days (n = 18)	9.8	All three days (n = 18)	15.5 [b]
With 10 μM CuCl$_2$		With 2 mM CuCl$_2$		With 2 mM CuCl$_2$	
1 (n = 6)	4.5	1 (n = 6)	6.0	1 (n = 6)	5.8
2 (n = 6)	6.5	2 (n = 6)	4.3	2 (n = 6)	6.0
3 (n = 6)	6.7	3 (n = 6)	6.2	3 (n = 6)	8.0
All three days (n = 18)	6.1	All three days (n = 18)	5.6	All three days (n = 18)	7.3

[a]Interday precision was calculated by pooling data from all three days.

[b]Precision was limited due to results being near the assay LOD.

CHAPTER 7

CONCLUSION AND FUTURE DIRECTIONS

In this dissertation, glycan node analysis was optimized, adapted, and applied to multiple unique, biologically important biomatrices for the purpose of evaluating its utility in cancer research. Specifically, the glycan node analysis procedure was applied to profile specific glycan features in cell culture supernatant. Glycan node analysis in cell culture supernatant was reproducible and consistent on a day to day basis, and cytokine-induced subtle changes in glycosyltransferase activity were detected using this approach. The inflammatory cytokine interleukin-6 (IL-6) was found to regulate multiple specific glycan tumor antigens, such as β1-6-branching, β1-4-branching, Tn antigen (GalNAc-Ser/Thr), terminal galactosylation, bisecting GlcNAc, and antennary fucosylation, in hepatocellular carcinoma (HepG2) cells. IL-1β appeared to regulate β1-6-branching and β1-4-branching in HepG2 cells, but the magnitude of the effect was not significant. Because β1-6-branching is a molecular surrogate of GnT-V activity, a Western blot confirmed increased β1-6-branching due to upregulated GnT-V upon IL-6 treatment. GnT-V adds a GlcNAc residue to an α-linked mannose of an N-glycan. Our glycan node analysis results revealed that the only GlcNAc residue that was upregulated was 3,4-GlcNAc. Because 3,4-GlcNAc represents antennary fucosylation, it was concluded that the β1-6-branched glycans tended to be extended antennary forms.

Abnormal glycosylation of blood plasma glycoproteins is a hallmark of cancer, and the mechanisms by which these processes occur are not well understood. It has been assumed that inflammatory cytokines modulate the way cells glycosylate their secreted glycoproteins. However, glycomics studies on cytokine induced glycosylation are rare, and often limited to N-glycan analysis using lectins. In this dissertation, it's been shown that glycan node analysis can be used to study cytokine induced changes in glycosylation, in

which a complete glycan profile (N-linked and O-linked) is provided. Future studies should investigate the molecular pathways by which inflammatory cytokines, such as IL-6 and IL-1β, change glycosyltransferase expression. The common molecular pathway of IL-6 is the STAT3 pathway, and for IL-1β signaling is through the NFκB pathway. Perhaps the glycosylation changes that we observed here are regulated through such pathways. Additionally, the role of other anti-inflammatory and pro-inflammatory cytokines, such as IL-10, IL-5, TNF, IL-2, and IL-8, should be investigated to understand the molecular mechanisms by which the inflammatory aspect of cancer changes the way "normal" cells glycosylate their secreted glycoproteins.

Glycan node analysis was also employed to profile antibody IgG glycosylation. Treatment of IgG antibodies with low amounts of neuraminidase enzyme results in subtle changes in terminal sialylation, which were consistently quantified by glycan node analysis. Changes in glycosylation are extremely important since they can affect the pharmacokinetic and pharmacodynamics of the antibody. Our glycan node analysis results suggest that glycan node analysis can potentially be applied to quantify glycosylation changes of therapeutic antibodies, for which glycosylation consistency is mandated in the therapeutic industry. The advantages of using glycan node analysis over other technologies are that specific glycan features can be quantified as single analytical signals, and that a complete glycan profile (N-linked and O-linked) is captured using this approach.

In this dissertation, it was demonstrated that the glycan node analysis can be applied to quantify glycosylation on extracellular vesicles (EVs) derived from cells and from blood plasma. EVs derived from metastatic cells and non-metastatic cells showed significant changes in several glycan nodes, particularly 3-GlcNAc, which represents hyaluronic acid. Additionally, EVs derived from normal donor blood plasma showed

148

particular glycan features that distinguish them from whole blood plasma glycans. The distinct glycan expression profile of EVs compared to whole plasma was promising for developing new diagnostic strategies. For example, glycan node analysis of exosomes can be a cost effective and time-efficient future method to assess glycosylation changes in cancer from a simple blood draw. These results suggest the legitimacy of applying glycan node analysis to compare EVs derived from normal donors vs cancer donors blood plasma. It would be particularly interesting to see if hyaluronic acid is upregulated or downregulated in patients with metastatic cancer. This would represent a promising biomarker since EVs have been shown to have a potential clinical utility in the diagnosis and therapy of cancer.

In this dissertation, a simplified "liquid phase permethylation" procedure for glycan node analysis was applied for the first time to whole biological specimens. A conventional "solid phase permethylation" procedure was performed in parallel to compare the permethylation efficiencies. Both methods showed permethylation efficiencies of ≥99 %, and it was found that the liquid phase permethylation procedure offered higher sensitivity than the solid phase permethylation procedure for detecting glycan nodes in cell lysates. Both permethylation methods were applied to cancer cell lysates for the first time, and specific glycan profiles were identified for each cell line. Both methods agreed on most of the glycan nodes identified, and it was found that the liquid phase permethylation procedure offered better intra- and inter-assay reproducible results. It was found that antennary fucosylation is elevated in HepG2 cell lysates relative to THP-1 cells, K562 cells, and PBMCs. Also, glycolipids were found upregulated in THP-1 cells and K562 cells, but not in HepG2 cells and PBMCs. These results suggest that liquid phase permethylation for glycan node analysis can be applied to cancer tissue and normal tissue

149

for biomarker discovery. Future studies should investigate the glycan node profile of cancer vs healthy tissues for clinical diagnosis.

Changes in glycosylation in cancer were extensively studied in this dissertation, but the roles of glycosylation changes were also addressed. In this dissertation, it was found a unique role of oxidized-desialylated low-density lipoprotein (LDL) in regulating the activity of lymphokine activated killer (LAK) cells. It was found that desialylation and oxidation significantly enhance the uptake of LDL by LAK cells, and this causes the LAK cells to have downregulated cytotoxicity against leukemia K562 cells. The downregulated cytotoxicity was explained by a downregulation of CD56 and NKG2D cytotoxicity receptors and an impairment of IFNγ production, all induced by oxidized-desialylated LDL. These phenomena have implications in both cancer and atherosclerosis. Cancer and atherosclerosis are two similar diseases that share multiple pathways, and it has been suggested that atherosclerosis can lead to cancer. Oxidized-desialylated LDL is a hallmark of atherosclerosis, and there is extensive research showing how this form of LDL leads to atherosclerotic plaques. However, studies on how oxidized-desialylated LDL modulates immunity and tumor progression are very limited. The findings in this dissertation will open up new avenues in research, in which a new link between atherosclerosis and cancer immunity has been identified. Future studies should investigate the effects of oxidized-desialylated LDL on other cytotoxic immune cells, such as T cells, and pre-purified NK cells. Results in this dissertation suggest that oxidized desialylated LDL will have an inhibitory effect on both T cells and NK cells. Additionally, future research should investigate the levels of oxidized-desialylated LDL in the blood of cancer patients, especially those with cardiovascular diseases. The glycan node analysis has been shown to distinguish particular glycan features from cancer vs healthy patients.

In this same manner, it should be investigated the levels of sialylated and desialylated LDL in cancer patients using glycan node analysis.

The TBARS assay described in this dissertation, however, should not be used as a diagnostic tool to identify oxidation of LDL in cancer vs healthy in future studies. In this dissertation, it has been shown that the TBARS assay should only be used as a tool to assess oxidative stress in general, in which TBARS levels are directly compared between one or more groups of biologically similar samples that are processed and/or stored together and separated by only a single variable that is fully controlled. TBARS assay results should not be compared across different laboratories unless such a comparison is warranted by explicit inter-laboratory analytical validation data. This recommendation is akin to how western blots are commonly used and interpreted: comparisons of band densities are valid for within-blot and perhaps within-laboratory studies, but comparing band densities between laboratories is generally considered an invalid practice. The TBARS assay described in this dissertation is a valuable tool to assess oxidation in LDL samples prior to incubating them with lymphocytes or immune cells. Future studies can use this assay to assess oxidation in biological samples or LDL samples to better understand the role of oxidized-desialylated LDL in biology.

REFERENCES

1.   Varki A KS (2017) Historical Background and Overview. In: Varki A, Cummings RD, Esko JD et al. (ed) Essentials of Glycobiology [Internet], 3rd ed. Cold Spring Harbor Laboratory Press, Cold Spring Harbor (NY)

2.   Seeberger PH (2017) Monosaccharide Diversity. In: Varki A, Cummings RD, Esko JD et al. (ed) Essentials of Glycobiology [Internet], 3rd ed. Cold Spring Harbor (NY): Cold Spring Harbor Laboratory Press; 2015-2017.

3.   Maley F, Trimble RB, Tarentino AL, Plummer TH (1989) Characterization of glycoproteins and their associated oligosaccharides through the use of endoglycosidases. Anal Biochem 180:195–204 .

4.   Apweiler R., Hermjakob H. SN (1999) On the frequency of protein glycosylation, as deduced from analysis of the SWISS-PROT database. Biochim Biophys Acta 1473:4–8

5.   Mulloy B, Dell A, Stanley P et al. (2017) Structural Analysis of Glycans. In: Varki A, Cummings RD, Esko JD, et al. E (ed) Essentials of Glycobiology [Internet], 3rd ed. Cold Spring Harbor Laboratory Press, Cold Spring Harbor (NY)

6.   Stanley P, Taniguchi N AM (2017) N-Glycans. In: Varki A, Cummings RD, Esko JD et al. (ed) Essentials of Glycobiology [Internet]., 3rd ed. Cold Spring Harbor (NY): Cold Spring Harbor Laboratory Press; 2015-2017.

7.   Fuster MM, Esko JD (2005) The sweet and sour of cancer: Glycans as novel therapeutic targets. Nat Rev Cancer 5:526–542 .

8.   Walimbe T, Panitch A (2020) Proteoglycans in biomedicine: Resurgence of an underexploited class of ECM molecules. Front Pharmacol 10:1–13 .

9.   Zachara N, Akimoto Y HG (2017) The O-GlcNAc Modification. In: Varki A, Cummings RD, Esko JD et al. (ed) Essentials of Glycobiology, 3rd ed. Cold Spring Harbor Laboratory Press, Cold Spring Harbor (NY).

10.   Bjork S, Breimer ME, Hansson GC, Karlsson K, Leffler H (1987) Structures of Blood Group Glycosphingolipids of Human Small Intestine. J Biol Chem 262:6758–6765.

11.   Schnaar RL KT (2017) Glycosphingolipids. In: Varki A, Cummings RD, Esko JD et al. (ed) Essentials of Glycobiology [Internet], 3rd ed. Cold Spring Harbor (NY): Cold Spring Harbor Laboratory Press; 2015-2017.

12.   Cordat E, Reithmeier RAF (2014) Structure, function, and trafficking of SLC4 and SLC26 anion transporters, 1st ed. Elsevier Inc.

13.   Rini JM EJ (2017) Glycosyltransferases and Glycan-Processing Enzymese. In: Varki A, Cummings RD, Esko JD et al. (ed) Essentials of Glycobiology [Internet].,

3rd ed. Cold Spring Harbor (NY): Cold Spring Harbor Laboratory Press; 2015-2017.

14. Freeze HH, Hart GW SR (2017) Glycosylation Precursors. In: Varki A, Cummings RD, Esko JD et al. (ed) Essentials of Glycobiology, 3rd ed. Cold Spring Harbor Laboratory Press, Cold Spring Harbor (NY).

15. Colley KJ, Varki A KT (2017) Cellular Organization of Glycosylation. In: Varki A, Cummings RD, Esko JD et al. (ed) Essentials of Glycobiology, 3rd ed. Cold Spring Harbor Laboratory Press, Cold Spring Harbor (NY).

16. Mellquist JL, Kasturi L, Spitalnik SL, Shakin-Eshleman SH (1998) The amino acid following an Asn-X-Ser/Thr sequon is an important determinant of N-linked core glycosylation efficiency. Biochemistry 37:6833–6837.

17. Schjoldager KT, Narimatsu Y, Joshi HJ, Clausen H (2020) Global view of human protein glycosylation pathways and functions. Nat Rev Mol Cell Biol 21:729–749.

18. Bieberich E (2014) Synthesis, Processing, and Function of N-glycans in N-glycoproteins. 47–70.

19. Brockhausen I SP (2017) O-GalNAc Glycans. In: Varki A, Cummings RD, Esko JD et al. (ed) Essentials of Glycobiology [Internet]., 3rd ed. Cold Spring Harbor (NY): Cold Spring Harbor Laboratory Press; 2015-2017.

20. Costa NR, Mendes N, Marcos NT, Reis CA, Caffrey T, Hollingsworth MA, Santos-Silva F (2008) Relevance of MUC1 mucin variable number of tandem repeats polymorphism in Hpylori adhesion to gastric epithelial cells. World J Gastroenterol 14:1411–1414.

21. Stanley P CR (2017) Structures Common to Different Glycans. In: Varki A, Cummings RD, Esko JD et al. (ed) Essentials of Glycobiology [Internet]., 3rd ed. Cold Spring Harbor Laboratory Press; 2015-2017.

22. Dillekås H, Rogers MS, Straume O (2019) Are 90% of deaths from cancer caused by metastases? Cancer Med 8:5574–5576.

23. Häuselmann I, Borsig L (2014) Altered tumor-cell glycosylation promotes metastasis. Front Oncol 4 MAR:1–15.

24. Adamczyk B, Tharmalingam T, Rudd PM (2012) Glycans as cancer biomarkers. Biochim Biophys Acta - Gen Subj 1820:1347–1353.

25. Dennis JW, Demetrio M, Dennis JW (1991) β1-6 Branched Oligosaccharides as a Marker of Tumor Progression in Human Breast and Colon Neoplasia. Cancer Res 51:718–723.

26. Rodrigues E, Macauley MS (2018) Hypersialylation in cancer: Modulation of inflammation and therapeutic opportunities. Cancers (Basel) 10:1–19.

27. Zhao YP, Xu XY, Fang M, Wang H, You Q, Yi CH, Ji J, Gu X, Zhou PT, Cheng C, Gao CF (2014) Decreased core-fucosylation contributes to malignancy in gastric cancer. PLoS One 9: .

28. Grosso M, Vitarelli E, Giuffrè G, Tuccari G, Barresi G (2000) Expression of Tn, sialosyl-Tn and T antigens in human foetal large intestine. Eur J Histochem 44:359–363.

29. Stowell SR, Ju T, Cummings RD (2015) Protein glycosylation in cancer. Annu Rev Pathol Mech Dis 10:473–510.

30. Wang W, Guo H, Geng J, Zheng X, Wei H, Sun R, Tian Z (2014) Tumor-released galectin-3, a soluble inhibitory ligand of human NKp30, plays an important role in tumor escape from NK cell attack. J Biol Chem 289:33311–33319.

31. Qi J, Li N, Fan K, Yin P, Zhao C, Li Z, Lin Y, Wang L, Zha X (2014) β1,6 GlcNAc branches-modified PTPRT attenuates its activity and promotes cell migration by STAT3 pathway e98052. PLoS One 9:.

32. Kirwan A, Utratna M, O'Dwyer ME, Joshi L, Kilcoyne M (2015) Glycosylation-Based Serum Biomarkers for Cancer Diagnostics and Prognostics. Biomed Res Int 2015: .

33. Munkley J, Elliott DJ (2016) Hallmarks of glycosylation in cancer. Oncotarget 7:35478–35489.

34. Ferdosi S, Rehder DS, Maranian P, Castle EP, Ho TH, Pass HI, Cramer DW, Anderson KS, Fu L, Cole DEC, Le T, Wu X, Borges CR (2018) Stage Dependence, Cell-Origin Independence, and Prognostic Capacity of Serum Glycan Fucosylation, β1-4 Branching, β1-6 Branching, and α2-6 Sialylation in Cancer. J Proteome Res 17:543–558.

35. Ferdosi S, Ho TH, Castle EP, Stanton ML, Borges CR (2018) Behavior of blood plasma glycan features in bladder cancer. PLoS One 13:1–20.

36. McCarthy C, Saldova R, Wormald MR, Rudd PM, McElvaney NG, Reeves EP (2014) The role and importance of glycosylation of acute phase proteins with focus on alpha-1 antitrypsin in acute and chronic inflammatory conditions. J Proteome Res 13:3131–3143.

37. Stowell, S. R., Ju, T., & Cummings RD (2015) Protein Glycosylation in Cancer. Annu Rev Pathol 10:473–510.

38. Venkitachalam S, Revoredo L, Varadan V, Fecteau RE, Ravi L, Lutterbaugh J, Markowitz SD, Willis JE, Gerken TA, Guda K (2016) Biochemical and functional characterization of glycosylation-associated mutational landscapes in colon cancer. Sci Rep 6:1–11.

39. Wörmann SM, Diakopoulos KN, Lesina M, Algül H (2014) The immune network in pancreatic cancer development and progression. Oncogene 33:2956–2967.

40.   Mackiewicz A, Schultz D, Mathison J, Ganapathi M, Kushner I (1989) Effect of cytokines on glycosylation of acute phase proteins in human hepatoma cell lines. Clin Exp Immunol 75:70–75.

41.   Van Dijk W, Pos O, Van der Stelt ME, Moshage HJ, Yap SH, Dente L, Baumann P, Eap CB (1991) Inflammation-induced changes in expression and glycosylation of genetic variants of α1-acid glycoprotein: Studies with human sera, primary cultures of human hepatocytes and transgenic mice. Biochem J 276:343–347.

42.   Mackiewicz A, Ganapathi MK, Schultz D KI (1987) Monocytes regulate glycosylation of acute-phase proteins. J Exp Med 166:253–258.

43.   Mackiewicz A KI (1989) Affinity Electrophoresis for Studies of Mechanisms Regulating Glycosylation of Plasma Proteins. Electrophoresis 10:830–835.

44.   Mackiewicz, A. Kushner I (1989) Interferon beta 2/B-cell stimulating factor 2/interleukin 6 affects glycosylation of acute phase proteins in human hepatoma cell lines. Scand J Immunol 29:265–271.

45.   Gryska K, Słupianek A, Laciak M, Górny A, Mackiewicz K, Baumann H MA (1995) Inflammatory cytokines controlling branching of N-heteroglycans of acute phase protein. In: Alavi, Azita JSA (ed) Glycoimmunology. Plenum Press, New York, New York, pp 239–246.

46.   Patel S, Vetale S, Teli P, Mistry R, Chiplunkar S (2012) IL-10 production in non-small cell lung carcinoma patients is regulated by ERK, P38 and COX-2. J Cell Mol Med 16:531–544.

47.   Enewold L, Mechanic LE, Bowman ED, Zheng YL, Yu Z, Trivers G, Alberg AJ, Harris CC (2009) Serum concentrations of cytokines and lung cancer survival in African Americans and Caucasians. Cancer Epidemiol Biomarkers Prev 18:215–222.

48.   Cigrovski Berković M, Catela Ivković T, Marout J, Zjačić-Rotkvić V, Kapitanović S (2012) Interleukin 1β gene single-nucleotide polymorphisms and susceptibility to pancreatic neuroendocrine tumors. DNA Cell Biol 31:531–536.

49.   Lesina M, Kurkowski MU, Ludes K, Rose-John S, Treiber M, Klöppel G, Yoshimura A, Reindl W, Sipos B, Akira S, Schmid RM, Algül H (2011) Stat3/Socs3 Activation by IL-6 Transsignaling Promotes Progression of Pancreatic Intraepithelial Neoplasia and Development of Pancreatic Cancer. Cancer Cell 19:456–469.

50.   Bellone G, Smirne C, Mauri FA, Tonel E, Carbone A, Buffolino A, Dughera L, Robecchi A, Pirisi M, Emanuelli G (2006) Cytokine expression profile in human pancreatic carcinoma cells and in surgical specimens: Implications for survival. Cancer Immunol Immunother 55:684–698.

51.   Zaynagetdinov R, Sherrill TP, Gleaves LA, McLoed AG, Saxon JA, Habermann AC, Connelly L, Dulek D, Peebles RS, Fingleton B, Yull FE, Stathopoulos GT,

Blackwell TS (2015) Interleukin-5 facilitates lung metastasis by modulating the immune microenvironment. Cancer Res 75:1624–1634.

52. Poch B, Lotspeich E, Ramadani M, Gansauge S, Beger HG, Gansauge F (2007) Systemic immune dysfunction in pancreatic cancer patients. Langenbeck's Arch Surg 392:353–358.

53. Padró M, Mejías-Luque R, Cobler L, Garrido M, Pérez-Garay M, Puig S, Peracaula R, De Bolós C (2011) Regulation of glycosyltransferases and Lewis antigens expression by IL-1β and IL-6 in human gastric cancer cells. Glycoconj J 28:99–110.

54. Narisada M, Kawamoto S, Kuwamoto K, Moriwaki K, Nakagawa T, Matsumoto H, Asahi M, Koyama N, Miyoshi E (2008) Identification of an inducible factor secreted by pancreatic cancer cell lines that stimulates the production of fucosylated haptoglobin in hepatoma cells. Biochem Biophys Res Commun 377:792–796.

55. Bassagañas S, Allende H, Cobler L, Ortiz MR, Llop E, de Bolós C, Peracaula R (2015) Inflammatory cytokines regulate the expression of glycosyltransferases involved in the biosynthesis of tumor-associated sialylated glycans in pancreatic cancer cell lines. Cytokine 75:197–206.

56. Goto Y, Lamichhane A, Kamioka M, Sato S, Honda K, Kunisawa J, Kiyono H (2015) IL-10-producing CD4+ T cells negatively regulate fucosylation of epithelial cells in the gut. Sci Rep 5:1–11.

57. Chintalacharuvu SR, Emancipator SN (1997) The glycosylation of IgA produced by murine B cells is altered by Th2 cytokines. J Immunol 159:2327–23233.

58. Gonzalez H, Hagerling C, Werb Z (2018) Roles of the immune system in cancer: From tumor initiation to metastatic progression. Genes Dev 32:1267–1284.

59. Abel AM, Yang C, Thakar MS, Malarkannan S (2018) Natural killer cells: Development, maturation, and clinical utilization. Front Immunol 9:1–23.

60. Hu W, Wang G, Huang D, Sui M, Xu Y (2019) Cancer immunotherapy based on natural killer cells: Current progress and new opportunities. Front Immunol 10:1–16.

61. Suck G, Linn YC, Tonn T (2016) Natural Killer Cells for Therapy of Leukemia. Transfus Med Hemotherapy 43:89–95.

62. Daly J, Carlsten M, O'Dwyer M (2019) Sugar free: Novel immunotherapeutic approaches targeting siglecs and sialic acids to enhance natural killer cell cytotoxicity against cancer. Front Immunol 10:1–9.

63. Farkona S, Diamandis EP, Blasutig IM (2016) Cancer immunotherapy: The beginning of the end of cancer? BMC Med 14:1–18.

64.	García-Muñoz R, López-Díaz-de-Cerio A, Feliu J, Panizo A, Giraldo P, Rodríguez-Calvillo M, Grande C, Pena E, Olave M, Panizo C, Inogés S (2016) Follicular lymphoma: in vitro effects of combining lymphokine-activated killer (LAK) cell-induced cytotoxicity and rituximab- and obinutuzumab-dependent cellular cytotoxicity (ADCC) activity. Immunol Res 64:548–557.

65.	Chong AS, Aleksijevic A, Scuderi P, Hersh EM GW (1989) Phenotypic and functional analysis of lymphokine-activated killer (LAK) cell clones. Ability of CD3+, LAK cell clones to produce interferon-gamma and tumor necrosis factor upon stimulation with tumor targets. Cancer Immunol Immunother 29:270–278.

66.	Surgeons N, Disease C, Insti- N (1985) Lymphokine-Activated Killer (LAK) Cells. Cell Immunol 134:296–313.

67.	Lotze MT, Matory YL, Rayner AA, Ettinghausen SE, Vetto JT, Seipp CA, Rosenberg SA (1986) Clinical effects and toxicity of interleukin-2 in patients with cancer. Cancer 58:2764–2772.

68.	Lee S, Margolin K (2012) Tumor-infiltrating lymphocytes in melanoma. Curr Oncol Rep 14:468–474.

69.	Wyckoff JB, Jones JG, Condeelis JS, Segall JE (2000) A critical step in metastasis: In vivo analysis of intravasation at the primary tumor. Cancer Res 60:2504–2511.

70.	Zhou X, Yang G, Guan F (2020) Biological Functions and Analytical Strategies of Sialic Acids in Tumor. Cells 9:273.

71.	Hudak JE, Canham SM, Bertozzi CR (2014) Glycocalyx engineering reveals a Siglec-based mechanism for NK cell immunoevasion. Nat Chem Biol 10:69–75.

72.	Stanczak MA, Siddiqui SS, Trefny MP, Thommen DS, Boligan KF, Von Gunten S, Tzankov A, Tietze L, Lardinois D, Heinzelmann-Schwarz V, Von Bergwelt-Baildon M, Zhang W, Lenz HJ, Han Y, Amos CI, Syedbasha M, Egli A, Stenner F, Speiser DE, Varki A, Zippelius A, Läubli H (2018) Self-associated molecular patterns mediate cancer immune evasion by engaging Siglecs on T cells. J Clin Invest 128:4912–4923.

73.	Lyons JJ, Milner JD, Rosenzweig SD (2015) Glycans Instructing Immunity: The Emerging Role of Altered Glycosylation in Clinical Immunology. Front Pediatr 3.

74.	Tsuboi S (2015) Roles of Glycans in Immune Evasion from NK Immunity. In: Suzuki T., Ohtsubo K. TN (ed) Sugar Chains. Springer, Tokyo, pp 177–188.

75.	Madsen CB, Lavrsen K, Steentoft C, Vester-Christensen MB, Clausen H, Wandall HH, Pedersen AE (2013) Glycan Elongation Beyond the Mucin Associated Tn Antigen Protects Tumor Cells from Immune-Mediated Killing. PLoS One 8:1–11.

76.	Park JJ, Lee M (2013) Increasing the α 2, 6 sialylation of glycoproteins may contribute to metastatic spread and therapeutic resistance in colorectal cancer.

Gut Liver 7:629–641.

77. Adams OJ, Stanczak MA, Von Gunten S, Läubli H (2018) Targeting sialic acid-Siglec interactions to reverse immune suppression in cancer. Glycobiology 28:640–647.

78. Alipov VI, Sukhorukov VN, Karagodin VP, Grechko A V., Orekhov AN (2017) Chemical composition of circulating native and desialylated low density lipoprotein: what is the difference? Vessel Plus 107–115.

79. Borén J, Chapman MJ, Krauss RM, Packard CJ, Bentzon JF, Binder CJ, Daemen MJ, Demer LL, Hegele RA, Nicholls SJ, Nordestgaard BG, Watts GF, Bruckert E, Fazio S, Ference BA, Graham I, Horton JD, Landmesser U, Laufs U, Masana L, Pasterkamp G, Raal FJ, Ray KK, Schunkert H, Taskinen MR, van de Sluis B, Wiklund O, Tokgozoglu L, Catapano AL, Ginsberg HN (2020) Low-density lipoproteins cause atherosclerotic cardiovascular disease: pathophysiological, genetic, and therapeutic insights: a consensus statement from the European Atherosclerosis Society Consensus Panel. Eur Heart J 41:2313–2330.

80. Orekhov AN, Ivanova EA, Melnichenko AA, Sobenin IA (2017) Circulating desialylated low density lipoprotein. Cor Vasa 59:e149–e156.

81. Harada LM, Carvalho MD t., Passarelli M, Quintão EC r. (1998) Lipoprotein desialylation simultaneously enhances the cell cholesterol uptake and impairs the reverse cholesterol transport system: In vitro evidences utilizing neuraminidase-treated lipoproteins and mouse peritoneal macrophages. Atherosclerosis 139:65–75.

82. Grewal T, Bartlett A, Burgess JW, Packer NH, Stanley KK (1996) Desialylated LDL uptake in human and mouse macrophages can be mediated by a lectin receptor. Atherosclerosis 121:151–163.

83. Summerhill VI, Grechko A V., Yet SF, Sobenin IA, Orekhov AN (2019) The Atherogenic Role of Circulating Modified Lipids in Atherosclerosis. Int J Mol Sci 20.

84. Tertov V V., Kaplun V V., Sobenin IA, Boytsova EY, Bovin N V., Orekhov AN (2001) Human plasma trans-sialidase causes atherogenic modification of low density lipoprotein. Atherosclerosis 159:103–115.

85. Delimaris I, Faviou E, Antonakos G, Stathopoulou E, Zachari A, Dionyssiou-Asteriou A (2007) Oxidized LDL, serum oxidizability and serum lipid levels in patients with breast or ovarian cancer. Clin Biochem 40:1129–1134.

86. Ivanova EA, Myasoedova VA, Melnichenko AA, Grechko A V., Orekhov AN (2017) Small Dense Low-Density Lipoprotein as Biomarker for Atherosclerotic Diseases. Oxid Med Cell Longev 2017.

87. Tsikas D (2017) Assessment of lipid peroxidation by measuring malondialdehyde (MDA) and relatives in biological samples: Analytical and biological challenges.

Anal Biochem 524:13–30.

88. Aguilar Diaz De Leon J, Borges CR (2020) Evaluation of oxidative stress in biological samples using the thiobarbituric acid reactive substances assay. J Vis Exp 2020:1–10.

89. Niavarani SR, Lawson C, Bakos O, Boudaud M, Batenchuk C, Rouleau S, Tai LH (2019) Lipid accumulation impairs natural killer cell cytotoxicity and tumor control in the postoperative period. BMC Cancer 19:11–14.

90. Rodrigues N V., Correia D V., Mensurado S, Nobrega-Pereira S, deBarros A, Kyle-Cezar F, Tutt A, Hayday AC, Norell H, Silva-Santos B, Dias S (2018) Low-density lipoprotein uptake inhibits the activation and antitumor functions of human Vg9Vd2 T cells. Cancer Immunol Res 6:448–457.

91. Tanabe F, Sato A, Ito M, Ishida E, Ogata M, Sigeta S (1988) Low-density lipoprotein oxidized by polymorphonuclear leukocytes inhibits natural killer cell activity. J Leukoc Biol 43:204–210.

92. Varki A, Kannagi R, Toole B et al. (2017) Glycosylation Changes in Cancer. In: Varki A, Cummings RD, Esko JD et al. (ed) Essentials of Glycobiology [Internet], 3rd ed. Cold Spring Harbor Laboratory Press, Cold Spring Harbor (NY).

93. Pilobello KT, Krishnamoorthy L, Slawek D ML (2005) Development of a lectin microarray for the rapid analysis of protein glycopatterns. Chembiochem 6:985–989.

94. Zaia J (2008) Mass Spectrometry and the Emerging Field of Glycomics. Chem Biol 15:881–892.

95. Williams C, Royo F, Aizpurua-Olaizola O, Pazos R, Boons GJ, Reichardt NC, Falcon-Perez JM (2018) Glycosylation of extracellular vesicles: current knowledge, tools and clinical perspectives. J Extracell Vesicles 7: .

96. Borges CR, Rehder DS, Boffetta P (2013) Multiplexed surrogate analysis of glycotransferase activity in whole biospecimens. Anal Chem 85:2927–2936.

97. Hu Y, Ferdosi S, Kapuruge EP, Diaz de Leon JA, Stücker I, Radoï L, Guénel P, Borges CR (2019) Diagnostic and Prognostic Performance of Blood Plasma Glycan Features in the Women Epidemiology Lung Cancer (WELCA) Study. J Proteome Res.

98. Kang P, Mechref Y, Klouckova I, Novotny M V. (2005) Solid-phase permethylation of glycans for mass spectrometric analysis. Rapid Commun Mass Spectrom 19:3421–3428.

99. Goetz JA, Novotny M V., Mechref Y (2009) Enzymatic/chemical release of O-glycans allowing MS analysis at high sensitivity. Anal Chem 81:9546–9552.

100. Zaare S, Aguilar JS, Hu Y, Ferdosi S, Borges CR (2016) Glycan node analysis: A

bottom-up approach to glycomics. J Vis Exp 2016:1–11.

101. V ESPB (1984) A simple and rapid method for the permethylation of carbohydrates. Carbohydr Res 131:209–217.

102. Ciucanu I (2006) Per-O-methylation reaction for structural analysis of carbohydrates by mass spectrometry. Anal Chim Acta 576:147–155.

103. Pilsoo Kang, Yehia Mechref, Iveta Klouckova and MVN (2005) Solid-phase permethylation of glycans for mass spectrometric analysis. Rapid Commun Mass Spectrom 19:3421–3428.

104. Heiss C, Stacey Klutts J, Wang Z, Doering TL, Azadi P (2009) The structure of Cryptococcus neoformans galactoxylomannan contains β-d-glucuronic acid. Carbohydr Res 344:915–920.

105. Hossler P, Khattak SF, Li ZJ (2009) Optimal and consistent protein glycosylation in mammalian cell culture. Glycobiology 19:936–949.

106. Klasić M, Krištić J, Korać P, Horvat T, Markulin D, Vojta A, Reiding KR, Wuhrer M, Lauc G, Zoldoš V (2016) DNA hypomethylation upregulates expression of the MGAT3 gene in HepG2 cells and leads to changes in N-glycosylation of secreted glycoproteins. Sci Rep 6:1–14.

107. Drake RR, Jones EE, Powers TW, Nyalwidhe JO (2015) Altered glycosylation in prostate cancer, 1st ed. Elsevier Inc.

108. Walsh G (2018) Biopharmaceutical benchmarks 2018. Nat Biotechnol 36:1136–1145.

109. Ciucanu I, Costello CE (2003) Elimination of Oxidative Degradation during the per-O-Methylation of Carbohydrates. J Am Chem Soc 125:16213–16219.

110. Ciucanu I, Caprita R (2007) Per-O-methylation of neutral carbohydrates directly from aqueous samples for gas chromatography and mass spectrometry analysis. Anal Chim Acta 585:81–85.

111. Kang P, Mechref Y, Novotny M V. (2008) High-throughput solid-phase permethylation of glycans prior to mass spectrometry. Rapid Commun Mass Spectrom 22:721–734.

112. Hu Y, Borges CR (2017) A spin column-free approach to sodium hydroxide-based glycan permethylation. Analyst 142:2748–2759.

113. Gornik O, Keser T, Lauc G (2016) Separation and Purification of Glycans Out of Glycoproteins Glycoproteins : Molecules with Great Heterogeneity. In: M. M (ed) Sample Preparation Techniques for Soil, Plant, and Animal. Humana Press, New York, pp 377–386.

114. Kramer RM, Shende VR, Motl N, Pace CN, Scholtz JM (2012) Toward a

molecular understanding of protein solubility: Increased negative surface charge correlates with increased solubility. Biophys J 102:1907–1915.

115. Dewald J, Colomb F, Bobowski-Gerard M, Groux-Degroote S, Delannoy P (2016) Role of Cytokine-Induced Glycosylation Changes in Regulating Cell Interactions and Cell Signaling in Inflammatory Diseases and Cancer. Cells 5:43.

116. Nie H, Liu X, Zhang Y, Li T, Zhan C, Huo W, He A, Yao Y, Jin Y, Qu Y, Sun XL, Li Y (2015) Specific N-glycans of Hepatocellular Carcinoma Cell Surface and the Abnormal Increase of Core-α-1, 6-fucosylated Triantennary Glycan via N-acetylglucosaminyltransferases-IVa Regulation. Sci Rep 5:1–11.

117. Liang J, Zhu J, Wang M, Singal AG, Odewole M, Kagan S, Renteria V, Liu S, Parikh ND, Lubman DM (2019) Evaluation of AGP Fucosylation as a Marker for Hepatocellular Carcinoma of Three Different Etiologies. Sci Rep 9:1–13.

118. Link-Lenczowski P, Bubka M, Balog CIA, Koeleman CAM, Butters TD, Wuhrer M, Lityńska A (2018) The glycomic effect of N-acetylglucosaminyltransferase III overexpression in metastatic melanoma cells. GnT-III modifies highly branched N-glycans. Glycoconj J 35:217–231.

119. Kalluri R, LeBleu VS (2020) The biology, function, and biomedical applications of exosomes. Science (80-) 367.

120. Qin J, Xu Q (2014) Functions and applications of exosomes. Acta Pol Pharm - Drug Res 71:537–543.

121. Williams C, Pazos R, Royo F, González E, Roura-Ferrer M, Martinez A, Gamiz J, Reichardt NC, Falcón-Pérez JM (2019) Assessing the role of surface glycans of extracellular vesicles on cellular uptake. Sci Rep 9:1–14.

122. Cheng Y, Zeng Q, Han Q, Xia W (2019) Effect of pH, temperature and freezing-thawing on quantity changes and cellular uptake of exosomes. Protein Cell 10:295–299.

123. Huang T, Deng CX (2019) Current progresses of exosomes as cancer diagnostic and prognostic biomarkers. Int J Biol Sci 15:1–11.

124. Sun B, Li Y, Zhou Y, Ng TK, Zhao C, Gan Q, Gu X XJ (2019) Circulating exosomal CPNE3 as a diagnostic and prognostic biomarker for colorectal cancer. J Cell Physiol 234:1416–1425.

125. Hennig R, Cajic S, Borowiak M, Hoffmann M, Kottler R, Reichl U, Rapp E (2016) Towards personalized diagnostics via longitudinal study of the human plasma N-glycome. Biochim Biophys Acta - Gen Subj 1860:1728–1738.

126. Suhre K, Trbojević-Akmačić I, Ugrina I, Mook-Kanamori DO, Spector T, Graumann J, Lauc G, Falchi M (2019) Fine-mapping of the human blood plasma N-glycome onto its proteome. Metabolites 9.

127. Moyano AL, Li G, Boullerne AI, Feinstein DL, Hartman E, Skias D, Balavanov R, van Breemen RB, Bongarzone ER, Månsson JE GM (2016) Sulfatides in extracellular vesicles isolated from plasma of multiple sclerosis patients. J Neurosci Res 94:1579–1587.

128. Purushothaman A, Bandari SK, Chandrashekar DS, Jones RJ, Lee HC, Weber DM, Orlowski RZ (2017) Chondroitin sulfate proteoglycan serglycin influences protein cargo loading and functions of tumor-derived exosomes. Oncotarget 8:73723–73732.

129. Chandran VI, Welinder C, Mansson AS, Offer S, Freyhult E, Pernemalm M, Lund SM, Pedersen S, Lehtio J, Marko-Varga G, Johansson MC, Englund E, Sundgren PC, Belting M (2019) Ultrasensitive immunoprofiling of plasma extracellular vesicles identifies syndecan-1 as a potential tool for minimally invasive diagnosis of glioma. Clin Cancer Res 25:3115–3127.

130. Lv J , Wang Z , Li F , Zhang Y LH (2019) Reverse capture for selectively and sensitively revealing the N-glycome of serum exosomes. Chem Commun 55:14339–14342.

131. Esko JD, Kimata K LU (2009) Proteoglycans and Sulfated Glycosaminoglycans. In: Varki A, Cummings RD, Esko JD, Freeze HH, Stanley P, Bertozzi CR, Hart GW EM (ed) Essentials of Glycobiology, 2nd ed. Cold Spring Harbor (NY): Cold Spring Harbor Laboratory Press, Spring Harbor (NY), pp 207–221.

132. Ghosh A, Kuppusamy H, Pilarski LM (2009) Aberrant splice variants of HAS1 (hyaluronan synthase 1) multimerize with and modulate normally splicedHAS1 protein. J Biol Chem 284:18840–18850.

133. Chao KL, Muthukumar L, Herzberg O (2007) Structure of human hyaluronidase-1, a hyaluronan hydrolyzing enzyme involved in tumor growth and angiogenesis. Biochemistry 46:6911–6920.

134. Chen YB, Jiang CT, Zhang GQ, Wang JS PD (2009) Increased expression of hyaluronic acid binding protein 1 is correlated with poor prognosis in patients with breast cancer. J Surg Oncol 100:382–386.

135. Goebeler M, Kaufmann D, Bröcker EB, Klein CE (1996) Migration of highly aggressive melanoma cells on hyaluronic acid is associated with functional changes, increased turnover and shedding of CD44 receptors. J Cell Sci 109:1957–1964.

136. Karjalainen JM, Tammi RH, Tammi MI, Eskelinen MJ, Ågren UM, Parkkinen JJ, Alhava EM, Kosma VM (2000) Reduced level of CD44 and hyaluronan associated with unfavorable prognosis in clinical stage I cutaneous melanoma. Am J Pathol 157:957–965.

137. Kanada M, Bachmann MH CC (2016) Signaling by Extracellular Vesicles Advances Cancer Hallmarks. Trends Cancer 2:84–94.

138. Hong CS., Funk S. WTL (2017) Isolation of Biologically Active Exosomes from Plasma of Patients with Cancer. Methods Mol Biol 1633:257–265.

139. Kimura K, Hohjoh H, Yamamura T (2018) The Role for Exosomal microRNAs in Disruption of Regulatory T Cell Homeostasis in Multiple Sclerosis. J Exp Neurosci 12:0–2.

140. Choi D, Spinelli C, Montermini L RJ (2019) Oncogenic Regulation of Extracellular Vesicle Proteome and Heterogeneity. Proteomics 19:1–2.

141. Möckl L (2020) The Emerging Role of the Mammalian Glycocalyx in Functional Membrane Organization and Immune System Regulation. Front Cell Dev Biol 8:1–14.

142. Amado M, Yan Q, Comelli EM, Collins BE, Paulson JC (2004) Peanut agglutinin high phenotype of activated CD8+ T cells results from de novo synthesis of CD45 glycans. J Biol Chem 279:36689–36697.

143. Comelli EM, Sutton-Smith M, Yan Q, Amado M, Panico M, Gilmartin T, Whisenant T, Lanigan CM, Head SR, Goldberg D, Morris HR, Dell A, Paulson JC (2006) Activation of Murine CD4 + and CD8 + T Lymphocytes Leads to Dramatic Remodeling of N -Linked Glycans. J Immunol 177:2431–2440.

144. Freire-de-Lima L, Previato JO, Mendonça-Previato L (2016) Editorial: Glycosylation changes in cancer: An innovative frontier at the interface of cancer and glycobiology. Front Oncol 6:1–2.

145. Ito H, Kaji H, Togayachi A, Azadi P, Ishihara M, Geyer R, Galuska C, Geyer H, Kakehi K, Kinoshita M, Karlsson NG, Jin C, Kato K, Yagi H, Kondo S, Kawasaki N, Hashii N, Kolarich D, Stavenhagen K, Packer NH, Thaysen-Andersen M, Nakano M, Taniguchi N, Kurimoto A, Wada Y, Tajiri M, Yang P, Cao W, Li H, Rudd PM, Narimatsu H (2016) Comparison of analytical methods for profiling N- and O-linked glycans from cultured cell lines: HUPO Human Disease Glycomics/Proteome Initiative multi-institutional study. Glycoconj J 33:405–415.

146. Wada Y, Dell A, Haslam SM, Tissot B, Canis K, Azadi P, Bäckström M, Costello CE, Hansson GC, Hiki Y, Ishihara M, Ito H, Kakehi K, Karlsson N, Hayes CE, Kato K, Kawasaki N, Khoo KH, Kobayashi K, Kolarich D, Kondo A, Lebrilla C, Nakano M, Narimatsu H, Novak J, Novotny M V., Ohno E, Packer NH, Palaima E, Renfrow MB, Tajiri M, Thomsson KA, Yagi H, Yu SY, Taniguchi N (2010) Comparison of methods for profiling O-glycosylation: Human proteome organisation human disease glycomics/proteome initiative multi-institutional study of IgA1. Mol Cell Proteomics 9:719–727.

147. Ciucanu I KF (1984) a Simple and Rapid Method for the Permethylation of Carbohydrates Ionelciucanuandfrancsckerek. Carbohydr Res 131:209–217.

148. Anumula KR, Taylor PB (1992) A comprehensive procedure for preparation of partially methylated alditol acetates from glycoprotein carbohydrates. Anal Biochem 203:101–108 .

149. Heiss PA and C (2009) Mass Spectrometry of N-Linked Glycans. In: Karlsson NHP and NG (ed) Methods in Molecular Biology, Glycomics: Methods and Protocols. Humana Press, Hatfield, Hertfordshire, pp 37–51.

150. Nix DB, Kumagai T, Katoh T, Tiemeyer M, Aoki K (2014) Improved in-gel reductive β-elimination for comprehensive O-linked and sulfo-glycomics by mass spectrometry. J Vis Exp 1–11.

151. Wessel D, Flügge UI (1984) A method for the quantitative recovery of protein in dilute solution in the presence of detergents and lipids. Anal Biochem 138:141–143.

152. Ito H, Kaji H, Togayachi A, Azadi P, Ishihara M, Geyer R, Galuska C, Geyer H, Kakehi K, Kinoshita M, Karlsson NG, Jin C, Kato K, Yagi H, Kondo S, Kawasaki N, Hashii N, Kolarich D, Stavenhagen K, Packer NH, Thaysen-Andersen M, Nakano M, Taniguchi N, Kurimoto A, Wada Y, Tajiri M, Yang P, Cao W, Li H, Rudd PM, Narimatsu H (2016) Comparison of analytical methods for profiling N- and O-linked glycans from cultured cell lines: HUPO Human Disease Glycomics/Proteome Initiative multi-institutional study. Glycoconj J 33:405–415.

153. van Kooyk Y, Kalay H, Garcia-Vallejo JJ (2013) Analytical tools for the study of cellular glycosylation in the immune system. Front Immunol 4:1–6.

154. Zhou S, Dong X, Veillon L, Huang Y, Mechref Y (2017) LC-MS/MS analysis of permethylated N-glycans facilitating isomeric characterization. Anal Bioanal Chem 409:453–466.

155. Hamouda H, Kaup M, Ullah M, Berger M, Sandig V, Tauber R, Blanchard V (2014) Rapid analysis of cell surface N-glycosylation from living cells using mass spectrometry. J Proteome Res 13:6144–6151.

156. Zou X, Yoshida M, Nagai-Okatani C, Iwaki J, Matsuda A, Tan B, Hagiwara K, Sato T, Itakura Y, Noro E, Kaji H, Toyoda M, Zhang Y, Narimatsu H, Kuno A (2017) A standardized method for lectin microarray-based tissue glycome mapping. Sci Rep 7:1–12.

157. de Oliveira RM, Ricart CAO, Martins AMA (2018) Use of mass spectrometry to Screen Glycan early markers in hepatocellular carcinoma. Front Oncol 7:1–10.

158. Daniotti JL, Lardone RD, Vilcaes AA (2016) Dysregulated expression of glycolipids in tumor cells: From Negative Modulator of Anti-tumor Immunity to Promising Targets for Developing Therapeutic Agents. Front Oncol 5:1–11.

159. Birklé S, Zeng G, Gao L, Yu RK, Aubry J (2003) Role of tumor-associated gangliosides in cancer progression. Biochimie 85:455–463.

160. Cheng KW, Agarwal R, Mitra S, Lee JS, Carey M, Gray JW, Mills GB (2012) Rab25 increases cellular ATP and glycogen stores protecting cancer cells from bioenergetic stress. EMBO Mol Med 4:125–141.

161. López-Díaz de Cerio A, García-Muñoz R, Pena E, Panizo Á, Feliu J, Giraldo P, Rodríguez-Calvillo M, Martínez-Calle N, Grande C, Olave MT, Andrade-Campos M, Bandrés E, Núñez-Córdoba JM, Inogés S, Panizo C (2020) Maintenance therapy with ex vivo expanded lymphokine-activated killer cells and rituximab in patients with follicular lymphoma is safe and may delay disease progression. Br J Haematol 189:1064–1073.

162. Wrangle JM, Patterson A, Johnson CB, Neitzke DJ, Mehrotra S, Denlinger CE, Paulos CM, Li Z, Cole DJ, Rubinstein MP (2018) IL-2 and beyond in Cancer Immunotherapy. J Interf Cytokine Res 38:45–68.

163. Kjærgaard J, Hokland ME, Agger R, Skovbo A, Nannmark U, Basse PH (2000) Biodistribution and tumor localization of lymphokine-activated killer T cells following different routes of administration into tumor-bearing animals. Cancer Immunol Immunother 48:550–560.

164. Wu J, Lanier LL (2003) Natural Killer Cells and Cancer. Adv Cancer Res 90:127–156.

165. Kim GG, Donnenberg VS, Donnenberg AD, Gooding W, Whiteside TL (2007) A novel multiparametric flow cytometry-based cytotoxicity assay simultaneously immunophenotypes effector cells: Comparisons to a 4 h 51Cr-release assay. J Immunol Methods 325:51–66.

166. Saito H, Ando S, Morishita N, Lee KM, Dator D, Dy D, Shigemura K, Adhim Z, Nibu KI, Fujisawa M, Shirakawa T (2014) A Combined Lymphokine-activated Killer (LAK) cell immunotherapy and adenovirus-p53 gene therapy for head and neck squamous cell carcinoma. Anticancer Res 34:3365–3370.

167. Spear P, Wu MR, Sentman ML, Sentman CL (2013) Nkg2d ligands as therapeutic targets. Cancer Immun 13:1–14.

168. Eleme K, Taner SB, Önfelt B, Collinson LM, McCann FE, Chalupny NJ, Cosman D, Hopkins C, Magee AI, Davis DM (2004) Cell Surface Organization of Stress-inducible Proteins ULBP and MICA That Stimulate Human NK Cells and T Cells via NKG2D. J Exp Med 199:1005–1010.

169. Fagan EA, Feddleston ALW (1987) Immunotherapy for cancer: The use of lymphokine activated killer (LAK) cells. Gut 28:113–116.

170. Toh U, Yamana H, Sueyoshi S, Tanaka T, Niiya F, Katagiri K, Fujita H, Shirozou K, Itoh K (2000) Locoregional cellular immunotherapy for patients with advanced esophageal cancer. Clin Cancer Res 6:4663–4673.

171. Qian X, Wang X, Jin H (2014) Cell transfer therapy for cancer: past, present, and future. J Immunol Res 2014:525913.

172. Polhill T, Zhang GY, Hu M, Sawyer A, Zhou JJ, Saito M, Webster KE, Wang Y, Wang Y, Grey ST, Sprent J, Harris DCH, Alexander SI, Wang YM (2012) IL-2/IL-2Ab complexes induce regulatory T cell expansion and protect against proteinuric

CKD. J Am Soc Nephrol 23:1303–1308.

173. Axelrod ML, Cook RS, Johnson DB, Balko JM (2019) Biological consequences of MHC-II expression by tumor cells in cancer. Clin Cancer Res 25:2392–2402.

174. Yang W, Bai Y, Xiong Y, Zhang J, Chen S, Zheng X, Meng X, Li L, Wang J, Xu C, Yan C, Wang L, Chang CCY, Chang TY, Zhang T, Zhou P, Song BL, Liu W, Sun SC, Liu X, Li BL, Xu C (2016) Potentiating the antitumour response of CD8+ T cells by modulating cholesterol metabolism. Nature 531:651–655.

175. Lagadari M, Truta-Feles K, Lehmann K, Berod L, Ziemer M, Idzko M, Barz D, Kamradt T, Maghazachi AA, Norgauer J (2009) Lysophosphatidic acid inhibits the cytotoxic activity of NK cells: Involvement of Gs protein-mediated signaling. Int Immunol 21:667–677.

176. Tertov V V., Orekhov AN (1997) Metabolism of native and naturally occurring multiple modified low density lipoprotein in smooth muscle cells of human aortic intima. Exp Mol Pathol 64:127–145.

177. FILIPOVIC I, BUDDECKE E (1979) Desialized Low-Density Lipoprotein Regulates Cholesterol Metabolism in Receptor-Deficient Fibroblasts. Eur J Biochem 101:119–122.

178. FILIPOVIC I, SCHWARZMANN G, AZ W, WIEGANDT H, BUDDECKE E (1979) Sialic-Acid Content of Low-Density Lipoproteins Controls Their Binding and Uptake by Cultured Cells. Eur J Biochem 93:51–55.

179. Levitan I, Volkov S, Subbaiah P V (2010) COMPREHENSIVE INVITED REVIEW Oxidized LDL: Diversity, Patterns of Recognition, and Pathophysiology. Antioxid Redox Signal 13:39–75.

180. Tapia-Vieyra JV, Delgado-Coello B, Mas-Oliva J (2017) Atherosclerosis and Cancer; A Resemblance with Far-reaching Implications. Arch Med Res 48:12–26.

181. Aguilar Díaz de león, J.S. and Borges C. (2020) Glycosylation Profiling of Glycoproteins Secreted from Cultured Cells Using Glycan Node Analysis and GC-MS. In: Methods in Molecular Biology, (In Press).

182. Walker SA, Aguilar Díaz De león JS, Busatto S, Wurtz GA, Zubair AC, Borges CR, Wolfram J (2020) Glycan Node Analysis of Plasma-Derived Extracellular Vesicles. Cells 9:1946.

183. Munkley J, Scott E (2019) Targeting Aberrant Sialylation to Treat Cancer. Medicines 6:102.

184. Hudak JE, Canham SM, Bertozzi CR (2014) Glycocalyx engineering reveals a Siglec-based mechanism for NK cell immunoevasion. Nat Chem Biol 10:69–75.

185. Stanczak MA, Siddiqui SS, Trefny MP, Thommen DS, Boligan KF, Von Gunten S, Tzankov A, Tietze L, Lardinois D, Heinzelmann-Schwarz V, Von Bergwelt-Baildon

M, Zhang W, Lenz HJ, Han Y, Amos CI, Syedbasha M, Egli A, Stenner F, Speiser DE, Varki A, Zippelius A, Läubli H (2018) Self-associated molecular patterns mediate cancer immune evasion by engaging Siglecs on T cells. J Clin Invest 128:4912–4923.

186. Del Zotto G, Marcenaro E, Vacca P, Sivori S, Pende D, Della Chiesa M, Moretta F, Ingegnere T, Mingari MC, Moretta A, Moretta L (2017) Markers and function of human NK cells in normal and pathological conditions. Cytom Part B - Clin Cytom 92:100–114.

187. Ni L, Lu J (2018) Interferon gamma in cancer immunotherapy. Cancer Med 7:4509–4516.

188. Ross J, Sagliano N, Donovan M, Breitbart R, Ginsburg G (2001) Atherosclerosis and Cancer: Common Molecular Pathways of Disease Development and Progression. Ann N Y Acad Sci 947:271–293.

189. Mantovani A, Allavena P, Sica A, Balkwill F (2008) Cancer-related inflammation. Nature 454:436–444.

190. Panth N, Paudel KR, Parajuli K (2016) Reactive Oxygen Species: A Key Hallmark of Cardiovascular Disease. Adv Med 2016:1–12.

191. Khan A, Alsahli M, Rahmani A (2018) Myeloperoxidase as an Active Disease Biomarker: Recent Biochemical and Pathological Perspectives. Med Sci 6:33.

192. Tomas L, Edsfeldt A, Mollet IG, Matic LP, Prehn C, Adamski J, Paulsson-Berne G, Hedin U, Nilsson J, Bengtsson E, Gonçalves I, Björkbacka H (2018) Altered metabolism distinguishes high-risk from stable carotid atherosclerotic plaques. Eur Heart J 39:2301–2310.

193. Jiménez-Corona AE, Damián-Zamacona S, Pérez-Torres A, Moreno A, Mas-Oliva J (2012) Osteopontin Upregulation in Atherogenesis Is Associated with Cellular Oxidative Stress Triggered by the Activation of Scavenger Receptors. Arch Med Res 43:102–111.

194. DamiaÂn-Zamacona S, Toledo-Ibelles P, Ibarra-Abundis M, Uribe-Figueroa L, HernaÂndez-Lemus E, Macedo-Alcibia KP, Delgado-Coello B, Mas-Oliva J, Reyes-Grajeda JP (2016) Early transcriptomic response to ldl and oxldl in human vascular smooth muscle cells. PLoS One 11:1–22.

195. Guo H, Callaway JB, Ting JPY (2015) Inflammasomes: Mechanism of action, role in disease, and therapeutics. Nat Med 21:677–687.

196. Duewell P, Kono H, Rayner KJ, Sirois CM, Vladimer G, Bauernfeind FG, Abela GS, Franchi L, Nũez G, Schnurr M, Espevik T, Lien E, Fitzgerald KA, Rock KL, Moore KJ, Wright SD, Hornung V, Latz E (2010) NLRP3 inflammasomes are required for atherogenesis and activated by cholesterol crystals. Nature 464:1357–1361.

197. Pittet MJ, Swirski FK (2011) Monocytes link atherosclerosis and cancer. Eur J Immunol 41:2519–2522.

198. Cedó L, Reddy ST, Mato E, Blanco-Vaca F, Escolà-Gil JC (2019) HDL and LDL: Potential New Players in Breast Cancer Development. J Clin Med 8:853.

199. Liu H, Wang S, Xin J, Wang J, Yao C, Zhang Z (2019) Role of NKG2D and its ligands in cancer immunotherapy. Am J Cancer Res 9:2064–2078.

200. Steinberg D, Witztum JL (2010) History of discovery: Oxidized low-density lipoprotein and atherosclerosis. Arterioscler Thromb Vasc Biol 30:2311–2316.

201. Ohkawa, H., N. Ohishi and KY (1978) Reaction of linoleic acid hydroperoxide with thiobarbituric acid. J Lipid Res 19:1053–1057.

202. Morales M, Munné-Bosch S (2019) Malondialdehyde: Facts and artifacts. Plant Physiol 180:1246–1250.

203. Devasagayam TPA, Boloor KK, Ramasarma T (2003) Methods for estimating lipid peroxidation: An analysis of merits and demerits. Indian J Biochem Biophys 40:300–308.

204. Dasgupta A, Klein K (2014) Methods for Measuring Oxidative Stress in the Laboratory. Antioxidants Food, Vitam Suppl 19–40.

205. Wade, C.R., van Rij A. (1989) Plasma malondialdehyde, lipid peroxides, and the thiobarbituric acid reaction. Clin Chem 35:336–336.

206. Khoubnasabjafari, M., Ansarin, K., Jouyban A (2015) Reliability of malondialdehyde as a biomarker of oxidative stress in psychological disorders. BioImpacts 5:123–127.

207. Khoubnasabjafari, M., Ansarin, K. & Jouyban A (2017) Comments on "An Investigation into the Serum Thioredoxin, Superoxide Dismutase, Malondialdehyde, and Advanced Oxidation Protein Products in Patients with Breast Cancer." Ann Surg Oncol 24:S573–S576.

208. Khoubnasabjafari M, Ansarin K, Vaez-Gharamaleki J, Jouyban A (2016) Comments on "Salivary 8-hydroxy-2-deoxyguanosine, malondialdehyde, vitamin C, and vitamin E in oral pre-cancer and cancer: diagnostic value and free radical mechanism of action." Clin Oral Investig 20:395–396.

209. Khoubnasabjafari, M., Ansarin, K. & Jouyban A (2015) Comments Concerning "Comparison of Airway and Systemic Malondialdehyde Levels for Assessment of Oxidative Stress in Cystic Fibrosis." Lung 193:867–868.

210. Azizi S, Shahrisa A, Khoubnasabjafari M, Ansarin K, Khoubnasabjafari M, Soleymani J, Jouyban A (2016) A possible reason for the low reproducibility of malondialdehyde determinations in biological samples. Bioanalysis 8:2179–2181.

211. Azizi, S., Khoubnasabjafari, M., Shahrisa, A., Khoubnasabjafari, M., Soleymani, J., & Jouyban A (2017) Effects of analytical procedures on the repeatability of malondialdehyde determinations in biological samples. Pharm Sci 23:193–197.

212. Wasowicz W, Neve J, Peretz A (1993) Optimized steps in fluorometric determination of thiobarbituric acid- reactive substances in serum: Importance of extraction pH and influence of sample preservation and storage. Clin Chem 39:2522–2526.

213. Jentzsch AM, Bachmann H, Fürst P, Biesalski HK (1996) Improved analysis of malondialdehyde in human body fluids. Free Radic Biol Med 20:251–256.

214. J. A. Buege and S. D. Aust (1975) Microsomal lipid peroxidation," Methods in Enzymology. J Phys Conf Ser 71:012004.

215. Gutteridge JMC (1982) Free-Radical Damage to Lipids, Amino-Acids, Carbohydrates and Nucleic-Acids Determined by Thiobarbituric Acid Reactivity. Int J Biochem 14:649–653.

216. Khoubnasabjafari, M., Soleymani, J., Jouyban A (2018) Avoid Using Spectrophotometric Determination of Malondialdehyde as a Biomarker of Oxidative Stress. Biomark Med 12:551–554.

217. Khoubnasabjafari, M., Ansarin, K. & Jouyban A (2016) Salivary malondialdehyde as an oxidative stress biomarker in oral and systemic diseases. J Dent Res Dent Clin Dent Prospect 10:71–74.

218. Halliwell B, Whiteman M (2004) Measuring reactive species and oxidative damage in vivo and in cell culture: How should you do it and what do the results mean? Br J Pharmacol 142:231–255.

219. Lee R et al (2012) "Evaluating oxidative stress in human cardiovascular disease: methodological aspects and considerations." Curr Med Chem 19:2504–2520.

220. Morel DW, Hessler JR, Chisolm GM (1983) Low density lipoprotein cytotoxicity induced by free radical peroxidation of lipid. J Lipid Res 24:1070–1076.

221. Guzmán-Chozas M, Vicario-Romero IM, Guillén-Sans R (1998) 2-thiobarbituric acid test for lipid oxidation in food: Synthesis and spectroscopic study of 2-thiobarbituric acid-malonaldehyde adduct. JAOCS, J Am Oil Chem Soc 75:1711–1715.

222. Shibata T, Iio K, Kawai Y, Shibata N, Kawaguchi M, Toi S, Kobayashi M, Kobayashi M, Yamamoto K, Uchida K (2006) Identification of a lipid peroxidation product as a potential trigger of the p53 pathway. J Biol Chem 281:1196–1204.

223. Skoog, D. A., West, D. M., Holler, F. J., and Crouch SR (2014) Sampling, standardization, and calibration. In: Fundamentals of analytical chemistry, 9th ed. Cengage – Brooks/Cole, Belmont, CA, pp 153–196.

224. Skoog, D. A., Holler, F. J., and Crouch SR (2007) Introduction. In: Principles of Instrumental Analysis, 6th ed. Cengage – Brooks/Cole, Belmont, CA, pp 1–24.

225. Seibig S, Van Eldik R (1997) Kinetics of [FeII(edta)] Oxidation by Molecular Oxygen Revisited. New Evidence for a Multistep Mechanism. Inorg Chem 36:4115–4120.

226. Jeffs JW, Jehanathan N, Thibert SMF, Ferdosi S, Pham L, Wilson ZT, Breburda C, Borges CR (2019) Delta-S-Cys-Albumin: A Lab Test that Quantifies Cumulative Exposure of Archived Human Blood Plasma and Serum Samples to Thawed Conditions. Mol Cell Proteomics 18:2121–2137.

227. K Y (1998) Simple Assay for the Level of Total Lipid Peroxides in Serum or Plasma. Methods Mol Biol 108:101–106.

228. Tsikas D (2017) Assessment of lipid peroxidation by measuring malondialdehyde (MDA) and relatives in biological samples: Analytical and biological challenges. Anal Biochem 524:13–30.

229. Bernheim, F., Bernheim, M. L. C. WKM (1948) The reaction between thiobarbituric acid and the oxidation products of certain lipides. J Biol Chem 174:257–264.

230. Wilbur, K. M., Bernheim F., Shapiro OW (1949) The thiobarbituric acid reagent as a test for the oxidation of unsaturated fatty acids by various agents. Arch Biochem 24:305–313.

231. Kwon T.W. WBM (1963) Determination of malonaldehyde by ultraviolet spectrophotometry. J Food Sci 28:627–630.

232. Esterbauer H., Schaur F.J. ZH (1991) Chemistry and biochemistry of 4-hydroxynonenal, malonaldehyde and related aldehydes. Free Radic Biol Med 11:81–128.

233. Dalle-Donne I, Rossi R, Colombo R, Giustarini D, Milzani A (2006) Biomarkers of oxidative damage in human disease. Clin Chem 52:601–623.

234. Jo C, Ahn DU (1998) Fluorometric Analysis of 2-Thiobarbituric Acid Reactive Substances in Turkey. Poult Sci 77:475–480.

235. Tsikas D, Rothmann S, Schneider JY, Suchy MT, Trettin A, Modun D, Stuke N, Maassen N, Frölich JC (2016) Development, validation and biomedical applications of stable-isotope dilution GC-MS and GC-MS/MS techniques for circulating malondialdehyde (MDA) after pentafluorobenzyl bromide derivatization: MDA as a biomarker of oxidative stress and its relation to 1. J Chromatogr B Anal Technol Biomed Life Sci 1019:95–111.

236. Barden AE, Mas E, Croft KD, Phillips M, Mori TA (2014) Minimizing artifactual elevation of lipid peroxidation products (F 2-isoprostanes) in plasma during collection and storage. Anal Biochem 449:129–131.

237. Jeffs JW, Ferdosi S, Yassine HN, Borges CR (2017) Ex vivo instability of glycated albumin: A role for autoxidative glycation. Arch Biochem Biophys 629:36–42.

238. Lee DM (1980) Malondialdehyde in Stored Plasma. Biochem Biophys Res Commun 95:1663–1672.

239. Tsikas D, Rothmann S, Schneider JY, Gutzki FM, Beckmann B, Frölich JC (2017) Simultaneous GC-MS/MS measurement of malondialdehyde and 4-hydroxy-2-nonenal in human plasma: Effects of long-term L-arginine administration. Anal Biochem 524:31–44.

APPENDIX A

PERMISSIONS

Brown, Carol
to jersus.aguilar@asu.edu ▾

Mon, Dec 21, 2020, 11:37 AM (11 days ago)

Hello Jesus,

I re-sent my previous email regarding three of the figures requested. Now in regard to Figs 3.1, 9.6 and 10.1, we are happy to grant permission for their use in your PhD thesis only. Please include credit to The Consortium of Glycobiology Editors, La Jolla, California.

Best wishes for success with your thesis,

Carol C. Brown
Books Development, Marketing and Sales
Cold Spring Harbor Laboratory Press
500 Sunnyside Blvd
Woodbury, New York 11797
516 422 4038 ph.
516 422 4095 fx.
brown@cshl.edu

From: Brown, Carol
Sent: Monday, December 14, 2020 3:07 PM
To: 'jesus.aguilar@asa.edu'
Subject: FW: CSHL Press Reprint Permission Request Form

Dear Jesus,

I am happy to grant permission for the use of Figs 6.1 and 11.1 in Essentials of Glycobiology in your PhD thesis only. Please include complete reference and copyright to The Consortium of Glycobiology Editors, La Jolla, California.

Multiplexed Surrogate Analysis of Glycotransferase Activity in Whole Biospecimens

Author: Chad R. Borges, Douglas S. Rehder, Paolo Boffetta

Publication: Analytical Chemistry

Publisher: American Chemical Society

Date: Mar 1, 2013

Copyright © 2013, American Chemical Society

ACS Publications
Most Trusted. Most Cited. Most Read.

PERMISSION/LICENSE IS GRANTED FOR YOUR ORDER AT NO CHARGE

This type of permission/license, instead of the standard Terms & Conditions, is sent to you because no fee is being charged for your order. Please note the following:

- Permission is granted for your request in both print and electronic formats, and translations.
- If figures and/or tables were requested, they may be adapted or used in part.
- Please print this page for your records and send a copy of it to your publisher/graduate school.
- Appropriate credit for the requested material should be given as follows: "Reprinted (adapted) with permission from (COMPLETE REFERENCE CITATION). Copyright (YEAR) American Chemical Society." Insert appropriate information in place of the capitalized words.
- One-time permission is granted only for the use specified in your request. No additional uses are granted (such as derivative works or other editions). For any other uses, please submit a new request.
If credit is given to another source for the material you requested, permission must be obtained from that source.

BACK

CLOSE WINDOW